UNIVERSIDADE D
COIMBRA

Magda Ferreira Rodrigues

Influence of elevated hydrostatic pressure on Müller cells phenotype

Do microglia-derived microvesicles play a role?

Dissertação no âmbito do Mestrado em Investigação Biomédica, com especialização em Neurobiologia, orientada pela Professora Doutora Ana Raquel Sarabando Santiago e coorientada pelo Doutor Henrique Manuel Paixão dos Santos Girão e apresentada à Faculdade de Medicina da Universidade de Coimbra.

Julho de 2021

INFLUENCE OF ELEVATED HYDROSTATIC PRESSURE ON MÜLLER CELLS PHENOTYPE

DO MICROGLIA-DERIVED MICROVESICLES PLAY A ROLE?

Magda Ferreira Rodrigues

Dissertação no âmbito do Mestrado em Investigação Biomédica, com especialização em Neurobiologia, orientada pela Professora Doutora Ana Raquel Sarabando Santiago e coorientada pelo Doutor Henrique Manuel Paixão dos Santos Girão e apresentada à Faculdade de Medicina da Universidade de Coimbra.

Dissertation for the attribution of the Master degree in Biomedical Research submitted to the Faculty of Medicine of the University of Coimbra, Portugal. The experimental work described in this dissertation was performed at Coimbra Institute for Clinical and Biomedical Research (iCBR), in Retinal Dysfunction & Neuroinflammation Group, under the supervision of Professor Ana Raquel Sarabando Santiago and Doctor Henrique Manuel Paixão dos Santos Girão. This work was funded by Fundação para a Ciência e a Tecnologia (FCT), Portugal (UID/NEU/04539/2019, UIDB/04539/2020 and UIDP/04539/2020), COMPETE-FEDER (FCOMP-01-0124-FEDER-028417; and POCI-01-0145-FEDER-007440), Centro 2020 Regional Operational Programme (CENTRO-01-0145-FEDER-000008: BRAINHEALTH 2020).

Dissertação para obtenção do grau de Mestre em Investigação Biomédica apresentada à Faculdade de Medicina da Universidade de Coimbra, Portugal. O trabalho experimental descrito nesta dissertação foi realizado no Instituto de Investigação Clínica e Biomédica de Coimbra, no grupo "Retinal Dysfunction & Neuroinflammation Group", sob a orientação científica da Professora Doutora Ana Raquel Sarabando Santiago e do Doutor Henrique Manuel Paixão dos Santos Girão. Este trabalho foi financiado pela Fundação para a Ciência e a Tecnologia (FCT), Portugal (UID/NEU/04539/2019, UIDB/04539/2020 e UIDP/04539/2020), COMPETE-FEDER (FCOMP-01-0124-FEDER-028417; e POCI-01-0145-FEDER-007440), Programa Operacional Regional do Centro - Centro 2020 (CENTRO-01-0145-FEDER-000008: BRAINHEALTH 2020).

Coimbra, 2021

1 2 9 0

FACULDADE DE MEDICINA
UNIVERSIDADE D
COIMBRA

“It always seems impossible until it's done.”

Nelson Mandela

Agradecimentos

Apesar do desafio que foi realizar esta tese não poderia deixar de tentar arranjar as melhores palavras para agradecer às pessoas sem as quais a realização deste trabalho não teria sido possível.

À Professora Doutora Raquel Santiago, orientadora desta tese, gostaria de agradecer a orientação e disponibilidade que providenciou ao longo do tempo que me teve como sua aluna. O apoio, incentivo e preocupação que concedeu permitiram a concretização deste trabalho. Agradeço a confiança que depositou em mim no laboratório, por acreditar nas minhas capacidades e todos os conhecimentos e experiência que me transmitiu, que decerto me aguçaram o pensamento e me tornaram mais experiente para a vida de investigadora.

Gostaria de agradecer ao Doutor Henrique Girão, coorientador desta tese, que me acompanhou ao longo deste trabalho e mestrado, que sempre se demonstrou disponível para responder às minhas dúvidas e perguntas. Agradeço o apoio contínuo que demonstrou pelos seus alunos.

Agradeço também ao Doutor Francisco Ambrósio que me abriu as portas do seu laboratório, concedendo-me as condições necessárias para a realização deste trabalho, e as reuniões semanais que permitiram alargar os meus conhecimentos.

À Doutora Mónica Zuzarte e à Teresa Rodrigues gostaria de agradecer por me terem ajudado na obtenção de resultados, por fazerem possível eu ver que o *pellet* invisível que andava a recolher não era apenas imaginário.

Também não poderia faltar um agradecimento aos membros do *Retinal Dysfunction & Neuroinflammation Group* com os quais partilhei o meu dia a dia no laboratório e que sempre se mostraram prontos a ajudar, nem que fosse apenas para encontrar um reagente ou uma chave perdida. Deixo agradecimentos especiais à Inês Aires e à Raquel Boia as minhas companheiras de gabinete, colegas de trabalho que se tornaram amigas, não sei para onde o futuro me leva, mas duvido que tenha colegas de gabinete como estas à minha espera. Sabia que quando atravessasse a porta do gabs qualquer que fosse a minha preocupação, stress ou notícia pelo menos uma delas estaria sempre lá para ouvir e passar a sua sabedoria. Deixo um agradecimento muito especial à Inês. Por toda a disponibilidade, por todos os ensinamentos que me passaste, por me fazeres continuar

em todos os momentos em que as coisas não estavam a funcionar. Quero agradecer-te por toda a ajuda que me deste, mesmo quando tinhas as tuas próprias preocupações.
Aos meus companheiros de mestrado Pita e Maria, por me aturarem sempre que estava a stressar com a tese. À Xana obrigada pelo apoio, compreensão, brincadeiras e amarguras que partilhamos diariamente, não me podia ter calhado melhor companheira nesta aventura.
Quero agradecer às pessoas que por incrível que parece ainda me lembro do dia em que nos tornamos amigas. À Costa e à Serdoura por terem sido as minhas companheiras desde o começo da minha vida em Coimbra e que desde aí nunca mais foram a lado nenhum. À Morais e à Jamanta que por já terem passado por esta fase tinham sempre um conselho para mim qualquer que fosse a situação. À Adriana, Maria e Ana que quando eu dizia "Tive um dia mau, vamos tomar café" estavam sempre lá para mim, mesmo quando tinham pouca disponibilidade. Ao Pedro e ao Brandão os melhores colegas de casa. Sem estas pessoas a minha experiência universitária não teria sido a mesma.
Quero agradecer ao Rafa por ter estado comigo praticamente todos os dias desta jornada, por ter ouvido todos os meus queixumes e todas as aventuras pelas quais passei durante este ano. Nunca esquecerei as boleias infinitas e os dias em que eu te arrastava comigo para o laboratório só para me fazeres companhia.
À Mel e ao Clark por serem os mais fofos e me darem o carinho que sempre precisei deles.
À minha irmã quero agradecer todas as vezes que ela disse "Não estejas assim, vai correr tudo bem" que me fizeram sentir todo o apoio e todo o conforto que eu precisava, por me aconselhar e ser o meu exemplo, e obrigada pelas fotos matinais do Valentim que animam sempre o meu dia. Também, não me posso esquecer de agradecer ao meu cunhadito por me aturar em Coimbra.
E finalmente, aos meus pais, um obrigado pelas sopas da mãe e pelas bricolagens do pai. Obrigada por me formarem e por me perdoarem as vezes que não ia a casa. Obrigada pelo apoio, pela paciência, pela dedicação e pelo carinho que sempre me ofereceram mesmo eu sendo rabuja, e mesmo que provavelmente não perceberem o que está escrito nas páginas seguintes.
Obrigada!

List of Contents

List of Figures

List of Tables

Abbreviations

ADP	Adenosine diphosphate
AP	Alkaline phosphatase
AQP4	Aquaporin-4
ARF	ADP-ribosylation factor
ARVO	Association for Research in Vision and Ophthalmology
A-Smase	Acidic sphingomyelinase
ATP	Adenosine triphosphate
BBB	Brain-blood barrier
BCA	Bicinchoninic acid
BDNF	Brain-derived neurotrophic factor
bFGF	Basic fibroblast growth factor
BLC	B lymphocyte chemoattractant
BRB	Blood-retinal barrier
Brn3a	Transcription factor of the Brn3a family
BSA	Bovine serum albumin
CD	Cluster of differentiation
Ck	Chemokine
CNS	Central nervous system
CNTF	Ciliary neurotrophic factor
CRALBP	Cellular retinaldehyde-binding protein
DAPI	4',6-diamidino-2-phenylindole
DIV	Days *in vitro*
DMEM	Dulbecco's Modified Eagle medium
DTT	1,4-Dithiothreitol
ECF	Chemifluorescence
ECL	Chemiluminescenc
EGF	Epidermal growth factor
EHP	Elevated hydrostatic pressure
EM	Electron microscopy
ENA-78	Epithelial neutrophil activating peptide-78
ESCRT	Endosomal sorting complex required for transport
EVs	Extracellular vesicles
Exo-free FBS	FBS depleted of vesicles
FBS	Fetal bovine serum
FGF	Fibroblast growth factor
Flt3L	Fms-like tyrosine kinase 3 ligand
GABA	γ-aminobutyric acid
GCL	Ganglion cell layer
GCP-2	Granulocyte chemotactic protein-2
GDNF	Glial cell line-derived neurotrophic factor
GFAP	Glial fibrillary acidic protein

GLAST	Glutamate-aspartate transporter 1
GM-CSF	Granulocyte-macrophage colony-stimulating factor
GRO	Growth regulated oncogene
GS	Glutamine synthetase
HGF	Hepatocyte growth factor
HIF-1α	Hypoxia-inducible factor-1 α
HRP	Horseradish peroxidase
HSP	Heat shock protein
I-309	Glycoprotein 309
Iba1	Ionized calcium-binding adapter molecule 1
ICAM-1	Intercellular adhesion molecule-1
IFN-y	Interferon γ
IFN-α	Interferon α
IGF-1	Insulin-like growth factor 1
IGFBP	Insulin-like growth factor-binding protein
IL	Interleukin
ILM	Inner limiting membrane
ILV	Intraluminal vesicles
INL	Inner nuclear layer
iNOS	Inducible nitric oxide synthase
IOP	Intraocular pressure
IP-10	Interferon-y-inducible protein
IPL	Inner plexiform layer
LIF	Leukemia inhibitory factor
LIGHT	TNF family member
LPS	Lipopolysaccharide
MCP1	Monocyte chemoattractant protein 1
MDC	Macrophage-derived chemokine
MHC	Major histocompatibility complex
MIF	Macrophage migration inhibitory factor
MIG	Monokine induced by interferon-y
MIO-M1	Human Müller cell line Moorfields/Institute of Ophthalmology-Müller 1
MIP-1	Macrophage inflammatory protein 1
MVB	Multivesicular bodies
MV-CT	MVs collected from BV-2 cells incubated at atmospheric pressure
MV-EHP	MVs collected from BV-2 cells incubated at EHP
MVs	Microvesicles
NAP-2	Neutrophil-activating peptide-2
NeuN	Neuronal nuclear protein
NFL	Nerve fiber layer
NF-L	Neurofilament-L
NGF	Nerve growth factor
NO	Nitric oxide
NT	Neurotrophins

NTA	Nanoparticle tracking analysis
OCT	Optical coherence tomography
ONL	Outer nuclear layer
OPL	Outer plexiform layer
ORBEA	Órgão para o Bem-Estar Animal (Animal Welfare and Ethics Body)
OS/IS	Outer and inner segments
PBS	Phosphate-buffered saline
PCR	Polymerase chain reaction
PDGF	Platelet-derived growth factor
PEDF	Pigmented epithelium-derived factor
PFA	Paraformaldehyde
PS	Phosphatidylserine
RANTES	Regulated upon activation, normal T cell expressed and secreted
RBPMS	RNA-binding protein with multiple splicing
RGC	Retinal ganglion cell
RIPA	Radioimmunoprecipitation assay
RNA	Ribonucleic acid
ROS	Reactive oxygen species
RPE	Retinal pigment epithelium
RPMI	Roswell Park Memorial Institute medium
RT	Room temperature
SCF	Stem cell factor
SD	Spectral domain
SDF-1	Stromal cell-derived factor 1
SDS-PAGE	Sodium dodecyl sulphate-polyacrylamide gel electrophoresis
SEM	Standard error of the mean
TARC	Thymus and activation regulated chemokine
TBS-T	Tris-buffered saline
TEM	Transmission electron microscopy
TGF	Transforming growth factor
Thy1	RCG cell surface protein
TIMP	Tissue inhibitor of metalloproteinase
TLR	Toll-like receptors
TNF	Tumour necrosis factor
TSPO	18 kDa Translocator protein
TUNEL	Terminal deoxynucleotidyl transferase (TdT)-mediated dUTP nick end labelling
VCAM-1	Vascular cell adhesion molecule-1
VEGF	Vascular endothelial growth factor
VIS	Vitreous infiltration score
WB	Western blot
β-III-Tub	β-III-Tubulin

Resumo

O glaucoma é das principais causas de cegueira a nível mundial. Esta doença é caracterizada pela atrofia do nervo ótico e morte de células ganglionares da retina (CGR). A pressão intraocular (PIO) elevada é o principal fator de risco para o desenvolvimento e progressão desta doença. A neuroinflamação mediada pelas células da glia contribui para a neurodegeneração da retina no glaucoma. No entanto, os mecanismos que estão envolvidos neste processo ainda não foram clarificados. As microvesículas (MVs) são vesículas extracelulares (VE) formadas pela fissão para o exterior da membrana plasmática e estão envolvidas na comunicação celular. A contribuição das MVs derivadas de microglias para a inflamação da retina é desconhecida. Tendo em conta o envolvimento das células da microglia e das células de Müller no glaucoma, neste estudo, pretendeu-se investigar se as MVs derivadas das células da microglia interferem com as células de Müller e avaliar os efeitos das MVs nas células de Müller e na retina.

As células da microglia (linha celular BV-2) foram expostas a pressão hidrostática elevada (PHE), mimetizando o aumento da PIO. As células da condição controlo foram incubadas a pressão atmosférica. As MVs provenientes de células BV-2 (MV-CT e MV-PHE) foram isoladas por ultracentrifugação de baixa velocidade e caracterizadas por análise de rastreamento de nanopartículas, microscopia eletrónica de transmissão e expressão de marcadores proteicos característicos de VE. As células de Müller (linha celular MIO-M1) foram incubadas com MV-CT ou MV-PHE e expostas a PHE ou pressão atmosférica. Em seguida, os efeitos da PHE e das MVs foram avaliados nas células MIO-M1. Para além disso, MVs foram injetadas no vítreo de murganhos C57BL/6J e os efeitos foram avaliados 24h e 7 dias após a injeção.

As células MIO-M1 expostas a PHE e incubadas com MVs não apresentaram alterações que indiquem gliose. As células MIO-M1 sob PHE aumentaram a produção de fatores pró-inflamatórios e a expressão de quimiocinas, no entanto, as MVs derivadas de microglias induziram, de uma forma geral, a resposta oposta nas células MIO-M1. As células MIO-M1 têm uma resposta moderada à PHE e as MVs de microglias são capazes de influenciar a resposta das células de Müller, no entanto, são necessários mais estudos para explorar aprofundadamente estes efeitos.

Após a administração intravítrea das MVs nos murganhos C57BL/6J, a análise por tomografia de coerência ótica mostrou que as MVs não alteraram significativamente a espessura da retina e observaram-se "spots" no vítreo, sugerindo a presença de células no vítreo, provavelmente células pertencentes ao sistema imunitário. A análise dos infiltrados vítreos revelou que estas células se encontram mais presentes 24h após a injeção de MV-PHE, comparando com o efeito das MV-CT. Sete dias após a injeção, ocorreu um decréscimo substancial na presença destas células no vítreo de animais em que MV-PHE foram administradas em comparação com a injeção de MV-CT. Os níveis das proteínas TSPO e iNOS aumentaram 24h após a exposição de MVs, sugerindo um aumento da inflamação. Imunohistoquímica revelou um aumento na imunomarcação de GFAP e no número de células MHC-II^{+}/Iba1^{+}, o que indica ativação das células de Müller e da microglia após a injeção de MVs. Além disso, as MVs induziram a morte de células da retina e a perda de CGR. De modo geral, as MVs derivadas de microglias induziram neuroinflamação da retina, gliose reativa e perda de CGR, mostrando que as MVs de origem microglial podem contribuir para a degeneração da retina. Curiosamente, ambas as populações de MVs causaram efeitos na retina, o que indica que estas conseguem disseminar o sinal inflamatório independentemente do estado de ativação das microglias.

Em resumo, os resultados demonstraram que as microglias libertam MVs capazes de interagir com células de Müller e células da retina, modulando a sua resposta, o que segure que as MVs derivadas de microglias podem ser uma via de comunicação entre células gliais e propagar sinais inflamatórios na retina.

Palavras-chaves: Células de Müller; comunicação intercelular; glaucoma; microglia; microvesículas; neuroinflamação.

Abstract

Glaucoma is a leading cause of blindness worldwide. This disease is characterized by optic nerve atrophy and retinal ganglion cell (RGC) death. Elevated intraocular pressure (IOP) is the main risk factor for the onset and progression of the disease. Neuroinflammation mediated by glial cells contributes to retinal neurodegeneration in glaucoma. However, the mechanisms that contribute to this process are not identified yet. Microvesicles (MVs) are extracellular vesicles (EV) formed by outward budding of the plasma membrane and are involved in cell-to-cell communication. The contribution of microglial MVs to retinal inflammation is unknown. Microglia and Müller cells play important roles in glaucoma, therefore, in this study, we aimed to explore if MVs derived from microglial cells communicate with Müller cells, and evaluate the effects of MVs on Müller cells and in the retina.

Microglia cells (BV-2 cell line) were exposed to atmospheric and elevated hydrostatic pressure (EHP) to mimic elevated IOP. Control BV-2 cell cultures were maintained under atmospheric pressure conditions. MVs from BV-2 cells (MV-CT and MV-EHP) were isolated by low-speed ultracentrifugation and characterized by nanoparticle tracking analysis, transmission electron microscopy, and expression of protein markers characteristic of EV. Müller cells (MIO-M1 cell line) were incubated with MV-CT or MV-EHP under EHP or atmospheric pressure. The effects of EHP and MVs on MIO-M1 cells were evaluated. Additionally, MVs were injected in the vitreous of C57BL/6J mice and 24h and 7 days post-injection the effects were evaluated.

The results show that MIO-M1 cells, exposed to EHP and incubated with MVs, did not express Müller cells gliotic markers. MIO-M1 cells under EHP increased pro-inflammatory factor production and upregulated chemokine expression, while, in general terms, MVs from microglial cells induced the opposite response in MIO-M1 cells. The results show that MIO-M1 cells have a mild response to EHP and that microglial MVs can influence Müller cells response, however, more studies are necessary to further explore these results.

After administration of MVs into the vitreous of C57BL/6J mice, optical coherence tomography (OCT) showed that MVs do not significantly change retinal thickness. However, “spots” were observed in the vitreous, suggesting the presence of cells in the

vitreous, likely corresponding to immune cells. The densitometric analysis of the cell infiltrates showed that eyes injected with MV-EHP presented more cells in the vitreous cavity 24h after injection compared with MV-CT. After 7 days post-injection, there was a significant decrease in cells infiltrates in MV-EHP condition when compared with MV-CT. TSPO and iNOS protein levels increased 24h after MVs exposure, suggesting an increase in inflammation. Immunohistochemistry revealed an increase in GFAP staining and the number of MHC-II$^+$/Iba1$^+$ cells in retinas, indicating Müller cell and microglia activation after MVs injection. Moreover, MVs induced retinal cell death and decreased RGC survival. Overall, microglia-derived MVs induced retinal neuroinflammation, reactive gliosis, and RGC loss, showing that MVs derived from microglia may contribute to retinal degeneration. Both populations of MVs affect the retina, suggesting that microglial-derived MVs propagate the inflammatory signal, independently from the microglial cells state of activation.

In summary, the results demonstrated that microglia release MVs that are able to interact with Müller cells and retinal cells, modulating their response, suggesting that MVs derived from microglial cells could be a via of communication between glial cells and propagate inflammatory signals in the retina.

Keywords: Glaucoma; intercellular communication; microglia; microvesicles; Müller cells; neuroinflammation.

Chapter 1

Introduction

1. Introduction

1.1 The eye

Of the 5 senses, vision is the one that gives us the most information about the world, its colours, shapes, and sizes, and allows us to appreciate the surroundings. The eye captures light and transforms it into electrochemical signals that are converted into images in the brain.

Protected in the orbit, the eye is formed by three layers, each one with an essential purpose. The external layer protects the internal structure and allows light to enter the eye. Next, the intermediate layer is constituted by the anterior and the posterior part that, respectively, control the amount of light falling into the eye and the vascular layer that nurtures the outer layers of the retina. At last, the internal layer converts the visible light into electrochemical information (Figure 1)[1].

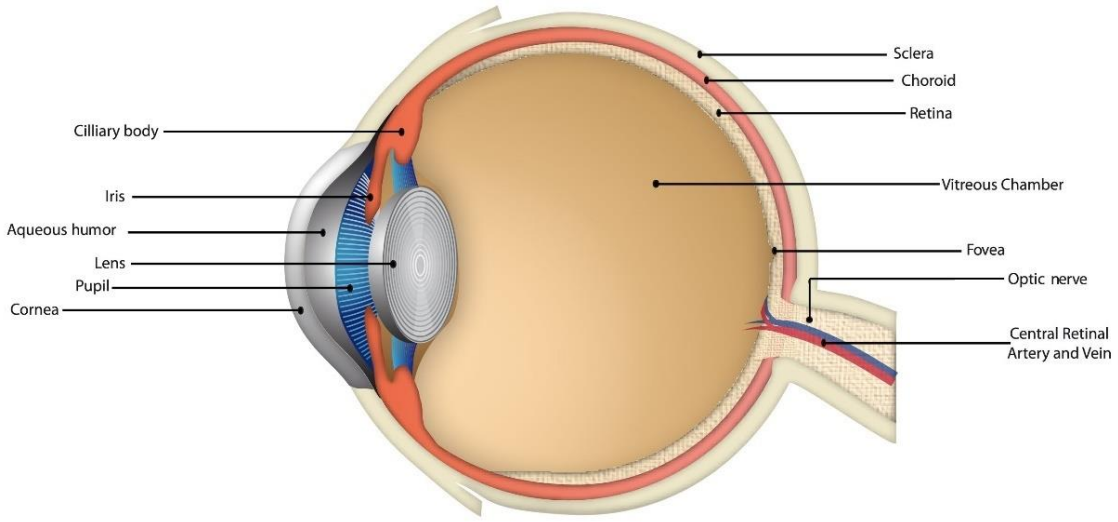

Figure 1 Anatomy of the human eye. Illustration of the eye structure, including the ciliary body, iris, aqueous humour, lens, pupil, cornea, sclera, choroid, retina, vitreous, fovea, and the optic nerve. Adapted from: https://www.freevector.com/.

The sclera is the outermost part of the eye. It is composed of conjunctive tissue that protects the internal layers and helps to maintain the form of the eye, in the front of the

eye the fibrous white tissue that composes the sclera becomes transparent creating the cornea. The cornea allows the light to enter the eye and it is the first ocular structure that refracts light. The iris, localized in the anterior part of the eye, is a coloured structure, comprised of muscles that contract or expand to control the size of the diameter of the pupil to regulate the amount of light that enters the eye. The lens and the ciliary body work as one, the ciliary muscles can adjust the lens shape by muscle contraction, allowing the eye to focus on different distances. The posterior part of the eye is constituted by the choroid, a highly vascularized connective tissue, that nourishes the photoreceptors, by providing oxygen and nutrients. The retina is the most inner layer and it is part of the central nervous system (CNS), being capable of converting light photons into neuronal stimuli that are interpreted in the brain[1,2].

In humans, 80% of the eye volume corresponds to the vitreous chamber, limited by the lens and the retina, which is filled with vitreous humour. The vitreous humour gives the eye its fluid-filled spherical appearance and possesses phagocytic cells that remove debris, maintaining a clear path for the light[1]. The anterior and the posterior chambers, respectively, located between the cornea and the iris and between the iris and the lens, are filled with aqueous humour. In the posterior chamber, the ciliary body produces and secretes the aqueous humour that then flows through the pupil into the anterior chamber. This fluid is drained by the trabecular meshwork, located between the cornea and the iris, into the Schlemm's canal, or the uveal meshwork, the nonconventional outflow pathway that drains the fluid into the ciliary muscle interstitium[2,3].

1.2 Retina

The retina is a neural tissue that lines in the back of the eye capable of converting photons into neuroelectrical impulses that are transported to the brain through the optic nerve. This tissue is constituted by neurons, glial cells (microglia, Müller cells, and astrocytes), epithelial cells, and blood vessels. To maintain its efficient function, the retina is organized in layers comprised of cell bodies (nuclear layers) and cellular processes (plexiform layers), and a monolayer of epithelial cells (Figure 2).

Adjacent to the vitreous, the innermost layer is the nerve fiber layer (NFL) composed of the retinal ganglion cells (RGC) axons, while the RGC somas constitute the ganglion cell layer (GCL). Next, separated by the inner plexiform layer (IPL), the inner nuclear layer (INL) is formed by the cell bodies of bipolar, amacrine, horizontal, and Müller cells. The outer plexiform layer (OPL) contains the dendrites of bipolar and horizontal cells that communicate with the axons and terminal endings of photoreceptors. Followed by the outer nuclear layer (ONL) formed by the cell bodies of photoreceptors, and, at last, the outer and inner segments (OS/IS) of photoreceptors. A monolayer of epithelial cells constitutes the retinal pigment epithelium (RPE) forming the outermost layer of the retina[2,4].

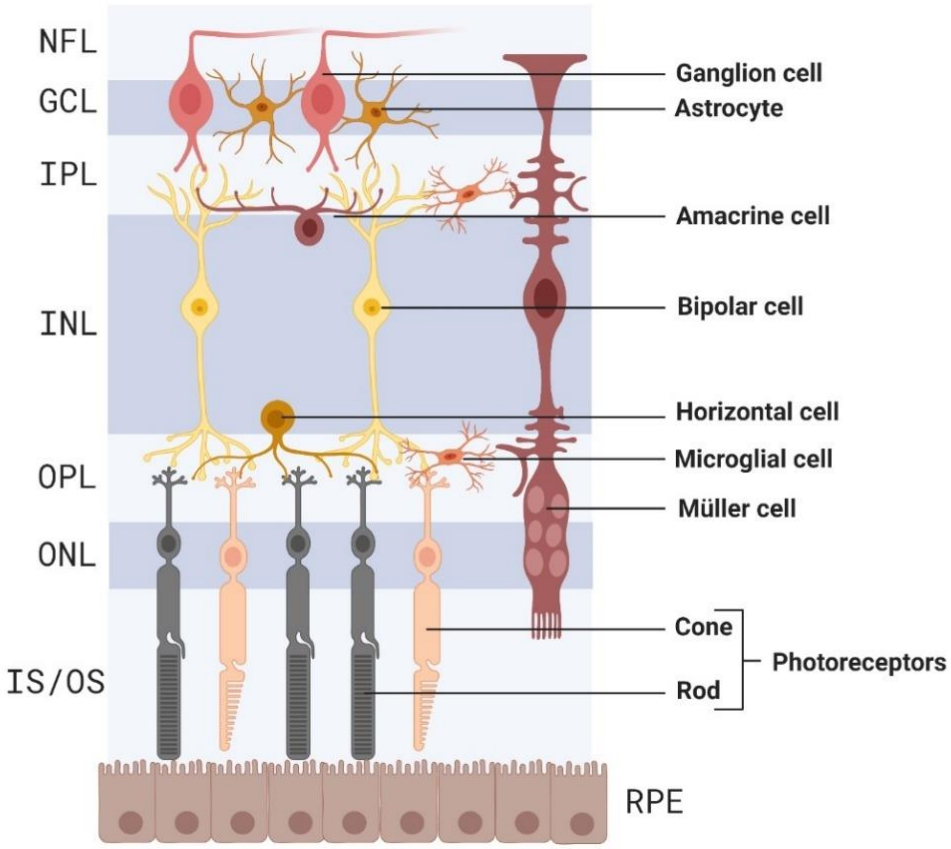

Figure 2 Anatomy of the retina. Schematic representation of the retinal structure. NFL – nerve fiber layer; GCL – ganglion cell layer; IPL – inner plexiform layer; INL – inner nuclear layer; OPL – outer plexiform layer; ONL – outer nuclear layer; OS/IS – outer and inner segments of photoreceptors; RPE – retinal pigment epithelium. The figure was created using Biorender (https://biorender.com/).

1.2.1 Blood vessels

To maintain an efficient visual function, the retina needs a constant supply of oxygen and nutrients. The oxygenation of the retina presents a higher rate than many other tissues, being one of the most metabolic active human tissues. The retina is organized in multiple layers and was two distinct vascular sources that provide blood supply to the tissue, the choroidal blood vessels nourish the photoreceptors, whereas the central retinal artery develops into capillaries that nurture the inner layers of the retina[5]. Furthermore, two main barriers of the vascular system, the blood-aqueous barrier and the blood-retinal barrier (BRB), ensure a regulated microenvironment for neuronal function, providing metabolic stability to the retina[6]. The BRB is divided into inner and outer blood-retinal barriers. The inner BRB is composed of endothelial cells connected by well-developed tight junctions, accompanied by astrocytes, Müller cells, and pericytes. The outer BRB is composed of tight junctions between RPE cells, only separated by the Brunch's membrane from the choriocapillaris (Figure 3). The BRB preserves the ocular homeostasis, however, in several retinal diseases, BRB breakdown is related to neurodegeneration, due to vascular impairments, and, consequently, vision loss[5].

The BRB also prevents the entry of cells from the circulation into the tissue, however, lymphocytes can cross the BRB during ocular inflammation. In ocular diseases, such as uveoretinitis, glaucoma, and diabetic retinopathy, disruption of the BRB and leukocyte infiltration occur in inflammation[7–9]. The cytokine production during inflammation activates endothelial cells, up regulating their expression of adhesion molecules. As a result, circulating leukocytes respond to the changes induced in the endothelium and immune cells are recruited to the inflammatory site[10]. Consequentially, macular edema, chorioretinal infiltrates, and exudates along with inflammatory cells in the vitreo occur due to BRB breakdown.

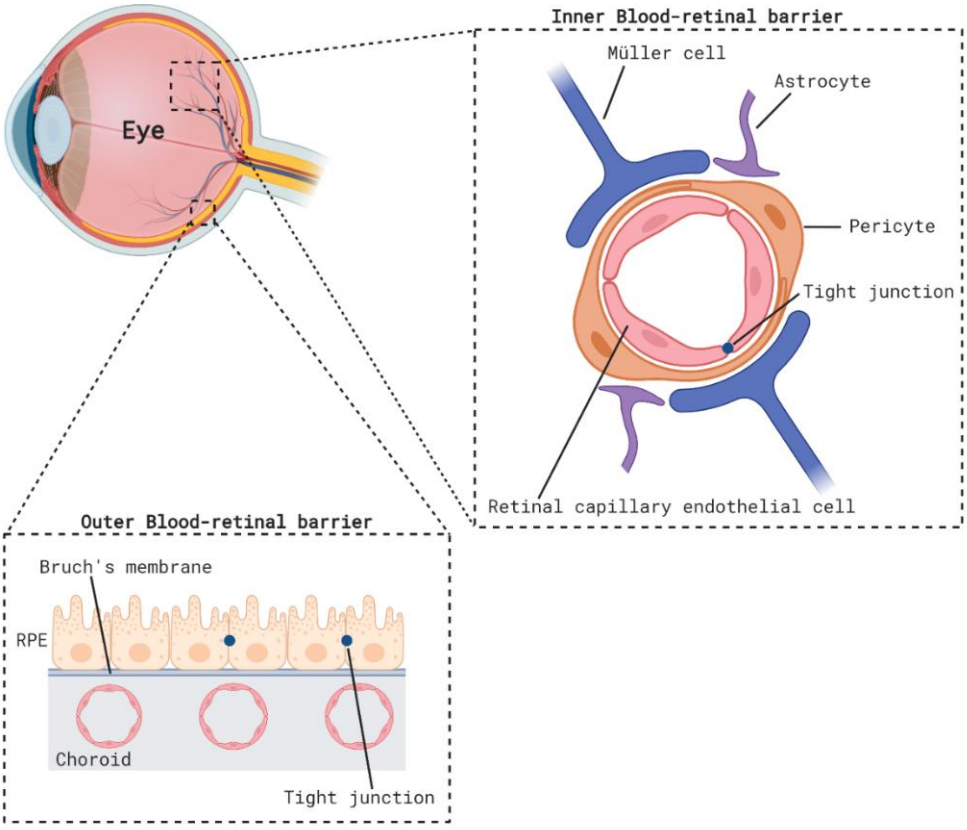

Figure 3 Illustration of the inner and outer blood-retinal barriers. The capillary endothelial cells and retinal epithelial cells sealed by complex junctions form the inner and outer BRB. Endothelial cells, pericytes, astrocytes, and Müller cells comprise the inner BRB and retinal pigment epithelial cells are overlaid on the Bruch's membrane forming the outer BRB. The BRB controls the transport of fluids and solutes and the extravasation of immune cells into the retinal parenchyma, being essential for homeostasis and neuron maintenance. The figure was created using Biorender (https://biorender.com/).

1.2.2 Visual pathway

Synapses between the several cell types occur in the plexiform layers of the retina to transmit the neuronal signals through the retina. The neurotransmission of information in the retina can be categorized into vertical or horizontal visual pathways. In the vertical pathway, the most important excitatory neurotransmitter is glutamate, and signals are transmitted from the photoreceptors directly to bipolar cells and then to RGC. In the horizontal pathway, mediated mainly by γ-aminobutyric acid (GABA) and glycine, horizontal cells in the OPL and amacrine cells in the IPL modulate the vertical

transmission[11]. Two pathways are classified based on the response of bipolar cells. When a stimulus reaches the bipolar cell, it can hyperpolarize the cell (OFF bipolar cell) or depolarize it (ON bipolar cell). This parallel process allows detecting light areas on dark backgrounds (ON) and dark areas on light backgrounds (OFF). Rods communicate exclusively with ON bipolar cells, whereas cones are connected to ON and OFF bipolar cells. In the IPL, ON and OFF bipolar cells transmit signals to the respective ON and OFF RGC[11,12].

1.2.3 Neurons

As part of the CNS, the retinal tissue is composed of 5 types of neurons: photoreceptors, horizontal cells, bipolar cells, amacrine cells, and RGC, each one executes distinct functions in the visual pathway[11].

Rods and cones are the two types of photoreceptors that exist in the human retina. The retinal photoreceptors convert light into neuronal signals through a process named phototransduction, this process is the first step in the visual pathway. Adjacent to the RPE, photoreceptors present an outer segment (OS) that contains membranous disks packed with a light-sensitive protein, the photopigments rhodopsin and cone opsin. The structural organization of the disks comprised in the OS provides a conical shape to cones and a cylindrical shape to rods[12,13]. Furthermore, photoreceptors are comprised of the inner segments (IS) that provide metabolic support to the OS, containing mitochondria and other cellular organelles, followed by the nucleus region and the synaptic terminals that communicate with bipolar and horizontal cells[13]. Horizontal cells are categorised by their communication with photoreceptors, contacting with rods and cones or exclusively with cones, in the human retina. Horizontal cells modulate photoreceptor response to light, their feedback pathway controls the synaptic input that bipolar cells receive from photoreceptors, and this function modulates light sensitivity[12]. Next, in the OPL, bipolar cells receive the stimuli from photoreceptors and horizontal cells and transmit it to RGC or amacrine cells. At least 11 different types of bipolar cells were identified in the human retina[12]. These are classified into two categories: ON and OFF bipolar cells. The expression of different glutamate receptors on bipolar cells dendrites allows cells to respond distinctively to the same synaptic impulse in the OPL, ON-bipolar cells express

metabotropic receptors, while OFF-bipolar cells express ionotropic receptors[12]. Then, amacrine cells modulate the synaptic impulse between bipolar cells and RGC in the IPL. Additionally, amacrine cells are capable of processing movement and light contrast, and modulate the signal transmission of bipolar cells[11,12].

Finally, the RGC are the output neurons in the visual pathway. Their soma is located in the GCL and their dendrites in the IPL where they receive the synaptic signals transmitted by bipolar and amacrine cells. Additionally, studies reported the occurrence of displaced amacrine cells in the GCL[14–16]. The RCC axons form the optic nerve that carries the visual information to the brain. The optic nerve is formed by all the axons of the RGC, and in humans is comprised of more than a million fibers[11]. RGC transport different impulses that complete each other allowing the creation of complex visual images in specific brain regions. In the brain of mammals, the information is processed in the lateral geniculate nucleus and the superior colliculus[17]. RGC can be divided into several subtypes, classified by their axonal projections in the brain, morphology, and photosensitivity. For example, mouse RGC can be classified into 25 types[18]. Molecular markers of RGC include transcription factors of the Brn3 family (Brn3a), the cell surface protein Thy1, and the ribonucleic acid (RNA)-binding protein with multiple splicing (RBPMS)[18]. RGC are the main retinal cells affected during optic neuropathies, in which RGC dysfunction and death have been described[19].

1.2.4 Glial cells

The glial cells are important for retinal support and homeostasis maintenance, but glial cells also respond to harmful stimuli like injuries and infection. There are three types of glial cells in the retina: astrocytes, microglia, and Müller cells[4].

1.2.4.1 Astrocytes

Astrocytes are almost exclusively located in the NFL; they are composed of a flatted cell body and radial processes that extend to the blood vessels and RGC axons. Astrocytes support neurons by maintaining the homeostasis of ionic levels, regulating neurotransmitters metabolism, and providing glucose to the RGC[20]. The distribution of

astrocytes is related to the retinal vasculature, being part of the BRB, these cells link neurons and blood vessels. In response to harmful situations, astrocytes became reactive, change their morphology, protein expression, and proliferation rate in a process designated by astrogliosis. One typical marker of gliosis is the increase in the expression of the glial fibrillary acidic protein (GFAP)[21].

1.2.4.2 Microglia

Microglia are the resident innate immune cells of the CNS. Their main functions are surveillance of the surrounding environment and maintenance of neuronal connections[22]. Microglia originate from hematopoietic progenitors that early in embryonic development migrate and colonize the CNS parenchyma[23,24]. In the retina, these cells first appear on the vitreal surface near the optic nerve, migrating from the inner to the outer retinal layers[24].

Under physiological conditions, in the mature retina, microglia can be found in the plexiform layers of the retina (IPL and OPL), monitoring the interactions between retinal neurons and glial cells (Figure 4A)[24]. These highly ramified cells, in their resting state, are known to remodel the dendrites of neurons during neuronal development, extend and retract their processes to scan the tissue, phagocyte cells debris, produce anti-inflammatory cytokines and neuroprotective mediators, involved in RGC and photoreceptors survival[25–28]. Overall, microglia sense the environment regulating homeostasis. In response to harmful stimuli, such as infection, trauma, and pathological conditions, microglia became activated and quickly migrate to the injured site. Reactive microglia change their morphology from a ramified state to an amoeboid shape with retracted processes. Upon activation, these cells produce and release pro-inflammatory mediators, such as interleukin (IL)-1β, IL-6, tumour necrosis factor (TNF), reactive oxygen species (ROS), and nitric oxide (NO) [27,29,30]. Once, in the damaged site microglia proliferate and phagocyte apoptotic cells and debris[29] (Figure 4B).

In the early stages of the disease, the activation of microglia occurs to control the damage, but prolonged microglial activation contributes to chronic neuroinflammation which leads to retinal neurodegeneration[31,32] (Figure 4C). For instance, in glaucoma,

studies have shown the involvement of microglia in the degeneration of RGC, but more studies are necessary to understand the role played by microglia in RGC dysfunction and death[33,34].

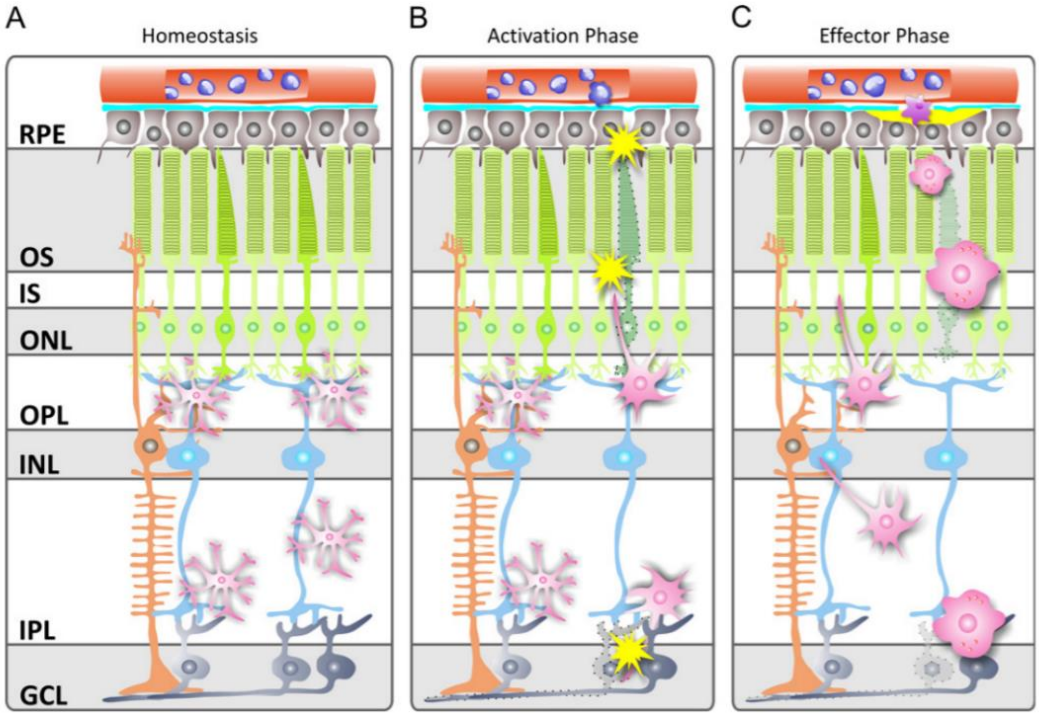

Figure 4 Schematic representation of three common phases of microglia activity in the retina. (**A**) In physiological conditions microglia can be found in the plexiform layers, constantly monitoring the environment, phagocyting cell debris and secreting neuronal factors, maintaining the homeostasis of the retina; (**B**) In response to several noxious stimuli microglia migrate through the tissue following the distress signals; (**C**) Microglia migrate to the injury site, once activated microglial cells alter their morphology to an amoeboid shape; GCL – ganglion cell layer; IPL – inner plexiform layer; INL – inner nuclear layer; OPL – outer plexiform layer; ONL – outer nuclear layer; OS/IS – outer and inner segments of photoreceptors; RPE – retinal pigment epithelium. Image from Karlstetter, Ebert, & Langmann, 2010[32].

1.2.4.3 Müller cells

The Müller cells are the most abundant glial cell type in the retina[35]. These radial cells span the entire width of the retinal tissue from the inner limiting membrane (ILM) to the ONL. Previous studies showed that Müller cells derive from neural crest cells and are the last neuronal element to be generated[36]. The cell bodies of Müller cells are located in the INL, two main processes ramify from the cell soma, the apical process spreads

towards the ONL, whereas the end foot of the cell extends towards the NFL. Additionally, the processes are highly ramified, and lateral ramifications extend towards the plexiform and nuclear layers ensuring the complete coverage of the retinal space. This specific placement of Müller cells allows them to metabolic and structurally support retinal neurons[37,38].

The cytoskeleton of these glial cells possesses vimentin and GFAP, which are proteins usually used as Müller cell markers. Moreover, glutamine synthetase (GS), glutamate aspartate transporter 1 (GLAST, excitatory amino acid transporter-1, EAAT1), and cellular retinaldehyde-binding protein (CRALBP) are the most commonly used markers that are specific associated with Müller cells metabolism[37–39].

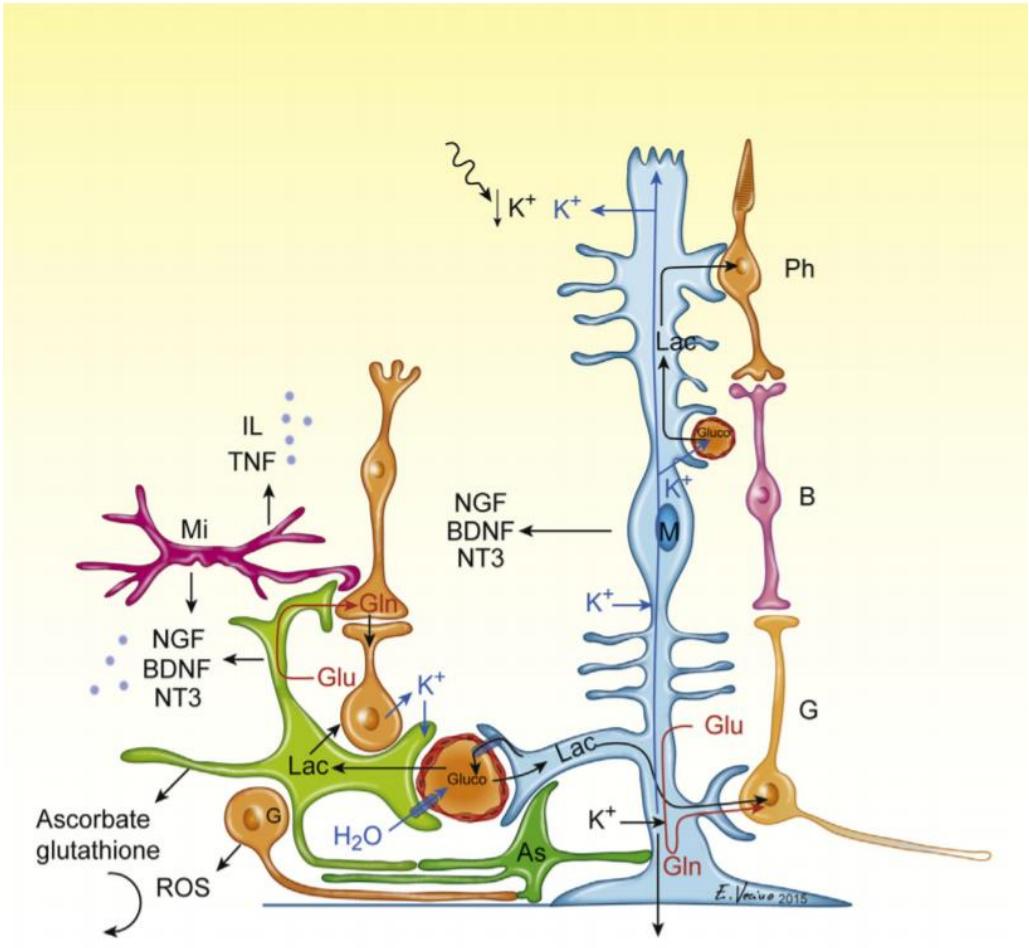

Figure 5 Schematic image of Müller cells interaction with retinal neurons. Representation of Müller cells metabolism; glutamate (Glu) to glutamine (Gln) transformation; homeostasis regulation and secretion of interleukins; A – astrocytes; B – bipolar cells; G – ganglion cells; M – Müller cells; Mi – microglia; Ph – photoreceptors[37]. Image from Vecino, Elena et al., 2016.

Müller cells and retinal neurons have a cooperative relationship, the glial cells support the survival of photoreceptors and RGC (Figure 5)[40–43]. One of the main functions of Müller cells is the recycling of glutamate, the most abundant neurotransmitter in the retina. The constant uptake of glutamate, via GLAST by Müller cells, avoids the diffusion of the neurotransmitter from the synaptic space modulating the synaptic activity, additionally, protects the neurons from glutamate excitotoxicity[44–47]. Subsequently, the enzyme GS converts glutamate into glutamine. Müller cell-derived glutamine is utilized by RGC and amacrine cells, and partially by photoreceptors to produce glutamate and GABA[39,48]. Moreover, the secretion of antioxidants, such as pyruvate, reduced ascorbate, and glutathione by macroglial cells provide anti-oxidative support to the neurons. The antioxidant glutathione is produced from the up taken glutamate and is involved in the neuroprotection of photoreceptors[46,49,50].

Furthermore, Müller cells contribute to the remodelling of synaptic circuits and release growth factors, neurotrophic factors, and cytokines, factors that are essential for proper neuronal function and survival. For example, in response to injuries, these cells release neurotrophins (Figure 5), such as brain-derived neurotrophic factor (BDNF), nerve growth factor (NGF), and glial cell line-derived neurotrophic factor (GDNF) that protect retinal neurons[37,39,51–54]. Also, ciliary neurotrophic factor (CNTF) and leukemia inhibitory factor (LIF) released by Müller cells are involved in photoreceptors regeneration and RGC neuronal protection against retinal damage[5,37,55].

In physiological conditions, Müller cells store extracellular glucose in the form of glycogen, being the major suppliers of glucose in the retina. This function, combined with their anatomical position within the retina, allows them to control the distribution of glucose across distinct neurons (Figure 5)[56–58]. For example, under metabolic stress, photoreceptors use lactate, produced by the anaerobic degradation of glucose by Müller cells[39].

Microglia are the most active phagocytic cells in the retina, but Müller cells also phagocyte dead cells and debris under physiological and pathological conditions[59,60]. Additionally, they are capable of phagocyte foreign bodies that are injected into the eye[61,62]. Furthermore, Müller cells play crucial roles in the maintenance of the inner BRB and the preservation of the extracellular homeostasis (Figure 5). The glial cells preserve

the BRB integrity by the secretion of neurotrophic factors[63,64]. These cells ensure the exchange of molecules, such as nutrients, ions, water, waste products, and transmitters, through Müller glia between blood vessels and neurons. Moreover, the osmotic and ionic balance is regulated by the membrane channels Kir (Kir4.1 and Kir2.1) and aquaporin-4 (AQP4) that regulate extracellular potassium buffering and water flow in the synaptic space, respectively[65,66].

Müller cells also act as light-guides through the retina. Their structural organization allows light to be gathered by their end feet and transmitted to the photoreceptor, allowing the reduction in light scattering and reflection in the inner retinal layer[39,67,68].

All noxious stimuli can activate Müller cells, changing their morphology, metabolism, and, consequently, their function. Müller cell gliosis is intended to protect the retina from further damage, but sustained macroglia activation has deleterious effects in neurons[69]. The expression of GFAP by Müller cells is an early marker of retinal distress. Other gliotic markers are the upregulation of vimentin and the increased expression of inflammatory factors. Some studies have shown that after retinal damage, a population of Müller cells can dedifferentiate into similar pluripotent retinal progenitors that proliferate and migrate to nuclear layers, giving rise to neural stem cells[70–73]. Prolonged Müller cell gliosis results in the dysregulation of GS, CRALBP, and Kir channels, causing changes in homeostasis. The neuroprotective and detrimental effects of Müller cell activation have been described in several retinal diseases, such as glaucoma and diabetic retinopathy[65,74].

1.2.4.3.1 Microglia and Müller cells communication

Chronic neuroinflammation, involving the activation of microglia and Müller cells, is associated with retinal neurodegenerative diseases, such as diabetic retinopathy, glaucoma, and age-related macular degeneration[39]. The interactions between retinal glial cells can influence the beneficial or detrimental outcomes of the inflammatory response modulating the neurodegeneration progression.

Following injury, microglia activation precedes Müller cell gliosis[75,76]. Previous studies reported that the exposure of Müller cells to activated microglia affects Müller cells morphology and proliferation rate[77,78]. Moreover, Müller cells expression of intermediate filament proteins (GFAP and vimentin), glutamate transporters (GLAST), inflammatory mediators, like inducible nitric oxide synthase (iNOS), and adhesive proteins such as vascular cell adhesion molecule-1 (VCAM-1) and intercellular adhesion molecule-1 (ICAM-1) change in the presence of activated microglia. Along with the release of inflammatory factors (IL-1β and IL-6), growth factors (LIF and GDNF), and chemotactic chemokines (monocyte chemoattractant protein 1, MCP1 and macrophage inflammatory protein 1, MIP-1)[77–79]. This interaction between glial cells modulates their neuroprotective effects. For example, activated microglia increases the production of NGF, and NGF consequently decreases the production of basic fibroblast growth factor (bFGF) by Müller cells, augmenting photoreceptor apoptosis. At the same time, the release of CNTF and GDNF by activated microglia stimulates the expression of CNTF and bFGF, which simultaneously improves the survival of photoreceptors[80]. Furthermore, activated microglia modulates Müller cell phagocytic capacity, gradually decreasing it after microglia migration to the injury site[59,81]. Müller cell response to microglia activation is affected by the nature of the injury, prolonged microglia activation, and, by the other cell types.

Overall, the understating of the cell-to-cell communication between these glial cells is necessary to further comprehend retinal pathologies and to uncover potentially new therapeutic targets that can regulate the neuroprotection, inflammation, and neuronal death in retinal injuries and diseases.

1.3 Glaucoma

Glaucoma is a group of eye disorders associated with progressive degeneration of RGC[82]. This disease is a leading cause of irreversible blindness worldwide and it is estimated that the number of people with glaucoma will increase to 111.8 million in 2040[83]. Glaucoma is classified as a degenerative optic neuropathy, characterized by loss of RGC, thinning of the NFL, and excavation of the optic disc, which can cause

permanent vision loss[84]. Genetics and vascular dysregulation are some factors that affect the susceptibility to glaucomatous nerve damage, however, elevated intraocular pressure (IOP) and older age are the main risk factors for the onset and progression of the disease[84,85]. Glaucoma is a silent disease in which most patients are diagnosed when the disease is in advanced stages. The treatment is mainly centred on lowering IOP by topical application of eye drops and surgery (laser or incisional), however, the disease may still progress despite the decrease in IOP[86,87]. Understanding the mechanisms that mediate the loss of RGC can be the key to develop new therapeutic strategies to halt RGC neurodegeneration.

1.3.1 Glaucoma models

Proper glaucoma models are essential to understand the molecular mechanisms of the disease and to develop new and more efficient therapies. *In vivo* and *in vitro* models were established to study glaucoma. Most animal models are centred in elevated IOP, the main risk factor in glaucoma, whereas other models address the normal tension glaucoma[88]. Some rodent genetic models mimic glaucomatous damages, such as DBA/2J mice, Nee mice, and GLAST knockout mice[89]. Microbead occlusion, intracameral injection of viscous agents, obstruction of aqueous outflow, cauterization of extraocular veins, circumlimbal suture, cannulation of the anterior chamber, compression of the conjunctival limbus are some of the pressure-dependent models[89]. The pressure-independent models of glaucoma address other features of the disease associated with neuronal death that allows studying mechanisms involved in RGC loss and optic nerve damage, such as the retinal ischemia-reperfusion injury, intravitreal injection of glutamate, or TNF[89]. Animal models are crucial to study the pathophysiology of the disease, however, they are too complex systems to understand the specific cellular roles. *In vitro* models emerge as valuable methods to identify the cellular pathways in glaucoma. The *in vitro* systems of elevated hydrostatic pressure (EHP) mimic ocular hypertension and can be used in several retinal cellular types[90].

1.3.1.1 Elevated hydrostatic pressure model: Focus on microglia and Müller cells

The current *in vitro* models to study elevated pressure are used to provide new perceptions into the individual cells' roles in the neurodegeneration characteristic of glaucoma. Previous studies assessed the responses of cells and tissues to several pressures, ranging from 30 to 100 mmHg above atmospheric pressure, and exposed for different times, from 10 minutes to 72 hours[90]. The EHP model applied in this study uses a customized pressure chamber that is connected to a tank that injects a mixture of gas (95% air/5% CO_2) through a pressure regulator. To maintain stable environmental conditions (temperature and humidity), the pressure chamber is kept with a reservoir with water in a standard incubator at 37°C. The pressure gauge (stable within ±1 mm Hg) connected to the chamber allows to regulate and maintain constant pressure, in this case, 70 mmHg above atmospheric pressure[90,91].

Reports have been describing the response of microglial cells to EHP, via exposure of primary retinal microglial cells, microglial cell lines, primary retinal neural cultures, and retinal organotypic cultures to elevated pressure. Furthermore, the studies show that EHP triggers changes in microglia number, reactivity, and morphology, increasing the mRNA expression of microglial activation associated markers and prompting amoeboid like changes in microglial cells morphology[92,93]. In addition, microglia migration, proliferation, and phagocytosis increase with EHP[93–95]. Challenging microglia with elevated pressure increases the expression of pro-inflammatory factors (TNF and IL-1β) and cytotoxic factors (NO), which are accompanied by increased levels of iNOS[93,94]. Another study shows that EHP considerably up-regulates IL-6 expression in microglia[96]. Moreover, microglia exposure to EHP increases oxidative stress, along with increase in adenosine triphosphate (ATP) and adenosine expression[93,95]. These alterations consequently contribute to RGC loss[92].

The effects of EHP in Müller cells have been described in some studies. In a rat Müller cell line, EHP exposure causes alterations in genes associated with elevated IOP[97]. In primary retinal Müller cell cultures exposed to 40 mmHg above atmospheric pressure for 24h increased the mRNA expression of GS and GLAST, suggesting that modulation

of the extracellular glutamate uptake is affected by elevated pressure[98]. Moreover, primary Müller cell cultures exposed to EHP increased mRNA expression of Kir2.1 and 4.1 channels, showing that EHP can induce cation channels dysregulation and, consequently, homeostasis imbalance[99]. Additionally, Müller cells increased pigmented epithelium-derived factor (PEDF), a potential neuroprotective factor, production upon EHP exposure, along with increased PEDF receptor expression and retraction of Müller cells processes[100].

1.3.2 Glaucoma and neuroinflammation

Neuroinflammation is the immune-inflammatory response within the CNS, modulated by the production of several mediators[101]. Evidence suggests neuroinflammation as a main player in glaucoma, however, a lot is still not known about the mechanisms involved in the neuropathology[90].

In glaucoma patients, the analysis of the vitreous humour showed elevated levels of IL-2, IL-5, MCP-1, TNF, and interferon-y-inducible protein (IP-10)[102], and the assessment of the aqueous humour revealed increased concentrations of IL-8, IL-9, IL-10, IL-12, interferon-α, and γ (IFN-α and IFN-γ) and monokine induced by interferon-γ (MIG)[103]. Also, increased levels of NO were detected in samples from aqueous humour of patients with glaucoma[104], accompanied by increased superoxide dismutase and glutathione peroxidase activity[105], suggesting that oxidative stress may also play a role in glaucoma. Additionally, analysis of blood samples of glaucoma patients revealed that superoxide dismutase, glutathione peroxidase, and catalase activities are increased in red blood cells[106]. Moreover, the analysis of human glaucoma donor eyes showed an increase in toll-like receptors (TLR) expression, showing an immune cells response to glaucoma. TLR are expressed in immune cells, like T and B cells, macrophages, and dendric cells, being part of the innate immune system[107]. Furthermore, a recent study reported the presence of B cells and natural killer cells infiltrates in the aqueous humour of glaucoma patients, suggesting that an immune imbalance may be involved in glaucomatous conditions[9].

The resident glial cells of the retina are responsible for the inflammatory response in glaucomatous conditions. After optic nerve damage, increase in IOP and excitotoxicity stimuli, glial cells can relocate in the retina and become activated, modulating the production of factors, such as cytokines and chemokines, that might have neuroprotective or detrimental effects in neuronal survival[108,109]. The presence of reactive microglia has already been described following optic nerve axotomy, retinal ischemia-reperfusion injury, and glaucoma[109]. Microglia reactivity and dysregulation of cytokine signalling in RGC have been reported in the DBA/2J mouse model of inherited glaucoma, which precedes the increase in IOP and axonal degeneration[33,110]. Additionally, in the DBA/2J mouse model, depletion of microglia by irradiation or treatment with minocycline or triamcinolone, which inhibit reactive microglia, improves RGC survival, further demonstrating the role of microglia in RGC death[111,112]. Moreover, inducing deficiency of fractalkine communication between RGC and microglia aggravates axonal transport dysfunction, as reported in the DBA/2J mouse model of glaucoma [113]. The expression of IL-6, a crucial factor of pressure-induced apoptosis, is increased in microglial cells in the DBA/2J model[114]. Interestingly, IL-6 was shown to protect RGC from degeneration induced by pressure[115], but its absence can prevent axonal degeneration and improve visual function[116]. Furthermore, EHP differently affects the IL-6 production by astrocytes and microglial cells, resulting in distinct effects in RGC survival[115]. The levels of TNF, a pro-inflammatory cytokine, are increased in the retina in human and experimental models of glaucoma and the aqueous humour of glaucoma patients[117–119]. The upregulation of TNF was been associated with microglia activation and RGC death in animals with ocular hypertension[117]. The inhibition of TNF signalling prevents optic nerve degeneration and reduce RGC loss[117,120]. Further studies have corroborated the detrimental effects of activated microglia in RGC degeneration and how the manipulation of microglia reactivity prevents neuronal loss[121,122]. In a model of ocular hypertension, microglia inhibition prevented axoglial alterations in the glaucomatous optic nerve[123]. Likewise, the control of microglia reactivity protects RGC in an excitotoxicity induced neuronal death model[124]. Also, blockade of the A_{2A} receptor controls microglia reactivity preventing RGC death induced by EHP *in vitro* and transient ischemic injury *in vivo*[92,94,125]. Additionally, it was reported that depletion of microglia from primary retinal neural cultures decreases cell death[93].

Müller cells are also involved in the inflammatory response, altering their morphology and production of inflammatory mediators, which can have a neuroprotective impact or further aggravate the detrimental effects on RGC[74,126]. Activated Müller cells have been identified in experimental animal models of glaucoma[74,127–129] and human glaucomatous eyes[130]. In glaucoma, excitotoxicity by glutamate has already been identified as a contributor to RGC loss[131], and reports showed that *in vitro* incubation of Müller cells under excitotoxic conditions induce the expression of several neurotrophins, such as BDNF, NGF, GDNF, and neurotrophins 3 and 4 (NT-3 and NT-4)[132]. Moreover, hypoxia tissue has been detected in the retina and optic nerve head of glaucoma patients by the identification of hypoxia-inducible factor-1 α (HIF-1α) regions[133]. In Müller cells, HIF-1α expression was increased after IOP elevation, along with vascular endothelial growth factor (VEGF), erythropoietin and heat shock protein-27 (HSP-27) upregulation[134], which also are detected in glaucomatous patients' eyes[135]. Additionally, the neuroprotective capabilities of these factors released by Müller cells were identified following glaucoma retinal injuries[136–139]. Retinal ischemia impairs the glutamatergic system of Müller cells leading to excitotoxicity and RGC damage[140]. Furthermore, the release of other factors, such as TNF, NO, and ROS by activated Müller cells also contribute to RGC death[65].

The mechanisms that contribute to the inflammatory signal in the retina are still unclear. However, the control of glial activation appears as a potential new approach in glaucoma treatment, preventing RGC death and further progression of optic nerve degeneration.

1.4. Extracellular vesicles

The exchange of information between cells is crucial in intercellular communication. Cell-to-cell interactions can be mediated by direct cell contact or transmission of soluble factors, such as cytokines, chemokines, and growth factors[141]. Additionally, a third mechanism involving extracellular vesicles (EVs) was identified in intercellular communication[142]. Initially, EVs were portrayed as cell waste carriers, however, these small vesicles, formed by a lipidic membrane, carry a variety of factors,

such as proteins, RNAs, and lipids, functioning as signalling vehicles to nearby and remote cells. Furthermore, the cargo transported by EVs can be influenced by the environmental conditions that the donor cell is exposed to, and their production and release can be modulated by different stimuli[143]. All cells can release EVs, which can carry cargo related to the cell of origin or undifferentiated content generally found in most vesicles[144]. Secreted EVs can be found in most body fluids, including blood, saliva, urine, bile, and semen[145–147]. EVs are categorised into exosomes, microvesicles (MVs), and apoptotic bodies (Figure 6), based on their biogenesis and size[141,148]. The combination of several microscopy and biochemical techniques is necessary to differentiate the distinct types of EV. Additionally, there are no universal markers for MVs besides cell surface markers which can differ in composition depending on the cell type. For example, the presence of endosomal markers is highly used as a conventional method for exosome identification[149,150].

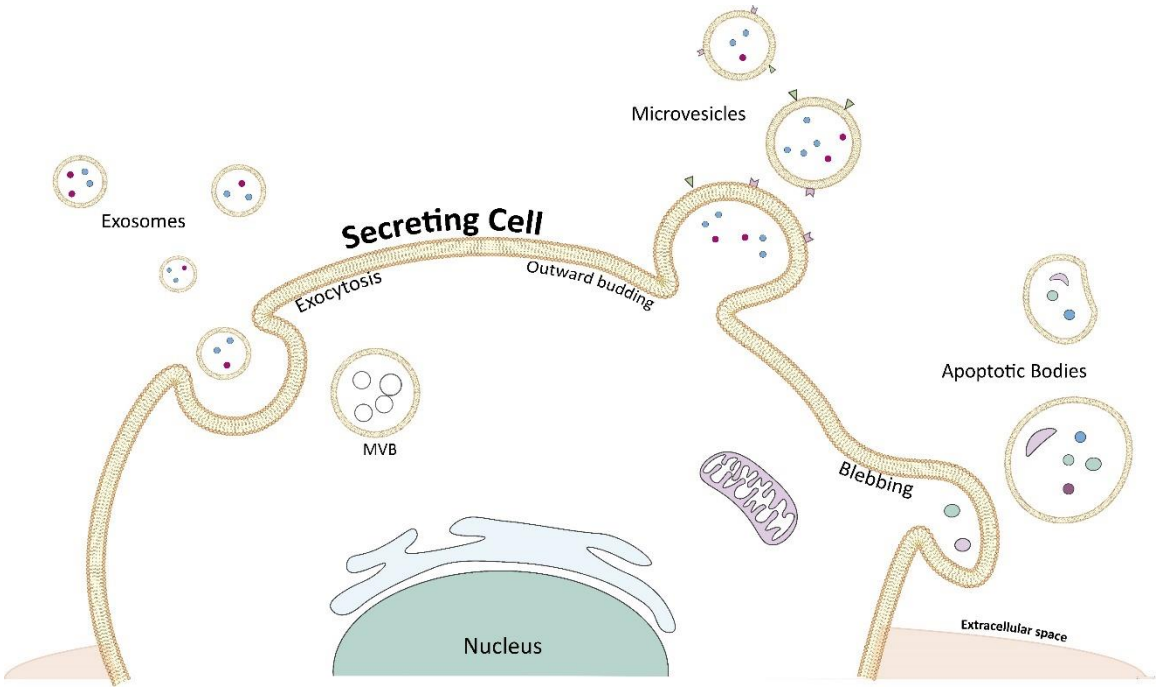

Figure 6 Schematic representation of biogenesis and secretion of extracellular vesicles. Exosomes are formed by budding of the membrane of multivesicular bodies (MVB), which fuse with the plasma membrane allowing the release of exosomes to the extracellular milieu. MVs result from outward budding and fission of the plasma membrane. During apoptosis, apoptotic bodies are formed by membrane blebbing.

1.4.1 Isolation and characterization methods of extracellular vesicles

The method used for EVs isolation should be planned based on the experimental aim and the properties of the sample. EVs can be isolated from body fluids and cell culture medium. Usually, isolation methods are based on EVs size, density, or specific markers expressed in EVs membrane surface[151]. Each manipulation of vesicles samples can disrupt EVs concentration, therefore few techniques may be applied to concentrate samples or use the combination of different methods[152]. The International Society for Extracellular Vesicles established guidelines to isolate and characterize the different types of EVs, to overcome the deficiency of specific markers of each type of EVs[153]. Differential centrifugation, density gradient centrifugation, size exclusion chromatography, ultrafiltration, precipitation, and immunocapture are the mainly used methods for EVs isolation[154,155]. The use of these methods does not ensure the isolation of ideal samples of EVs[156]. For example, although differential centrifugation is commonly used it does not isolate pure EVs samples, whereas density gradient centrifugation provides highly purified EVs, but with low yield[151,157]. Each isolation method has limitations and EVs characterization is required to further study the vesicles and their application[156].

Adequate methods are required to characterize the population of EVs by their size distribution, morphology, and biomarkers. Furthermore, quantification of the total number of EVs is crucial for the study of vesicles and their applications. A combination of methods is used to characterize EVs. Nanoparticle tracking analysis (NTA) measures the Brownian motions of individuals particles in suspension, gathering information regarding the size distribution and particle concentration[158]. However, NTA detects particle size only and does not differentiate between subpopulations of vesicles and non-EVs contaminants, which could have the same size as the vesicles' population in the study[159]. Electron microscopy (EM) techniques, such as transmission (TEM) and cryotransmission, are the standard methods for imagining EVs[160]. Cryotransmission-EM is a better alternative to TEM, because it preserves the integrity of the EVs, whereas during sample preparation for TEM the size can be compromised[157]. Furthermore, it is important to characterize the EVs cargo[156]. EVs can be characterized by the detection of specific markers using flow cytometry[156]. Flow cytometry provides a wide range of information regarding the molecular content of EVs surface, by multiple labelling of the

desire markers flow cytometry measures the emitted fluorescence signal, detecting the presence of the marker[159]. RNA purification, microarray analysis, quantitative reverse transcriptase-polymerase chain reaction (PCR) and PCR arrays, next generation sequencing and digital droplet PCR are techniques performed to characterize the RNA content in EVs[156]. In addition, the protein content of EVs is usually characterized through Western blot (WB), proteomic analysis, and fluorescent-activated cell-sorting[156]. WB is a widely used technique to confirm EVs presence in samples by showing the enrichment of various protein components in EVs isolated associated in the corresponding expression in donor cells[156]. However, WB should not be the only method applied to classify subpopulations of vesicles, especially between exosomes and MVs, since there are no universal recognized markers to differentiate them[161,162]. Lipidic components of EVs can also be characterized by mass spectrometry, however, the size of the sample is often a limitation[156]. Even though, identification of lipid classes in a subpopulation of EVs, and comparison to the cells that released the vesicles, could allow the identification of new EVs markers and uncover the biological role of EVs lipids in intercellular communication[163]. Moreover, EVs carry cellular metabolites, including sugars, amino acids, cofactors, and others[164]. Identification and quantification of these mediators transported by vesicles provide clues of the physiological environment, rising as possible biomarkers of disease[156].

1.4.2 Exosomes

Exosomes are small EVs, with a size range of 50-150 nm, formed as intraluminal vesicles (ILV) by inward budding of the membrane of multivesicular bodies (MVB)[143,165,166]. Following fusion of the MVB with the cell membrane, exosomes are released into the extracellular space (Figure 6)[167]. Different exosome subpopulations are distinguished by composition and morphology suggesting the involvement of multiple sorting types of machinery in exosome biogenesis[166]. Endosomal sorting complex required for transport (ESCRT), comprised of four distinct protein complexes, is essential in the biogenesis of exosomes. ESCRT-0 and ESCRT-1 are involved in the formation of microdomains in the MVB membrane, after that ESCRT-II recruits ESCRT-III, which executes the budding and fission of the microdomain, finally forming the ILV[143].

However, evidence indicates that MVB are still formed in the absence of ESCRT, indicating that exosomes can also be formed through ESCRT-independent mechanisms[168]. The molecular composition of exosomes includes endosomal-associated proteins (annexins and flotillin), tetraspanins (cluster of differentiation (CD)63, CD81, CD82, CD53), and lipids (cholesterol, sphingomyelin, and hexosylceramides)[169–173]. Additionally, exosome cargo can contain RNA (mRNA, miRNA, non-coding RNA) that can be subsequently transferred and processed by the recipient cells[174,175]. Exosomes are important players in intercellular communication, participating in countless healthy and disease processes of cell interaction, including homeostasis, development, cancer, and neurodegenerative diseases[176]. Previous studies have shown the importance of these EVs in pathological situations. Microglial cells propagate tau protein via secretion of tau enriched exosomes, contributing to neurotoxicity and progression of Alzheimer's disease[177]. In Parkinson's disease, exosomes released by both neurons and microglial cells contribute to the spread of α-synuclein, increasing neuroinflammation and aggravating neuronal disfunction[178]. Additionally, α-synuclein aggregation is promoted by certain lipids contained in exosomes[179]. It was recently demonstrated by our group that exosomes derived from microglia exposed to elevated pressure induce microglia reactivity, increase the production of proinflammatory mediators, cause retinal cell death, and impact RGC survival[180]. Exosomes may be seen as vehicles used by microglia to propagate the inflammatory signals, exacerbating cell dysfunction that contributes to retinal degeneration.

1.4.3 Microvesicles

MVs are formed through direct outward budding and fission of the plasma membrane (Figure 6) and present sizes ranging from 50 to 1000 nm. The distinction between MVs and exosomes is mainly based on their different biogenesis, since the size range of these vesicles overlap[143]. Even though the characterization of MVs is challenging, due to the lack of specific markers and the similarity in sizes between EVs, the interest in these EVs has increased in the recent years. When first identified MVs were thought to be part of a cellular process of clearing cells' waste, subcellular material from platelets

or ectocytosis, and were also mistaken as apoptotic bodies and exosomes[149,181,182]. These vesicles participate in several physiological processes[183,184] and appear as possible biomarkers of disease, considering that shed MVs are involved in the progression of pathologies, including cancer, multiple sclerosis, and infections[185–189]. Over time, studies tried to unravel the mechanisms of MVs biogenesis and the involvement of these vesicles in cell-to-cell communication. The biogenesis of MVs requires molecular changes within the plasma membrane, such as phospholipid and cytoskeletal protein rearrangement[190]. Membrane microdomains are formed through the clustering of membrane-associated proteins and lipids as well as the recruitment of ESCRT-I[191]. After the translocation of phosphatidylserine (PS) to the outer membrane leaflet, the membrane budding is induced and, consequently, the formation of the vesicle[192]. This rearrangement is regulated by aminophospholipid translocases (flippases and floppases), scramblases, and calpain, which are Ca^{2+}-dependent enzymes[143,190,192]. Aminophospholipid translocases are responsible for the transport of PS and phosphatidylethanolamine from one side of a bilayer to the other, while scramblases translocate phospholipids between the inner and outer leaflets of a cell membrane[143,190]. One consequence of the lipidic reorganization within the membrane is the alteration in cholesterol flux, increase efflux of cholesterol increases membrane fluidity, compromising the integrity of the membrane[193–195]. Actin-myosin interactions cause the restructuring of the cell cytoskeleton[143,190]. Myosin contracts due to its phosphorylation by activated GTPase adenosine diphosphate (ADP)-ribosylation factors (ARF6 and ARF1), which leads to the budding of the MVs[196]. Previous studies also reported the shedding of ESCRT-dependent MVs in *C. elegans,* as well as the bending of the plasma membrane promoted by acidic sphingomyelinase (A-SMase) translocation in glial cells[197,198]. ESCRT proteins have been implicated in the shedding of MVs through microdomains formation induced by phosphatidylethanolamine asymmetry within the membrane[197]. Following MVs formation, the vesicle is released from the plasma membrane (Figure 7).

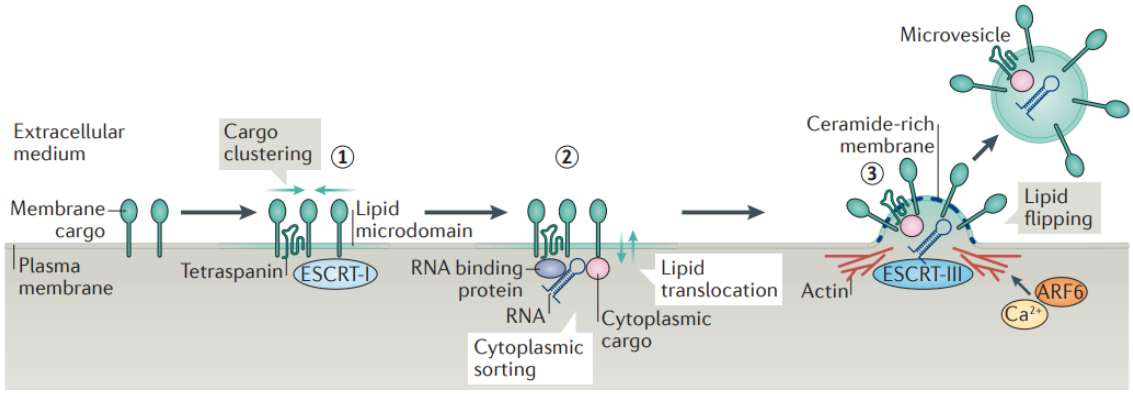

Figure 7 Biogenesis of microvesicles. Membrane microdomains are formed after lipids and membrane-associated proteins are clustered (step 1). Recruitment of components that are meant to be released in MVs (step 2). Membrane budding formation and vesicle release (step 3). Image from Van Niel, Guillaume, 2018[143].

After release, MVs can bind to recipient cells by receptor recognition, for example, exposed PS in the outer membrane of MVs is recognized through PS-receptors, followed by internalization. Nevertheless, several cells proceed differently, and in some cases, the interaction is restricted to the signalling mediated by surface contact via receptor binding[199]. In other cases, after receptor recognition, MVs fuse directly with the plasma membrane or are internalized via endocytosis[200]. In this case, the endocytic uptaken vesicle can stay isolated in the endosome and subsequently fuse with lysosomes; or discharge their content into the cytosol of recipient cell by fusion of their membrane with the endosome; alternatively, vesicles can return to the extracellular space (transcytosis) by endosome fusion with the plasma membrane[148]. Protein secretion is another alternative for MVs interaction with target cells, MVs suffer a rupture and release their content, which after modifies the recipient cell response[149].

Previous reports described the content of MVs, showing several membrane enzymes, such as tetraspanins (CD9, CD81, CD82), intracellular trafficking proteins (annexins, flotillin), membrane receptors (major histocompatibility complex II (MHC-II), CD14), and cytoplasmatic molecules, like ARF6, actin and chaperones proteins (HSP-70 and 90)[144,201–207]. These small vesicles are enriched with lipids such as cholesterol, PS, phosphatidylethanolamine, and sphingolipids. Additionally, microRNA, non-coding RNAs, mRNA can also be carried by MVs[141,143].

Further studies explored the effects of MVs derived from other cell types in different neurological conditions. For example, in the context of traumatic brain injury, brain endothelial cells release MVs enriched in occludin, a tight junction protein, that can be isolated from blood plasma[208]. This work shows that after a brain injury the cerebral endothelium is compromised, releasing MVs containing tight junction proteins that may provide clues regarding the integrity of the brain-blood barrier (BBB)[208]. In some cases, long-lasting changes in the permeability of the BBB induce inflammation, contributing to neuronal impairment[209]. Therefore, following brain trauma, the characterization of the cargo profile of MVs from blood plasma may serve as a biomarker of the condition of the neuronal environment, monitoring the BBB integrity and neuroinflammation[208].

1.4.4 Apoptotic bodies

Apoptosis is a mechanism of programmed cell death. It happens deliberately during development, homeostasis, and pathological conditions in all tissues[210,211]. Apoptotic bodies are released by cells undergoing apoptosis, formed by membrane enclosed vesicles that contain cellular cargo from disintegrating cells (Figure 6). Apoptotic bodies are the largest type of EVs, that may reach up to 4000 nm, however, smaller vesicles could be released by membrane blebbing[212,213]. During cell death, morphological alterations occur in the cell, such as PS translocation to the outer membrane, which binds to annexin, and oxidation of surface molecules[214]. Thrombospondin or the complement protein C3b recognize binding sites and, in turn, phagocytic cells, like microglia and macrophages, recognize the apoptotic bodies[215–217]. Therefore, annexin, thrombospondin, and C3b are well-recognized markers of apoptotic bodies[218,219]. Generally, these vesicles are phagocyted locally, consequently, apoptotic bodies participate in the cell-to-cell communication with nearby cells[219]. The contribution of these EVs in the cell-to-cell interaction was being demonstrated in previous studies. For example, apoptotic bodies are involved in the horizontal transference of tumour DNA after vesicle phagocytosis and endothelial cells derived apoptotic bodies affect growth and differentiation of endothelial progenitors cells[212,220].

1.4.5. Effects of microvesicles from microglia

Microglia release EVs to communicate with other cells, in both physiological and pathological conditions. Over the years, the interest in MVs released by microglial cells has increased, due to the role of these cells in inflammation and degeneration. The number of microglia-derived MVs and the cargo that they carry is affected by the conditions that the donor cells are exposed[221]. Previous reports revealed that in the brain activated microglia release MVs, which communicate with the surrounding cells and modulate the microenvironment[222].

Cells that express the purinergic receptor P2X7, an ion channel gated by extracellular ATP, have a specific mechanism of MVs shedding. Microglial cells express this receptor[223], which modulates the inflammatory cytokine release[224]. P2X7 receptor activation results in the rearrangement of cytoskeletal proteins and plasma membrane asymmetry[225–227]. This process induces translocation of A-SMase and, consequently, vesicle formation, followed by the detachment of blebs from the membrane, resulting in the release of MVs[198,228]. Activation of the receptor P2X7 stimulates inflammasome assembly, a caspase-1-associated complex, that leads to the release of IL-1β [224,228,229]. Therefore, this mechanism emerges as a secretory pathway of IL-1β through MVs. Interestingly, released MVs carry the P2X7 receptor in their membranes and are enriched in pro-caspase-1 and IL-1β[228,230,231]. Upon activation by extracellular ATP, pro-IL-1β is converted in mature IL-1β by the caspase-1 inflammasome complex in the MVs intravesicular lumen[232,233]. TNF, proteases, and the MHC-II could be some of the factors involved in the trafficking of membrane proteins, which may accompany IL-1β release by MVs shedding since they are modulated upon P2X7 receptor activation[206,233–235]. Furthermore, extracellular ATP induces apoptosis by P2X7 activation, thus shedding of MVs that carry the P2X7 receptor could be a mechanism of protection against apoptosis since it decreases receptor accessibility[230,236]. Moreover, a recent study described a new via to release MVs independent of extracellular ATP in myeloid cells during inflammation by showing that inhibition of ATP/P2X7 pathway does not decrease the number of MVs[237]. In such conditions, the production of MVs can be induced by pro- and anti-inflammatory cytokines, IFN-γ and IL-4, independent of the purinergic receptor[237]. The modulation of the two systems of MVs release present differences, ATP is relatively rapid

to induce MVs release, while MVs formation mediated by cytokines require longer times[228,237]. In addition, MVs production via cytokines stimulation is abolished by the inhibitor of transcription, which does not occur in ATP mediated MVs shedding, suggesting that the cytokine effects are dependent on activation of transcriptional factors[237]. The two pathways may be coordinated during inflammation in neurodegenerative diseases, in which ATP and cytokines are recognized as important mediators[238,239].

Cells can release cytokines by direct secretion, however, the use of MVs to release IL-1β as well as other factors presents advantages, such as the wide distribution of the mediators to distant target cells, prevention scattering of factors in the extracellular space, and avoiding factors degradation[149]. Therefore, MVs biogenesis may represent a via through which microglia communicate with other cells and, at the same time, regulate their factors production modulating their cellular response.

In lipopolysaccharide (LPS)-induced reactive microglia released MVs carry IL-1β, in its pro and maturated form, accompanied by the inflammasome-caspase associated enzyme pro-caspase-1, responsible for the cytokine maturation[230,240]. Furthermore, reports described that exposure of naïve microglial cells to MVs released by LPS stimulation induced microglia activation in *vitro*[240]. In addition, those MVs were also capable of inducing an inflammatory response *in vivo*[240]. These small vesicles have the potential to propagate inflammation and contribute to disease progression. Interestingly, elevated levels of myeloid MVs were detected in the cerebrospinal fluid of multiple sclerosis patients[186], and the cerebrospinal fluid of experimental autoimmune encephalomyelitis multiple sclerosis model[186]. Additionally, the recruitment of inflammatory cells after injection of MVs into the brain was described in the experimental autoimmune encephalomyelitis model[186]. Moreover, MVs emerge as a new therapeutic target to control inflammation since, in a knock-out mouse for A-SMase, animals were protected from injury induced by experimental autoimmune encephalomyelitis due to impairment in MVs formation[186]. Furthermore, other mediators identified in MVs were also suggested as possible factors of inflammation. The presence of glutaminase, a mitochondrial enzyme specialized in glutamate *de novo* synthesis, was described in MVs shed from microglia. MVs from activated microglia cause glutamate neurotoxicity, since

glutaminase release mediated by MVs is increased upon microglia activation[241]. Neuronal injury and inflammation can be amplified by exorbitant levels of extracellular glutamate, therefore MVs appear as a potential pathway of neurotoxicity induced by glutamate in neurologic diseases. Additionally, increased levels of miR-200c in MVs derived from microglia subjected to oxygen-glucose deprivation-hypoxia/reoxygenation were reported[241]. The miR-200c is involved in cell survival, contributing to brain cell death during ischemic injury[242]. Additionally, the inhibition of miR-200c in MVs from microglia showed neuroprotective effects[243], indicating that miRNA carried in MVs are able to mediate biological responses.

A report showed that MVs released by microglial cells interact with neurons, enhancing excitatory neurotransmission[244]. Hippocampal neurons incubated with MVs shed by microglial cells increase the miniature excitatory postsynaptic current frequency, without causing alterations in its amplitude, boosting the release of synaptic vesicles at the presynaptic site[244], showing that MVs derived from microglia can modulate the synaptic activity. Assessment of the effects of microglia MVs in neuronal cultures revealed an increased production in ceramide and sphingosine from sphingomyelin, indicating that the neuronal response to MVs is due to stimulation of the sphingolipid metabolism[198,244]. These effects require direct interaction between MVs and neurons since in this case, the results do not depend on cytokine release. Moreover, the surface components of MVs are responsible for the modulation in neurotransmission, since MVs depleted of content, by sequential freeze and thaw, stimulate the neuronal response[244]. These data reveal that not only the content carried by MVs can trigger a biological response, but also the lipid fraction of shed MVs plays a role as active biomolecules in the cell-to-cell communication[245].

Proteomic analysis of untreated and ATP stimulated microglial cells revealed a substantial overlap between protein markers expressed in MVs and exosomes[246]. Vesicles derived from ATP activated microglial cells presented an abundant incidence of proteins related to cellular metabolism, such as glycolysis, lactate production, the oxidative branch of the pentose phosphate pathway, and fatty acid synthesis related proteins[246]. This study provides additional information on the microglia response to ATP and how MVs derived from microglia can impact cells metabolism.

Recent studies have shown the potential role played by MVs derived from microglia in the progression of neurodegenerative diseases. For example, in the cerebrospinal fluid of patients with Alzheimer's disease, the levels of microglial-derived MVs loaded with amyloid-β are increased. The release of these vesicles with neurotoxic potential is correlated with microglia activation and neuronal loss[247]. Furthermore, the release of MVs containing p-tau contributes to the dissemination of tau aggregates in Alzheimer's disease[248,249]. Moreover, reports described the capacity of activated microglia to modulate the synapses in neurodegeneration[250,251], however, the role of reactive microglial cells in synaptic dysfunction is uncertain. A recent study showed that activated microglia release vesicles enriched in miR-146a-5p that decrease the levels of synaptic proteins (presynaptic synaptotagmin-1 and postsynaptic neuroligin-1), and adhesion protein in receiver neurons, leading to synaptic dysregulation and dendric spine loss[221,252]. These findings demonstrate how microglial activation and MVs production can affect neuronal synaptic function, and their involvement in neuroinflammation and neurodegeneration in diseases, such as in multiple sclerosis.

More studies are needed to understand the contribution of MVs to inflammation and neurodegeneration. Nevertheless, MVs released by microglia are emerging as biomarkers from damage and neuroinflammation. Because microglial cells are the primary sensor cell to notify alterations within the microenvironment, the identification of MVs from microglia may indicate the conditions of the CNS. This feature of MVs roused the interest in these vesicles as markers of CNS distress signals and thereby for the study of pathologies to identify the early stages of diseases and the processes of communication between cells.

Aims

Glaucoma is a neurodegenerative disease characterized by RGC death and progressive optic nerve atrophy. Neuroinflammation contributes to retinal glaucomatous damage, and microglia and Müller cell response to retinal damage can influence the outcome of the inflammatory process. Microglial cells are known to release EVs that spread information to the receiver cells and upon interaction can modulate their response. However, how these cells communicate and their consequences during retinal inflammation are uncertain. We hypothesized that microglial-derived MVs interact with Müller cells, changing their response and influencing their phenotype under different culture conditions.

The main aim of this work was to assess how microglia-derived MVs can modify Müller cells in the context of glaucoma. To achieve this goal an *in vitro* model of EHP was used to mimic the increase in IOP. Microglia cells were exposed to EHP (+70 mmHg above atmospheric pressure), or atmospheric pressure (control) for 24h, MVs were collected and characterized. Müller cells were also exposed to EHP or control pressure for 24h. The levels of neurotrophic factors, inflammatory cytokines, and gliosis markers were evaluated after incubating Müller cell with MVs and EHP. Additionally, MVs were injected in the vitreous of C57BL/6J mice and their effects were analysed in the retina after 24h and 7 days by determining structure and thickness, microglia, and Müller cells reactivity, retinal cell death, and RGC survival.

In summary, this study aimed to elucidate the role of microglial-derived MVs in microglia-Müller cell communication in the context of elevated pressure.

Chapter 2

Material and Methods

2. Materials and Methods

2.1 Animals

All animals handled in this study were used in agreement with the statement of the Association for Research in Vision and Ophthalmology (ARVO) for the use of animals in vision and ophthalmology research, in accordance with the European Community directive guidelines for the use of animals in laboratory (2010/63/EU) transposed to the Portuguese law (Decree-Law nº 113/2013 of August 7 and Decree-law 1/2019 of January 10). All procedures involving animals were approved by the Animal Welfare Body of the Coimbra Institute for Clinical and Biomedical Research (ORBEA nº 23/2015 and nº 09/2017).

Eleven days old and 4-7 months old C57BL/6J mice were used in this study. Animals were housed under a controlled environment (27.0±2.5 °C of temperature and 15.2±11.9% of relative humidity, 12h-light/dark cycle) with free access to food and water.

2.2 BV-2 cell line

BV-2 cells (murine microglial cell line) were cultured in 175 cm^2 flasks, maintained at 37 °C in a humidified atmosphere of 5% CO_2 in Roswell Park Memorial Institute (RPMI; GIBCO, Invitrogen) medium, supplemented with heat-inactivated 10% fetal bovine serum (FBS; GIBCO, Invitrogen), 2 mM L-glutamine (GIBCO, Invitrogen) and antibiotics (100 U/mL penicillin, 100 μg/mL streptomycin; GIBCO, Invitrogen). Briefly, BV-2 cells were passed every two days by washing the cells in a fresh medium and shake the culture flask until cell detachment. The BV-2 cell suspension was centrifuged at 150 g for 5 minutes and the pellet was resuspended in culture medium. Cells were then added to a new flask or plated for experiments. Cells were used until passage 30.

For experiments, heat-inactivated FBS depleted of vesicles (Exo-free FBS) was previously prepared by ultracentrifugation at 25400 g for 16h at 4 °C. BV-2 cells were plated at 6.25 x 10^4 cells/cm^2 in 100 mm plates in RPMI supplemented with 2% Exo-free FBS, 2 mM L-glutamine, and antibiotics (100 U/mL penicillin, 100 μg/mL streptomycin), and cultured at 37 °C in a humidified atmosphere of 5% CO_2.

2.3 Primary Müller cell cultures

Müller cell cultures were prepared as previously described[253], with some modifications as follow. Mice with 11 days old were sacrificed by decapitation and the eyes were immediately removed, washed, and soaked in Dulbecco's Modified Eagle medium (DMEM) with Glutamax, (GIBCO, Invitrogen) supplemented with gentamicin (10 μg/mL; GIBCO, Invitrogen) overnight at room temperature (RT) protected from light[253,254]. The eyes were rinsed twice in phosphate-buffered saline (PBS, in mM: 137 NaCl, 2.7 KCl, 10 Na_2HPO_4, 1.8 KH_2PO_4; pH 7.4) and incubated with 0.05% trypsin (in 0.5 mM EDTA; GIBCO, Invitrogen) and collagenase (200 U/mL; GIBCO, Invitrogen) for 2h at 37 °C in a humidified atmosphere of 5% CO_2. Eyes were washed with low glucose DMEM (5.5 mM glucose; GIBCO, Invitrogen) supplemented with 10% FBS and antibiotics (100 U/mL penicillin, 100 μg/mL streptomycin), further referred in this section as medium. The retinas were dissected in medium and 6-10 retinas were transferred to 10 mm plates. The tissue was mechanically dissociated into small fragments and incubated for 3 days at 37 °C in a humidified atmosphere of 5% CO_2. Cell growth was observed, and at day 5 *in vitro* (DIV5), the cultures were washed with culture medium until only an adherent cell population remained attached to the plate. Cells became fully confluent after 8-10 days in culture. Cells were then washed with PBS and detached from plate with trypsin (0.05% trypsin in 0.5 mM EDTA) for 2-3 minutes at 37 °C in a humidified atmosphere of 5% CO_2. Medium was added to stop trypsinization, and the cell suspension was centrifuged at 800 g for 5 minutes. The supernatant was carefully discarded, and the pellet was resuspended in medium. Cells were cultured in 175 cm^2 flasks in DMEM and used until passage 5, as described previously[255].

For experiments, cells were plated at a density of 1.05 x 10^4 cells/cm^2 in 6-well plates or 5.3 x 10^3 cells/cm^2 in 24-well plates with glass coverslips, pre-coated with poly-L-lysine (0.1 mg/mL), in DMEM low glucose supplemented with 10% Exo-free FBS and antibiotics (100 U/mL penicillin, 100 μg/mL streptomycin), and cultured at 37 °C in a humidified atmosphere of 5% CO_2.

2.4 MIO-M1 cell line

The human Müller cell line Moorfields/Institute of Ophthalmology-Müller 1 (MIO-M1)[256] was cultured in 175 cm^2 flasks in DMEM with Glutamax, supplemented with heat-inactivated 10% FBS and antibiotics (100 U/mL penicillin, 100 μg/mL streptomycin) and maintained at 37 °C in a humidified atmosphere of 5% CO_2. When cell confluency was obtained, cells were washed with PBS, and 0.05% trypsin (in 0.02 mM EDTA; Sigma-Aldrich) was added for 2-3 minutes at 37 °C. The cell suspension was centrifuged for 5 minutes at 450 g. The supernatant was carefully discarded and the pellet was resuspended in culture medium. MIO-M1 cell suspension was then used for plating or added to a new flask. MIO-M1 cell line was passed usually once a week and used until passage 40.

For experiments, cells were plated at a density of 1.05 x 10^4 cells/cm^2 in 6-well plates or 1.32 x 10^4 cells/cm^2 in 24-well plates with glass coverslips, pre-coated with poly-L-lysine (0.1 mg/mL), in DMEM with Glutamax supplemented with 10% Exo-free FBS and antibiotics (100 U/mL penicillin, 100 μg/mL streptomycin), and cultured at 37 °C in a humidified atmosphere of 5% CO_2.

2.5 Cell treatment

BV-2 cells were incubated for 24h in a 37 °C incubator equipped with a custom-made pressure chamber (Figure 8), supplied with a pressure regulator and a gauge, which allowed to maintain a constant hydrostatic pressure of 70 mmHg above atmospheric pressure (EHP), achieved by injecting a mix of 95% air 5% CO_2 [115]. The selected conditions for elevated pressure induction were based on previous findings[95,180,257].

Additionally, BV-2 cells were maintained in a standard 5% CO_2 humidified incubator at atmospheric pressure (control condition).

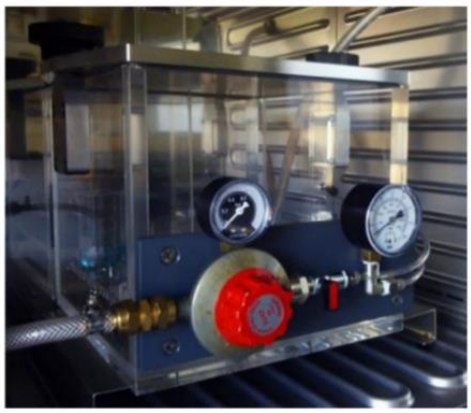

Figure 8 Customized pressure chamber inside a 37º C oven. The pressure chamber is equipped with a regulator to control the pressure.

2.6 Isolation of extracellular vesicles

BV-2 cell culture media were collected and centrifuged at 400 g for 10 minutes at 4 °C, and the supernatants were collected. The fraction of EVs corresponding to MVs was obtained from supernatants by low-speed ultracentrifugation at 16500 g for 20 minutes at 4 °C. The pelleted MVs were washed with sterile PBS and centrifuged for 20 minutes at 16500 g at 4 °C. The pellet was resuspended in sterile PBS. MVs collected from BV-2 cells incubated at atmospheric pressure (control) or challenged with EHP will be referred to as MV-CT and MV-EHP, respectively.

2.7 Nanoparticle tracking analysis

NTA was performed using a NanoSight NS300 instrument with a 488 nm laser and an sCMOS camera module (Malvern Panalytical Limited). The total of MVs samples was diluted in 1 mL of PBS and analysed following general instructions. A syringe pump with constant flow injection was used, and 5 videos of 1 minute were recorded for each sample with the camera level set at 12. Mean and estimated concentration for each particle size were obtained. All data were processed using NTA 3.3 analytical software (Malvern Panalytical Limited) with a Detection Threshold of 3.

2.8 Transmission electron microscopy

MVs were fixed with 4% paraformaldehyde (PFA) and prepared as previously described[258]. Briefly, Formvard-carbon coated grids (TAAB Laboratories) were used and MVs were washed with PBS and fixed with 1% glutaraldehyde for 5 minutes. Grids were washed with distilled water and contrasted with uranyl-oxalate (pH 7), for 5 minutes, and transferred to methyl-cellulose-uranyl acetate, for 10 minutes on ice. The preparations were observed in a Tecnai G2 Spirit BioTWIN electron microscope with analySIS 3.2 software (FEI).

2.9 Incubation with microvesicles

MIO-M1 cells (recipient cells) were incubated with MVs derived from BV-2 cells (donor cells) in the proportion of 1 donor cell to 1 recipient cell (MIO-M1 cells were incubated with the MVs derived from the same number of BV-2 cells). MIO-M1 cells were also challenged with EHP for 24h or cultured in normal pressure control.

2.10 Intravitreal injection

Four to seven months old C57BL/6J mice were anesthetized with 2.5% isoflurane in 1 L/min O_2 (IsoFlo; Abbott Laboratories). Topical anaesthesia (oxybuprocaine hydrochloride, Anestocil, 4 mg/mL, Edol) was used to anesthetize the ocular surface and the pupils were dilated with tropicamide (Tropicil Top, 10 mg/mL, Edol). BV-2 cells plated in six 100 mm plates per condition were used to isolate MVs in 100 μL of sterile PBS. In each eye, 3 μL of MVs suspension were injected in the vitreous using a 36G needle attached to an intraocular injection kit (NanoFil Application Kits, World Precision Instruments) coupled to a 10 μL syringe and an automated pump controlled with a footswitch (Micro4; World Precision Instruments). In each animal, one eye was injected with MV-CT and another eye with MV-EHP. A control animal group was defined by injecting 3 μL sterile PBS in one eye, and another eye was left untreated (naïve). Animals were randomly assigned to two time points (24h and 7 days post-injection).

2.11 Labelling of microvesicles

MVs were labelled with PKH67 Green Fluorescent Cell Linker Kit for General Cell Membrane Labelling (Sigma-Aldrich). Briefly, 50 μL of freshly isolated MVs were incubated with 1 μL of PKH67 for 5 minutes, in the dark previously prepared in 100 μL of diluent C. Samples were washed in sterile PBS and centrifuged for 20 minutes at 16500 g at 4 °C. The supernatant was gently discarded and MVs pellet was collected. The same procedure was performed in PBS to use as negative control.

2.11.1 Microvesicles interaction with MIO-M1

MIO-M1 cells, cultured at control pressure or exposed to EHP, were incubated for 1 or 2h with PKH67-labelled MVs that were previously diluted by ten-fold in DMEM with Glutamax. After, cells were washed in warm PBS and fixed for 10 minutes in 4% PFA with 4% sucrose. Coverslips were washed in PBS and permeabilized in 1% Triton X-100 in PBS for 5 minutes. Cells were incubated with phalloidin conjugated to Tetramethylrhodamine B isothiocyanate (TRITC; Sigma-Aldrich) (1:1000) and with the nuclear dye 4',6-diamidino-2-phenylindole (DAPI, 1:2000) for 30 minutes. Following washing with PBS, the preparations were mounted with fluorescent mounting medium (DAKO). Z-stack images (0.5 µm thickness) were acquired in a confocal microscope (LSM 710 Axio Observer Z1 microscope, QUASAR detection unit; ZEN Black 2010 software Carl Zeiss), using an EC Plan-Neofluar x40/1.30 Oil Dic M27 objective for phalloidin-stained cells, and a Plan Apochromat x63/1.40 Oil Dic M27 objective for preparations without phalloidin.

2.11.2 Interaction of microvesicles in the retina

Intravitreal injection of PKH67-labelled MVs was performed in 7 months old C57BL/6J mice, as previously described above. In the same animal, one eye was injected with PKH67-labelled MV-CT and the contralateral eye with PKH67-labelled MV-EHP. Animals injected with PKH67 in PBS in one eye and PBS alone in the contralateral eye were used as negative controls. After 24h, the animals were anesthetized with 2.5%

isoflurane in 1 L/min O_2 and sacrificed by decapitation. A suture was stitched to mark the upper eyelid and eyes were immediately removed and washed in PBS. A small incision was done in the cornea and the eyes were soaked overnight in 4% PFA. Then, retinas were removed from the eyecup, without losing eye orientation, and four cuts were made to allow the retinas to set flat (the deeper cut marked the superior part of the eye) in a glass slide. Once the tissue was flat, using a small piece of cellulose filter paper the retina was moved to a well where it was soaked for 1h in 4% PFA. Then, retinas were washed twice with PBS and incubated for 15 minutes with DAPI (1:2000). After three PBS washes, the retinas were mounted in mounting medium with the GCL facing up. MVs interaction with the retinas was observed in Z-stack images (0.5 µm thickness) captured in a confocal microscope (LSM 710 Axio Observer Z1 microscope, QUASAR detection unit; ZEN Black 2010 software Carl Zeiss) using Plan Apochromat x20/0.80 Oil DIC M27 objective. Additionally, whole-mounted retinal images were acquired with EC Plan-Neofluar x10/0.3 Ph1 M27 objective using an automated tile-scan imaging/stitching tool.

2.12 Preparation of vertical retinal sections

Animals were deeply anesthetized with an intraperitoneal injection of a solution of ketamine (80 mg/kg, Nimatek) and xylazine (5 mg/kg, Ronpum 2%) and then transcardially perfused with PBS followed by 4% PFA. A suture was stitched to mark the upper eyelid, the eyes were removed, and the cornea was punctured with a needle. Eyes were fixed for one additional hour in 4% PFA and then washed in PBS. For cryopreservation, the tissue was soaked in 15% sucrose in PBS for 1h followed by 30% sucrose in PBS overnight. The eyes were embedded in a tissue-freezing medium (Optimal Cutting Temperature, OCT; Shandon CryomatriX, Thermo Scientific) with 30% of sucrose in PBS (1:1), and stored at -80 °C. Retinal cryosections of 14 μm thickness were sectioned in a cryostat (Leica CM3050 S, Leica Biosystems) and mounted on Superfrost Plus glass slides (Menzel-Gläser, Thermo Scientific). Glass slides were stored at -20 °C until used.

2.13 Immunostaining

2.13.1 Immunocytochemistry

The cells plated on glass coverslips were washed with warm PBS and then fixed with 4% PFA with 4% sucrose for 10 minutes. Then, cultures were washed with PBS and permeabilized in 1% Triton X-100 in PBS for 5 minutes. After permeabilization, cells were blocked with 3% bovine serum albumin (BSA) and 0.2% Tween, in PBS, for 1h. Cultures were then incubated with the primary antibodies (Table 1) for 90 minutes at RT. Coverslips were washed with PBS and incubated with the corresponding secondary antibodies (see Table 1) for 1h at RT in the dark. Following incubation, cells were washed with PBS and incubated DAPI (1:2000) for 10 minutes. After a final wash with PBS coverslips were mounted with fluorescent mounting medium.

Table 1 List of primary and secondary antibodies used in immunocytochemistry.

	Supplier (Cat No)	**Host**	**Dilution**
Primary Antibodies			
Anti-Vimentin	Abcam (ab92547)	Rabbit	1:200
Anti-GS	Abcam (ab49873)		
Anti-EEAT1(GLAST)	Abcam (ab416)		1:100
Anti-NF-L	Cell Signalling Technology (2837)		1:200
Anti-NeuN	Abcam (ab128886)		1:250
Anti-β-III-Tubulin	Abcam (ab107216)	Chicken	1:500
Anti-CD11b	AbD Serotec (MCA275G)	Rat	1:200
Secondary antibodies			
Alexa Fluor 488 anti-rabbit IgG	Invitrogen (A21206)	Donkey	1:200
Alexa Fluor 568 anti-chicken IgG	Invitrogen (A11041)	Goat	
Alexa Fluor 568 anti-rat IgG	Invitrogen (A11077)		

2.13.2 Immunohistochemistry

The retinal sections were defrosted at RT overnight. The sections were fixed with cold acetone at -20 °C for 10 minutes, and then rehydrated in PBS until OCT

disappeared. A hydrophobic pen was used to limit the sections and the tissue was permeabilized with 0.25% Triton X-100 in PBS for 30 minutes and blocked in 10% normal goat serum and 1% BSA in PBS for 30 minutes at RT in a humidified environment. Then, the slides were washed with PBS and incubated overnight at 4 °C, in a humidified environment, with primary antibodies (Table 2) prepared in 1% BSA in PBS. The sections were immersed in PBS followed by incubation with the secondary antibodies (see Table 2) prepared in 1% BSA in PBS for 1h at RT, protected from light. The sections were washed with PBS and then incubated with DAPI (1:2000) for 10 minutes. Finally, the retinal sections were washed in PBS and mounted with a fluorescent mounting medium.

Table 2 List of primary and secondary antibodies used in immunohistochemistry.

	Supplier (Cat No)	**Host**	**Dilution**
Primary Antibodies			
Anti-GFAP	Millipore (AB5541)	Chicken	1:500
Anti-Brn3a	Millipore (MAB1585)	Mouse	
Anti-MHC-II	Abcam (ab139365)	Rat	
Anti-Iba1	Wako (019-19741)	Rabbit	1:1000
Secondary antibodies			
Alexa Fluor 488 anti-chicken IgG	Invitrogen (A11039)	Goat	1:500
Alexa Fluor 568 anti-mouse IgG	Invitrogen (A11004)		
Alexa Fluor 488 anti-rabbit IgG	Invitrogen (A11008)		
Alexa Fluor 568 anti-rat IgG	Invitrogen (A11077)		

2.14 Phagocytosis assay

First, to assess the ideal conditions for the evaluation of the phagocytic capacity of Müller cells, MIO-M1 cells were incubated for 1h, 2h, and 24h with 0.0025% and 0.005% of fluorescent latex beads. In the following experiments, MIO-M1 cells were incubated with 0.0025% fluorescent latex beads (1 μm diameter, Sigma-Aldrich) for 2h prior to the end of the experiment. Then, cultures were fixed with 4% PFA with 4% sucrose, washed with PBS, and permeabilized and blocked as previously described. Cells were stained with phalloidin (1:500) for 30 minutes, followed by a washing step with

PBS, and incubated with DAPI (1:2000) for 10 minutes. Coverslips were mounted with fluorescent mounting medium. Images of the preparations were acquired in an inverted fluorescence microscope (Zeiss Axio Observer.Z1 microscope equipped with an AxioCam HRm and Zen Blue 2012 software, Carl Zeiss) with a Plan Achromat x20/0.8 objective. From each condition, 10 random fields were acquired, and the number of phagocytized beads by each cell was counted as well as the number of cells with incorporated beads. Finally, the phagocytic efficiency (%) was calculated as described[259]:

$$Phagocytic\ efficiency = \frac{1 \times 1x + 2 \times 2x + 3 \times 3x + \cdots + n \times nx}{total\ number\ of\ cells} \times 100$$

nx represents the number of cells containing n microspheres ($n = 1,2,3, \ldots$ up to a maximum of 6 points for more than 5 beads ingested per cell).

2.15 Terminal deoxynucleotidyl transferase (TdT)-mediated dUTP nick end labelling (TUNEL) assay

Cell death was detected with DeadEnd™ Fluorometric TUNEL system following the instructions provided by the manufacture (Promega). Briefly, coverslips and cryosections were fixed and permeabilized as described above. The preparations were washed twice in PBS and incubated with equilibration buffer (200 mM potassium cacodylate, 25 mM Tris-HCl, 0.2 mM DTT, 0.25 mg/mL BSA and 2.5 mM cobalt chloride) for 10 minutes. Then, cultures and retinal sections were incubated with the recombinant TdT enzyme and with nucleotide mix containing dUTP conjugated to fluorescein at 37 °C for 1h. To stop the reaction, the preparations were immersed in saline-citrate buffer (175 g/L NaCl, 88.1 g/L sodium citrate) for 15 minutes at RT, followed by three washes with PBS for 5 minutes. Next, slides were incubated with DAPI (1:2000) and cultures were labelled with phalloidin (1:500) and DAPI. The preparations were mounted with a fluorescent mounting medium. In cell cultures, ten random fields were acquired for each condition. In retinal cryosections, four sections were acquired per eye then the total length of the retina and the total number of $TUNEL^+$ cells was normalized to the length of the section per image.

2.16 Preparation of protein extracts

Cells were washed with PBS and collected in ice-cold radioimmunoprecipitation assay (RIPA) buffer with 1 mM of DTT (Sigma-Aldrich) and complete mini protease inhibitor cocktail tablets (Roche Diagnostics). After, cell lysates were sonicated and centrifuged at 16100 g for 10 minutes at 4 ºC. Pellets were discarded, and the supernatants were immediately stored at -80 ºC.

Retinal lysates were prepared from eyes that were immediately removed from anesthetized animals with 2.5% isoflurane in 1 L/min O_2 and sacrificed by decapitation. The eyes were placed in ice-cold PBS and the retinas were dissected. The tissue was lysed in RIPA buffer with DTT and complete mini protease inhibitor cocktail tablets, sonicated and centrifuged, as described above. The supernatant was collected and stored at -80 ºC.

2.17 Bicinchoninic acid (BCA) assay

Quantification of total protein of protein extracts was performed using the BCA protein assay kit (Sigma-Aldrich), following the instructions supplied by the manufacture using known protein concentrations of BSA to obtain a standard curve. Then, in a 96-well plate, 25 μL of diluted samples were incubated with the provided BCA regent, for 30 minutes at 37 ºC in the dark. The absorbance at 570 nm was read in a microplate reader (Gen5 software, Synergy HT, BioTek Instruments).

2.18 Cytokine antibody array

A human cytokine array was used to simultaneous detect multiple cytokines, following the instructions provided by the manufacture (Abcam). All washes and incubations were performed under gentle rotation (60 rpm). Membranes were blocked in 1x blocking buffer at RT for 30 minutes and then incubated with the samples (300 μg of MIO-M1 lysates collected in provided cell lysis buffer) overnight at 4 ºC. Then, membranes were washed for 45 minutes at RT with wash buffer 1. After, serial washes with wash buffers 1 and 2 at RT (5 minutes each), membranes were incubated with 1x

Biotin-Conjugated Anti Cytokines overnight at 4 ℃. Following incubation, serial washes were performed as previously described, and 1x Horseradish peroxidase (HRP)-Conjugated Streptavidin was incubated overnight at 4 ℃. Serial washes were repeated, and the membranes were prepared for chemiluminescence detection. Finally, membranes were incubated for 2 minutes with the detection mix (equal volumes of detection buffer C and detection buffer D) at RT. ImageQuant LAS500 equipped with a CCD camera was used to detect chemiluminescence.

2.19 Western blot

Protein extracts were denaturated with 6x Sample Buffer 6x (0.5 M Tris, 30% glycerol, 10% SDS, 0.6 M DTT, 0.012% Bromophenol Blue) and heated for 5 minutes at 95 ℃. Equal amounts of protein were loaded into the gel, except for MVs samples of which the entire volume was loaded. Proteins were separated by 8-15% sodium dodecyl sulphate-polyacrylamide gel electrophoresis (SDS-PAGE) and transferred onto PVDF membranes (Millipore). Next, membranes were blocked with 5% low-fat milk in Tris-buffered saline (TBS-T, 137 mM NaCl, 20 mM Tris-HCl, pH 7.6 containing 0.1% Tween-20) for 1h at RT, and incubated overnight at 4 ℃ with primary antibodies (Table 3). Membranes were then washed three times with TBS-T, followed by incubation with the corresponding secondary antibodies (see Table 3) for 1h at RT. After final washes, protein detection was performed using enhanced chemiluminescence (ECL) (Clarity; Bio-Rad and WesternBright Sirius; Advansta) or enhanced chemifluorescence with ECF (GE Healthcare). Luminescence was detected in LAS550 and fluorescence in Typhoon FLA 9000 (GE Healthcare).

Table 3 List of primary and secondary antibodies used in WB.

	Supplier (Cat No)	Host	Dilution
Primary Antibodies			
Anti-Flotillin 1	BD Transduction Laboratories™ (610821)	Mouse	1:1000
Anti-GFAP	Millipore (IF03L)	Mouse	1:500
Anti-GS	Abcam (ab49873)	Rabbit	1:1000
Anti-Vimentin	Millipore (V5255)	Mouse	1:500
Anti-iNOS	Abcam (ab178945)	Rabbit	1:1000
Anti-IL-1β	Abcam (ab9722)	Rabbit	1:1000
Anti-LIF	Abcam (ab113262)	Rabbit	1:500
Anti-BDNF	Abcam (ab108319)	Rabbit	1:1000
Anti-GFAP	Millipore (G9269)	Rabbit	1:1000
Anti-GS	Santa Cruz Biotechnology (sc-74430)	Mouse	1:1000
Anti-TSPO	Abcam (ab109497)	Rabbit	1:1000
Anti-IL-1β	R&D Systems (AB-401-NA)	Mouse	1:500
Anti-Calnexin	SICGEN (AB0041-500)	Goat	1:10000
Secondary antibodies			
Anti-goat IgG, Alkaline phosphatas (AP)	Invitrogen (31-300)	Rabbit	1:10000
Anti-mouse IgG, AP	Millipore (A3562)	Goat	1:10000
Anti-mouse IgG, HRP	Invitrogen (A16072)	Goat	1:10000
Anti-Rabbit IgG, HRP	Invitrogen (A16104)	Goat	1:10000

2.20 Optical coherence tomography (OCT)

The structure and thickness of the retina were evaluated with Spectrum Domain (SD)-OCT (coupled to a Phoenix Micron IV Retinal Imaging Microscope, Phoenix Technology). Animals were anesthetized with an intraperitoneal injection of ketamine and xylazine (80 mg/kg and 5 mg/kg, respectively). Topical anaesthesia was applied to anesthetize the ocular surface and the pupils were dilated with tropicamide. Additionally,

carmellose sodium (Celluvisc, Allergan) was used to hydrate the cornea during the acquisition. OCT was performed at 24h and 7 days after MVs intravitreal injection. A SD-OCT system was used to capture B-scans of the retina. The first image was focused on the centre of the eye fundus and scans were acquired above and below the optical nerve head. For each eye, 5 images were analysed, two images above and two images bellow the optic nerve and one of the optic nerve[260]. Total retinal thickness was measured from the GCL to the RPE using Insight (Phoenix Technology).

The OCT scan images were used to quantify the presence of cell infiltrates in the vitreous using ImageJ software, similar to what was described previously[7], with some modifications as follows. The Max Entropy auto-thresholding macro was applied to the OCT scan images and the region of interest in each image was defined as the vitreous cavity visible. Vitreous infiltration score (VIS) was calculated using the following formula:

$$VIS = Integrated\ density - (area\ of\ selected\ cell \times mean\ of\ background\ reading)$$

2.21 Fluorescein angiography

Animals were deeply anesthetized with an intraperitoneal injection of ketamine and xylazine (80 mg/kg and 5 mg/kg, respectively). Topical anaesthesia was used to anesthetize the ocular surface and the pupils were dilated with tropicamide. Additionally, carmellose sodium (Celluvisc) was used to hydrate the cornea during the acquisition. Fluorescein angiography images were captured with the Micron IV Retinal Imaging Microscope, immediately after animals were intraperitoneally injected with 5% fluorescein (100 mg/mL, Serb Laboratories) and until saturation was achieved[260]. For this reason, only one eye per animal was analysed. Fluorescein angiography was performed to assess the effect of MVs interaction on vascular leakage. Only the timepoint of 24h was performed. The presence of leaky areas was evaluated in the acquired coded images, then images were graded by a researcher blinded to the experimental condition.

2.22 Statistical analysis

GraphPad Prism® 7.0 software was used for the statistical analysis of results. Graphics are presented as mean±standard error of the mean (SEM). The normal distribution of the data was analysed by the Shapiro-Wilk normality test. Data with normal distribution were analysed with parametric tests and data with non-gaussian distribution was analysed with non-parametric tests, as indicated in the figure legends. Statistical significance was considered for P value of < 0.05.

Chapter 3

Results

3. Results

In this study, we aimed to investigate the effects of microglia-derived MVs in Müller cells, using MIO-M1 cells (human Müller cell line) and an animal model.

MVs from microglial cells were derived from the BV-2 murine microglia cell line previously exposed to EHP (MV-EHP) or from atmospheric pressure conditions (MV-CT) for 24h. MIO-M1 cells were cultured at atmospheric pressure or EHP for 24h in the presence or absence of MVs. In addition, MVs were injected in the vitreous of C57BL/6J mice and their effects were assessed after 24h and 7 days of injection.

3.1 Characterization of Müller cell cultures

In this study, primary Müller cell cultures were established in the laboratory. First, the purity of the primary cultures was assessed by immunolabeling for the presence of Müller cell, neuronal and microglial cell markers. No labelling was observed for the neuronal markers neurofilament-L (NF-L) and neuronal nuclear protein (NeuN, Figure 9A), indicating that neurons are not present in the culture. Interestingly, primary Müller cells presented a weak expression of β-III-tubulin (β-III-tub), usually regarded as a neuronal marker (Figure 9A). Previous studies reported the expression of neuronal or ganglion cell-specific markers in Müller cells after injury (β-III tub, Thy-1 cell surface antigen, transcription factor Brn3.0, and neurotransmitter markers[261–265]). In addition, the β-III tub was also described to be constitutively expressed in fetal astrocytes of the human brain[266], and Müller cell lines, including MIO-M1 cells[267]. Additionally, the antibody for the CD11b (Figure 9A), a microglial marker, did not label cells, suggesting that microglia are not present in the culture. Müller cell cultures expressed specific proteins of Müller cell, such as, vimentin and GS (Figure 9B). These results, together with the fact that all cells in culture expressed vimentin, show that the cultures of primary Müller cells derived from post-natal mice are pure, express the selective markers and present a morphology compatible with Müller cells.

Taking the fact that the preparation of the primary cultures of Müller cells is expensive, laborious, and time-consuming, the decision was made to proceed with MIO-M1 cells, despite the fact that cells lines pose several disadvantages[268]. The human Müller

cell line MIO-M1 also expressed vimentin, GS, and GLAST (Figure 10), as previously described by others[256,269]. These cells have previously been used to explore the role of Müller cells in retinal diseases[270–273].

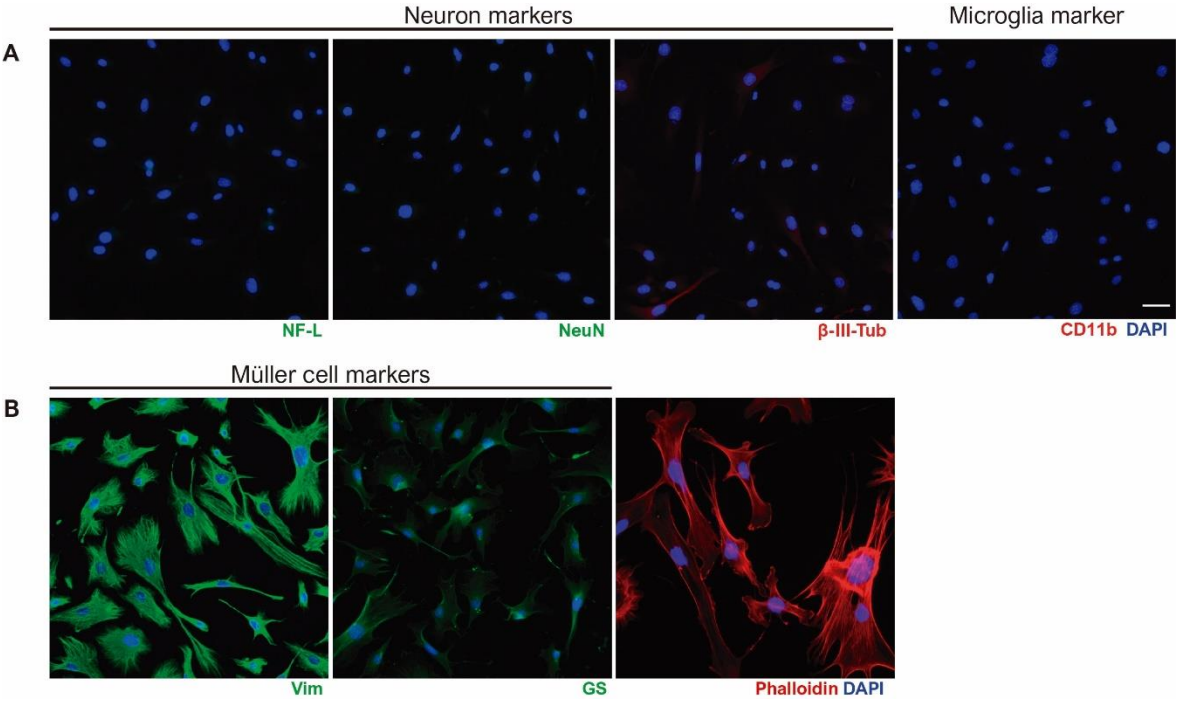

Figure 9 Evaluation of the purity of mouse primary Müller cell cultures. A. Expression of neuron markers, Neurofilament-L (NF-L; green), neuronal nuclear protein (NeuN; green) and β-III-tubulin (β-III-Tub; red), and microglia marker, cluster of differentiation 11b (CD11b; red) in Müller cell primary cultures. **B.** Expression of Müller cell markers (green): vimentin (Vim), glutamine synthetase (GS). Cell morphology was observed by staining actin filaments with phalloidin (red). Nuclei were stained with DAPI (blue). Scale bar: 50 μm.

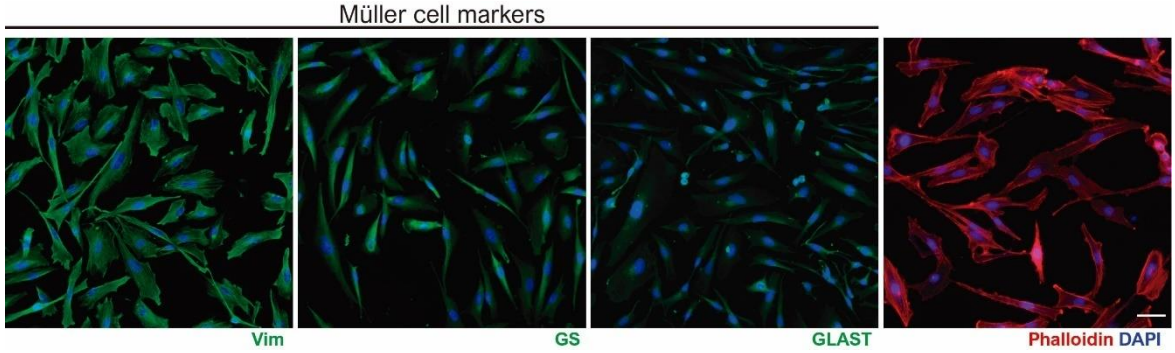

Figure 10 Expression of Müller cell markers in MIO-M1 cell line. Representative images of MIO-M1 cells labelled for vimentin (Vim), glutamine synthetase (GS), and glutamate aspartate transporter 1 (GLAST) (green). Actin filaments were stained with phalloidin (red). Nuclei were stained with DAPI (blue). Scale bar: 50 μm.

3.2 Characterization of extracellular vesicles released by BV-2 cells

BV-2 cells were exposed to EHP or kept at atmospheric pressure and the released EVs were collected from supernatant. EVs collected at low-speed ultracentrifugation were characterized in number, size, and presence of protein markers characteristic of MVs (Figure 11). NTA was performed to determine the size distribution of particles in suspension. The collected EVs presented an average size of 196.4±4.9 nm and 218.2±6.1 nm, respectively, for the control and EHP conditions (Figure 11A), consistent with the range size of MVs[143]. The concentration of MVs released in cells exposed to EHP ($9.32x10^8 \pm 4.1x10^7$ particles/mL, n=3) were not significantly different from control condition ($7.6x10^8 \pm 4.4x10^7$ particles/mL, n=3, Figure 11A). TEM was used to image the particles (Figure11B) that presented size similar to the results obtained by NTA and morphology compatible with EVs. The protein flotillin-1, present in lipid rafts during vesicle formation, has been used as a protein marker of exosomes[144], but it is also present in MVs[201]. In the protein extracts obtained from vesicles suspension, flotillin-1 was detected in both conditions, MV-CT and MV-EHP (Figure 11C). The endoplasmic reticulum protein calnexin is enriched in cellular extracts and was detected in the extracts from extracellular vesicles, which was already reported by others[163,274,275] (Figure 11C). Taking into account these results, the isolated fraction of EVs was characterized as MVs, and this nomenclature will be used subsequently.

3.3 Microvesicles derived from BV-2 cells interacted with MIO-M1 cells

Since the main hypothesis of this work is that MVs derived from microglial cells may change the phenotype of Müller cells, the effects of MVs derived from BV-2 cells in MIO-M1 cells were addressed. Firstly, to evaluate whether MVs obtained from BV-2 cells interacted with MIO-M1 cells, MV-CT and MV-EHP were labelled with the lipophilic dye PKH67 following incubation with MIO-M1 cells, for 1h or 2h (Figure 12A, n=1). The presence of green puncta inside the cells indicated that PKH67-labelled MVs, from both conditions, were internalized by MIO-M1 cells. With time, PKH67 staining inside the cells increased, as well as the number of cells stained (Figure 12A). Moreover, MIO-M1 cells were incubated with PKH67-labelled MV-CT and MV-EHP for 2h under EHP or atmospheric pressure and stained with phalloidin to allow better visualization of the

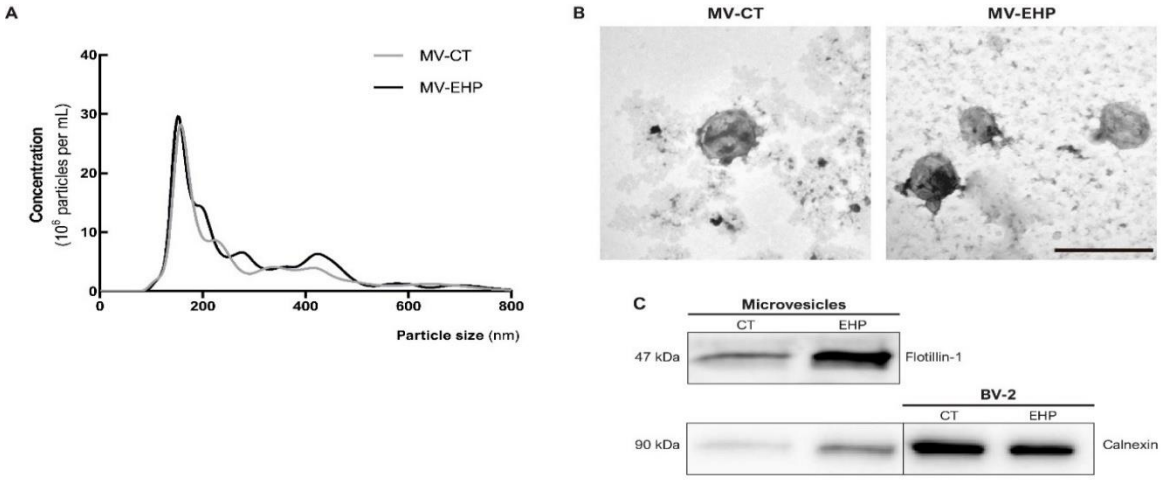

Figure 11 Characterization of extracellular vesicles collected by low speed-ultracentrifugation released by BV-2 cells. EVs were isolated from supernatants of microglial cells (BV-2 cell line) after exposure to EHP or atmospheric pressure. **A.** The size distribution and concentration of particles in vesicle suspensions were analysed by NTA. The presented graph is representative of 3 independent experiments. **B.** Vesicles were imaged by TEM and the depicted images are representative of 2 independent experiments. Scale bar: 1000 nm. **C.** The presence of Flotillin-1 and calnexin were analysed by WB.

cells morphology (Figure 12B, n=1). Results show that under elevated pressure MIO-M1 cells also internalize MVs. Interestingly, fewer PKH-67 labelled particles were observed inside the cells after phalloidin staining, suggesting that the protocol for phalloidin staining may affect PKH67 observation. The negative controls (PBS plus PKH67 and PBS alone) did not present any considerable labelling (Figure 12A and B).

3.4 Effect of BV-2 microvesicles and EHP in the death of Müller cells

MIO-M1 cells were incubated with MVs derived from BV-2 cells, MV-CT, and MV-EHP, and exposed to atmospheric pressure or EHP for 24h. Cell death was assessed by TUNEL assay (Figure 13A). In EHP conditions, $TUNEL^+$ cells were 138.1±68.65% of control, n=3 (Figure 13B). The incubation of MIO-M1 cells with MV-CT decreased the number of $TUNEL^+$ cells either in EHP or control conditions (40.26±20.46% and 57.31±11.6% of control, MV-CT under atmospheric pressure or MV-CT under EHP, respectively, n=3, Figure 13B), suggesting that MVs obtained from control BV-2 cells improve the survival of MIO-M1 cells. Incubation with MV-EHP in normal pressure did

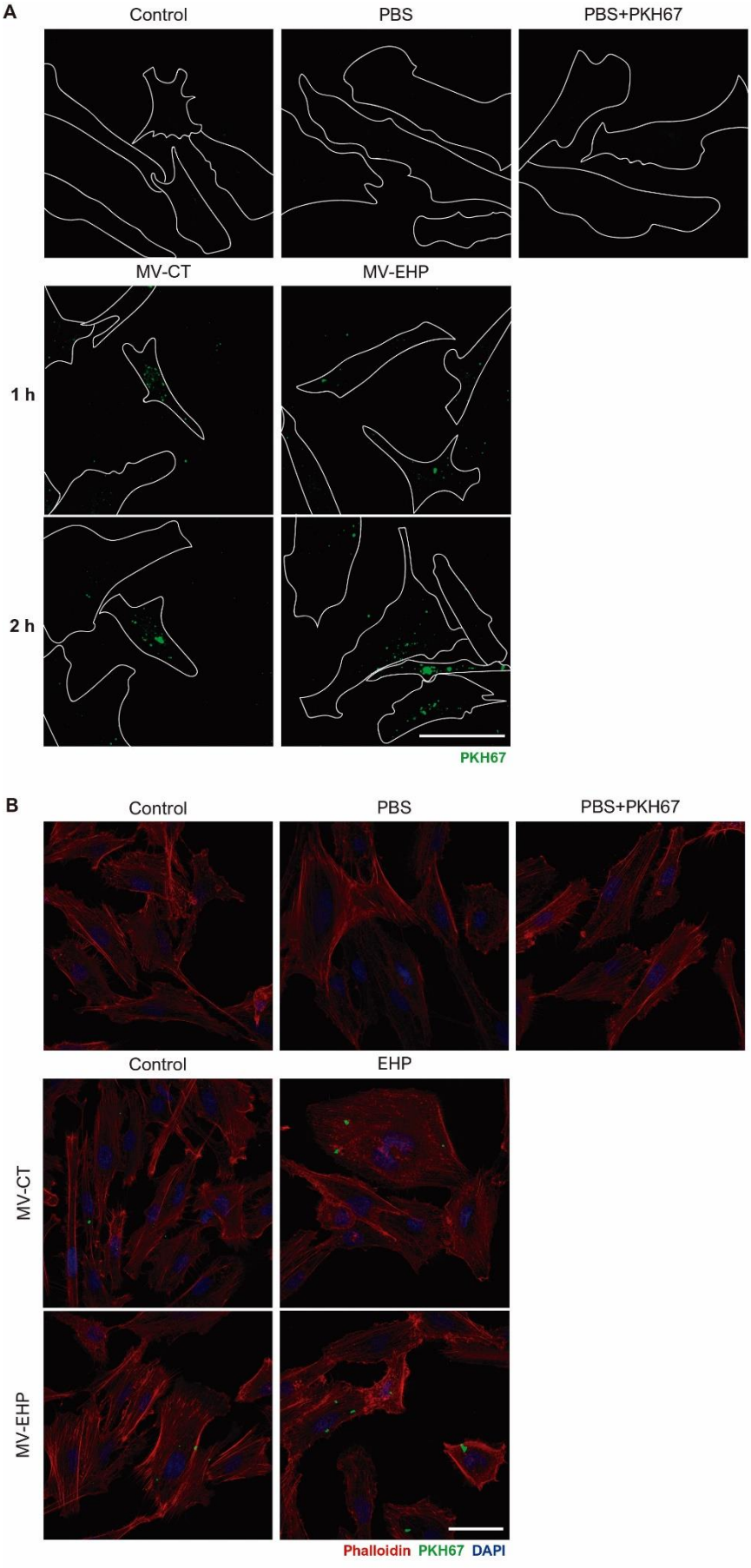

Figure 12 MVs derived from BV-2 cells interact with MIO-M1 cells. A. Representative images of the interaction between PKH67-labelled MVs (green) and MIO-M1 cells were observed after 1h and 2h of incubation. Images were acquired in light transmission and the border of the plasma membrane was outlined with a white line using Adobe Illustrator. **B.** Representative images of the interaction of PKH67-labelled MVs and MIO-M1 cells after 2h of incubation under atmospheric or EHP conditions. MIO-M1 cells were labelled with phalloidin (red) and nuclei were stained with DAPI (blue). Scale bar: 50 μm.

not significantly change cell death (97.38±41.45% of the control, n=3). Additionally, the incubation of MIO-M1 cells with MV-EHP during EHP did not significantly alter cell death (204.7±75.55% of control, n=3 Figure 13B).

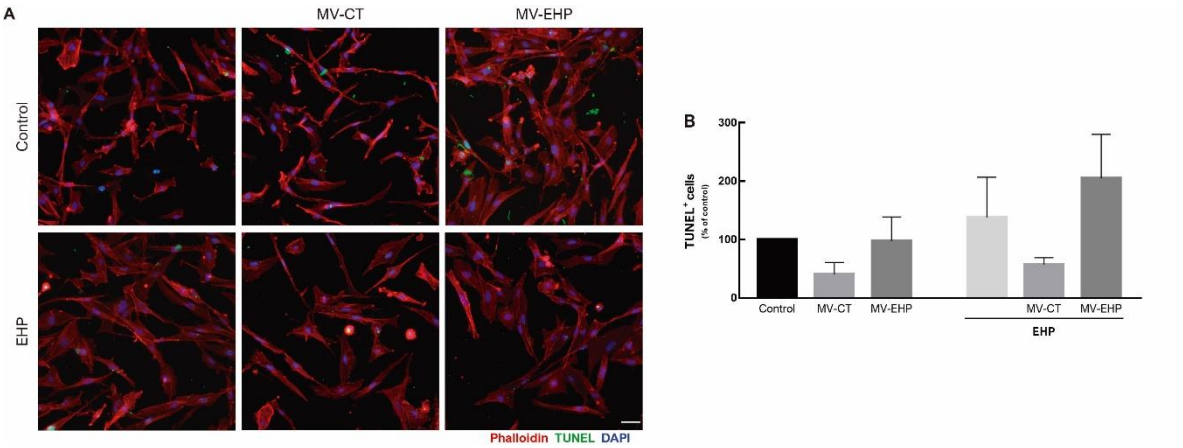

Figure 13 Effect of MVs and EHP exposure in cell death of Müller cells. A. MIO-M1 cells were incubated with MV-CT and MV-EHP under atmospheric or EHP for 24h and cell death was evaluated by TUNEL assay (green). Müller cells were stained with phalloidin (red). Nuclei were counterstained with DAPI (blue). Representative images are depicted **B.** The number of TUNEL$^+$ cells was normalized to the total number of cells (DAPI$^+$ cells) and the results are presented as percentage of control. Results were obtained from 3 independent experiments, performed in duplicate. Scale bar: 50 μm.

3.5 Effect of EHP and microglia-derived microvesicles in Müller cell gliosis

The expression levels of proteins involved in Müller cell gliosis were quantified by WB in protein extracts from MIO-M1 cells incubated with MVs derived from BV-2 cells (MV-CT and MV-EHP) and exposed to EHP or control pressure for 24h. Müller cell gliosis is characterized by the increase in the expression of the intermediate filaments of the cytoskeleton GFAP and vimentin and a decrease in the glutamate recycling enzyme GS[48]. The incubation of MIO-M1 cells for 24h with either MV-CT or MV-EHP did not cause major changes in the protein levels of GFAP (n=4, Figure 14A), vimentin (n=5, Figure 14B), and GS (n=6, Figure 14C). Also, the exposure of MIO-M1 cells to EHP for 24h did not cause Müller cell reactivity. Additionally, GFAP, vimentin, and GS levels were not altered upon the exposure of MIO-M1 cells to EHP in the presence of MV-CT (n=4) and MV-EHP (n=4, Figure 14).

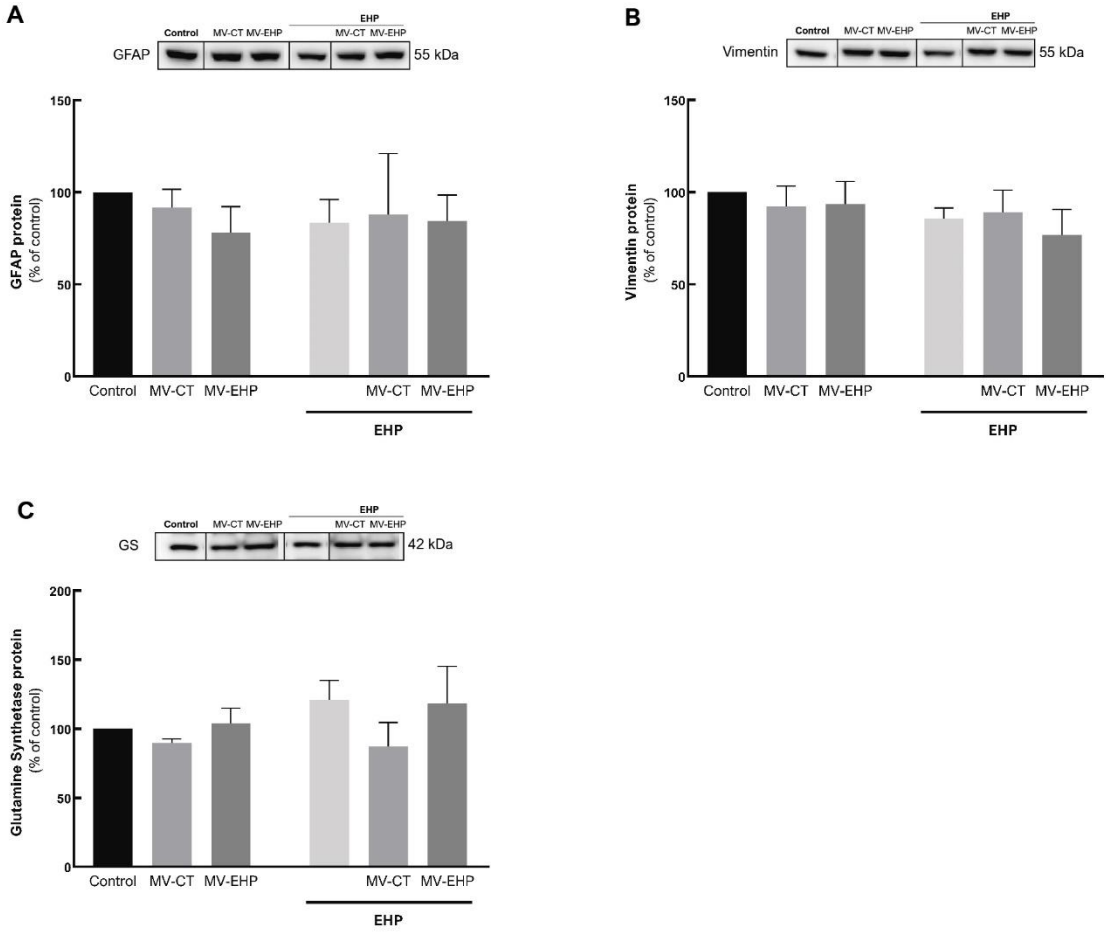

Figure 14 Effect of EHP and MVs derived from microglia in Müller cell gliosis. MIO-M1 cells were incubated with MV-CT and MV-EHP and cultured in normal pressure or exposed to EHP for 24h. Protein lysates were assayed for GFAP (**A**), vimentin (**B**), and GS (**C**). The results were normalized to control (performed in duplicate) and presented as percentage of control. Results were obtained from 4 to 6 independent experiments.

3.6 Effect of EHP and microvesicles derived from BV-2 cells in the inflammatory response of MIO-M1 cells

The effect of MV-CT and MV-EHP in the inflammatory profile of MIO-M1 cells was evaluated by WB, assessing the protein levels of iNOS, a biomarker of inflammation. iNOS levels did not significantly change when MIO-M1 cells were exposed to MV-CT and MV-EHP at atmospheric pressure (n=6, Figure 15). There was a tendency to a decrease in the protein levels of iNOS when the cells were exposed to EHP (n=6) and in the presence of MV-EHP (n=6, Figure 15). Moreover, the incubation with MV-CT under

EHP caused a significant decrease in iNOS levels (38.6±8.70% of control, n=6, Figure 15).

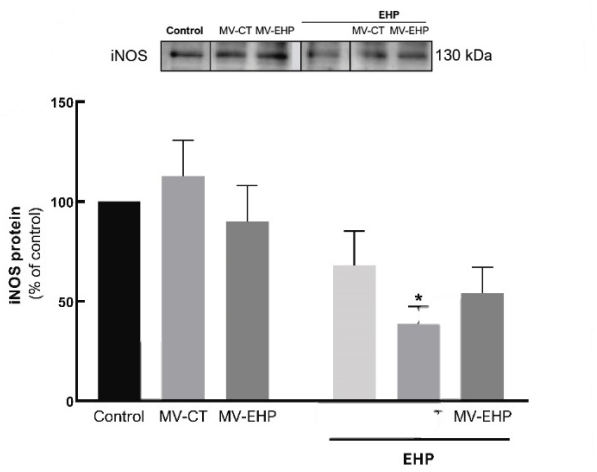

Figure 15 Effect of MVs derived from microglia under EHP and normal conditions in the inflammatory response of MIO-M1 cells. MIO-M1 cells were incubated with MV-CT and MV-EHP and cultured in normal pressure or exposed to EHP for 24h. Protein lysates were assayed for iNOS levels. The results were normalized to control (performed in duplicate) and presented as percentage of control. Results were obtained from 6 independent experiments. *p<0.05, compared with control, Kruskal–Wallis test followed by Dunn's multiple comparison test.

3.7 Effect of EHP and microvesicles derived from BV-2 in the soluble factors release by MIO-M1 cells

After, MIO-M1 cells MVs incubation under EHP and atmospheric pressure for 24h the release of soluble factors was evaluated by WB. No significant changes were observed in the protein levels of LIF, BDNF, and pro-IL-1β in MIO-M1 cells after MVs incubation under both pressure conditions, as well as under EHP alone (Figure 16). The incubation of MIO-M1 cells with MVs did not cause significant alterations in the protein levels of LIF (n=3, Figure 16A). Similarly, either EHP alone (n=3) or MVs incubation under pressure (n=1, Figure 16A) did not alter LIF expression by MIO-M1 cells. Additionally, MVs incubation and EHP alone did not alter the expression levels of BDNF by MIO-M1 cells (n=4, Figure 16B). MVs incubation under EHP tented to decrease BDNF levels in MIO-M1 cells (n=2, Figure 16B). No statistical differences in the protein levels of pro-IL-1β were found in MIO-M1 cells incubated with MVs under control pressure (n=4,

Figure 16C). Similarly, under EHP the results did not show significant difference in pro-IL-1β levels, either with EHP alone (n=4) or when MVs were added (n=4, Figure 16C).

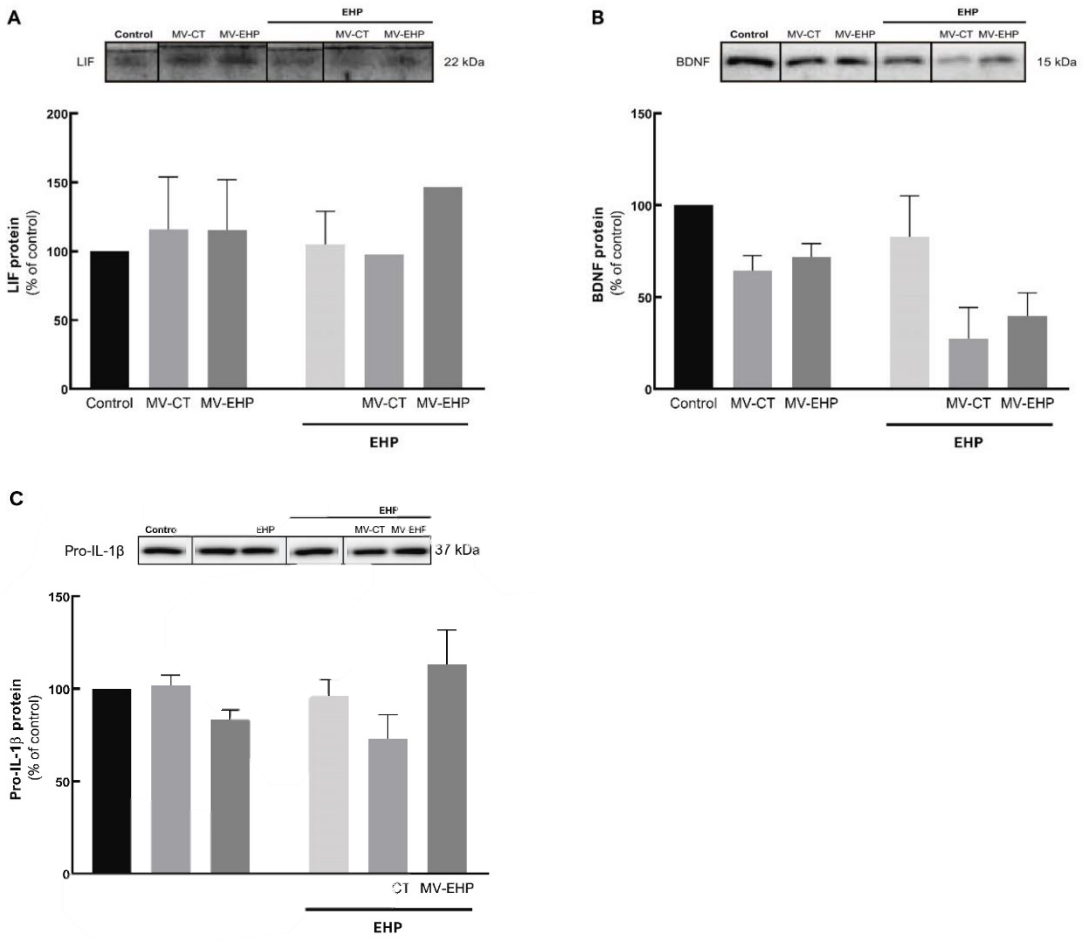

Figure 16 Effect of MVs derived from microglia under EHP and normal conditions in soluble factors protein levels. MIO-M1 cells were incubated with MV-CT and MV-EHP and cultured in normal pressure or exposed to EHP for 24h. Protein levels of LIF (**A**), BDNF (**B**), and BDNF (**C**) were assessed by WB. The results were normalized to control (performed in duplicate) and presented as percentage of control. Results were obtained from 1 to 4 independent experiments.

3.8 Effect of EHP and microvesicles derived from BV-2 in cytokine and trophic factors expression in MIO-M1 cells

To better characterize the phenotype of MIO-M1 cells upon incubation with BV-2 MVs and EHP, a cytokine array was performed to have a broader spectrum of factors analysed. The analysis was made using samples of MIO-M1 cell lysates pooled from 4

different conditions (n=1) to evaluate the levels of chemokines, growth factors, and cytokines (Table 4). The expression of these factors by MIO-M1 cells in each experimental condition was normalized to the expression levels in cells incubated in control conditions.

Table 4 Cytokine antibody array for MIO-M1 protein extracts after exposure to EHP, MV-CT, and MV-EHP.

	EHP	MV-CT	MV-EHP
Chemokines			
I-309	6,16	0,9	0,43
MCP-1	1,43	1	0,9
MIP-1b	1,17	0,83	0,69
RANTES	1,99	0,5	0,52
MCP-2	1,17	0,25	0,29
MCP-3	1,3	0,35	0,63
Eotaxin	0,81	0,21	0,47
MCP-4	0,55	0,11	0,11
TARC	1,29	0,56	0,47
MDC	1,55	0,44	0,93
Ckβ 1-8	0,55	0,23	0,47
Eotaxin-2	1,42	0,15	0,7
GRO	3,36	1,92	3,42
GRO-α	12,85	1,6	3,42
Fractalkine	0,48	0,4	0,45
ENA-78	1,21	1,07	1,36
GCP-2	0,98	0,58	0,81
NAP-2	1,79	0,11	0,36
MIG	2,14	1,21	1,21
IP-10	0,61	0,19	0,63
SDF-1	1,54	0,54	0,32
BLC	0,55	0,38	0,52
Growth factors			
GM-CSF	1,01	0,51	0,68
TGF-β1	0,97	0,29	0,32
TGF-β2	0,69	0,35	0,26
TGF-β3	0,27	0,25	0,19
EGF	1,2	0,54	0,82

>5
1.6 - 5
1.4 - 1.6
1.2 - 1.4
1 - 1.2
0.8 - 1
0.6 - 0.8
0.4 - 0.6
<0.6

IGF-1	1,52	0,53	0,74
VEGF	1,94	0,56	0,28
PDGF-BB	1,6	0,58	0,37
BDNF	0,87	0,53	0,58
FGF-4	6,78	1,16	1,32
FGF-6	1,92	0,56	0,43
FGF-7	1,79	0,42	0,4
FGF-9	0,95	0,41	0,43
GDNF	0,55	0,28	0,41
HGF	0,72	0,04	0,25
IGFBP-1	1,07	0,14	0,49
IGFBP-2	1,35	0,85	0,97
IGFBP-3	1,93	0,1	0,17
IGFBP-4	20,53	3,94	4,9
NT-3	1,33	0,26	0,36
Thrombopoietin	3,03	0,59	0,45
TNF superfamily			
TNF-α	0,79	0,5	0,67
TNF-β	0,75	0,47	0,73
LIGHT	0,64	0,37	0,37
Pro-inflammatory cytokines			
IL-1α	1,61	0,38	0,14
IL-1β	1,02	0,37	0,3
IL-2	1	0,34	0,26
IL-3	1,03	0,25	0,25
IL-6	0,62	0,42	1,47
IL-7	3,53	0,47	2,38
IL-8	1,24	1,21	1,54
IL-12 p40/p70	6,76	2,97	3,87
IL-15	1,33	0,46	0,38
IL-16	0,93	0,38	0,66
IFN-γ	1,14	0,41	0,34
SCF	1,97	0,59	0,4
Oncostatin M	4,48	0,97	1,24
Leptin	1,15	0,59	0,5
Flt3L	0,76	0,42	0,43
LIF	0,77	0,26	0,35

MIF	0,82	0,72	0,72
Osteopontin	1,24	4,59	4,19
Anti-inflammatory cytokines			
IL-4	0,89	0,37	0,42
IL-5	0,98	0,2	0,26
IL-13	2,35	0,41	0,35
Other factors			
Angiogenin	5,56	2,93	2,4
TIMP-1	0,61	0,75	0,74
TIMP-2	0,94	2,16	2,27

All data were normalized to the control (cells incubated at atmospheric pressure). Ratios above 1.2 (shades of red) were considered as an increase in protein levels, values below 0.8 (shades of blue) were considered a decrease in protein levels no changes are for values 1.2≤x≤0.8.
I-309 - Glycoprotein 309; **MCP** - Monocyte chemoattractant protein; **MIP-1b** - Macrophage inflammatory protein; **RANTES** - Regulated upon activation, normal T cell expressed, and secreted; **TARC** - Thymus and activation regulated chemokine; **MDC** - Macrophage-derived chemokine; **Ck** – Chemokine; **GRO** - Growth regulated oncogene; **ENA-78** - Epithelial neutrophil activating peptide-78; **GCP-2** - Granulocyte chemotactic protein-2; **NAP-2** - Neutrophil- activating peptide-2; **MIG** - Monokine induced by gamma interferon; **IP-10** - Interferon gamma-induced protein 10; **SDF-1** - Stromal cell-derived factor 1; **BLC** - B lymphocyte chemoattractant; **GM-CSF** - Granulocyte-macrophage colony-stimulating factor; **TGF** - Transforming growth factor; **EGF** - Epidermal growth factor; **IGF-1** - Insulin-like growth factor 1; **VEGF** - Vascular endothelial growth factor; **PDGF** - Platelet-derived growth factor; **BDNF** - Brain-derived neurotrophic factor; **FGF** - Fibroblast growth factor; **GDNF** - Glial-derived neurotrophic factor; **HGF** - Hepatocyte growth factor; **IGFBP** - Insulin-like growth factor-binding protein; **NT-3** - Neurotrophin-3; **TNF** - Tumor necrosis factor; **LIGHT** - TNF family member; **IL** - Interleukin, **IFN-γ** - Interferon γ; **SCF** - Stem cell factor; **Flt3L** - Fms-like tyrosine kinase 3 ligand; **LIF** - Leukemia inhibitory factor; **MIF** - Macrophage migration inhibitory factor; **TIMP** - Tissue inhibitor of metalloproteinase.

MIO-M1 cells responded to MV-CT incubation by downregulating the expression of most chemokines related to microglia, T-cells, and monocyte chemotaxis (MCP-2, MCP-4, SDF-1, IP-10, RANTES, and fractalkine), furthermore, GRO, GRO-α, and MIG were upregulated. I-309, MCP-1, and MIP-1b levels were not altered in MIO-M1 cells incubated with MV-CT. Moreover, in the same condition, MIO-M1 cells decreased the expression of the majority of the growth factors, being most of them related to neuroprotection (TGF, BDNF, GDNF, HGF, NT3). Furthermore, most of the FGF mediators were decreased after MV-CT incubation, except FGF-4 that did not present

alterations. Additionally, cytokine expression decreased in MIO-M1 incubated with MV-CT, including TNF, IL-1β, IL-6, and LIF, however, IL-8, IL-12, and osteopontin levels increased. When incubated with MV-EHP, MIO-M1 cells decreased chemokine expression, however, GRO, ENA-78, and MIG were upregulated, while MCP-1, MDC, and GCP-2 did not change compared to control cells. In general, MIO-M1 cells downregulated growth factors expression after MV-EHP incubation, except FGF-4 and IGFBP-4 that presented increased levels. MV-EHP incubation increased cytokines IL-6, IL-7, IL-8, IL-12, oncostatin M and osteopontin expression in MIO-M1 cells, while decreasing the remaining cytokines. The exposure of MIO-M1 cells to EHP upregulated the expression of most chemokines, however, the MCP-4, Ckβ 1-8, fractalkine, IP-10, and BLC levels were decreased. Additionally, MIP-1b, MCP-2, eotaxin, and GCP-2 expression did not change in MIO-M1 cells under EHP. Growth factors expression also increased in MIO-M1 cells exposed to EHP, however certain factors levels were not altered under EHP, such as GM-CSF, TGF-β1, EGF, BDNF, FGF-9, and IGFBP-1. Additionally, fewer were downregulated in the same condition (TGF-β2 and 3, GDNF and HGF). MIO-M1 cells responded to EHP incubation by increasing the expression of several cytokines, such as IL-1α, IL-7, oncostatin M among others. Additionally, the expression of cytokines of the TNF family, IL-6, Flt3L, and LIF was decreased after EHP exposure, while the remaining cytokines did not alter their expression.

MCP-1, RANTES, and fractalkine play important roles in microglia chemotaxis[27,276]. Notably, when incubated with MVs derived from microglia, RANTES and fractalkine expression were downregulated in MIO-M1 cells, while MCP-1 levels did not change compared with control cells. However, in EHP conditions MIO-M1 cells increased MCP-1 and RANTES expression, whereas fractalkine levels decreased. Interestingly, RANTES and MCP-1 are related to microglia activation signalling[27] and fractalkine modulates microglial homeostasis[277]. Furthermore, the majority of chemokines that belong to the CC chemokine family, such as MCP-3, TARC, eotaxin-2, and others, which mainly interact with monocytes, macrophages, and microglia[278], were upregulated in MIO-M1 cells exposed to EHP, contrarily MVs incubation decreased the expression of the majority of these chemokines. Moreover, the expression of CXC chemokines (GRO, ENA-78, NAP-2, MIG, SDF-1, IP-10, BLC), predominantly responsible for the recruitment of neutrophils[278], was also affected by MVs and EHP

incubation. GRO, ENA-78, and MIG were upregulated in MIO-M1 cells under EHP and incubated with MVs from both conditions. However, in general, EHP increased the expression of CXC chemokines, whereas incubation with MVs decreased their expression. Moreover, EHP increased the levels of growth factors while incubation with MVs decrease, suggesting that MIO-M1 cells modulated their neuroprotective capacities, implicating neuronal survival. Additionally, several mediators have angiogenic properties. EHP exposure caused an increase of pro-angiogenic factors expression, such as ENA-78, SDF-1, MIG, NAP-2, VEGF and angiogenin. MV-EHP increased ENA-78, MIG and angiogenin expression and decreased VEGF levels. Incubation with MV-CT increased angiogenin levels, while decreased the remaining pro-angiogenic factors expression[279]. Additionally, the anti-angiogenic protein TIMP-2[280] was upregulated in the presence of MVs, but not in cells exposed to EHP. Focusing on the cytokine expression profile of MIO-M1 cells, EHP induced an increase in the expression of most pro-inflammatory cytokines and of the anti-inflammatory cytokine IL-13, the other evaluated cytokines did not change their expression or decreased it. When incubated with MVs, generally, the cytokine expression was decreased. Particularly, expression of osteopontin and oncostatin M, which are involved in photoreceptors and RGC neuroprotection[281–283], were upregulated after MIO-M1 exposure to EHP and MV-EHP, while MV-CT incubation increased only osteopontin levels.

Overall, this assay showed that the expression of the majority of proinflammatory factors was elevated in MIO-M1 cells exposed to EHP compared with control cells. Additionally, MVs incubation decreased the levels of most of mediators expressed in comparison to control cells, however, MV-EHP increased more inflammatory factors than MV-CT, such as ENA-78, IL-6, IL-7, and oncostatin M, suggesting that MVs from different conditions modulated different responses in MIO-M1 cells.

3.9 Effect of EHP and microglia-derived microvesicles in Müller cell phagocytic efficiency

Müller cells have the capacity to phagocyte degenerating cells in healthy, diseased, and injured retinas, and the role of their phagocytic capacity in regeneration, degeneration, and neuroprotection has been reported[59]. Therefore, the phagocytic

efficiency of MIO-M1 cells was evaluated to understand whether MVs derived from BV-2 cells cause change in phagocytosis. In order to establish the conditions for the assessment of the phagocytic capacity of Müller cells, MIO-M1 cells were incubated for 1h, 2h, and 24h with 0.0025% and 0.005% of fluorescent latex beads (Figure 17A). The engulfment of latex beads by MIO-M1 cells increased overtime and with the increase in beads concentration, as expected (Figure 17C). Since these cells are plated in poly-L-lysine coated glass coverslips and it was observed that latex beads adhered to the coating, the preparations were observed in a confocal microscope to ensure that only engulfed beads were being counted. The orthogonal projection confirmed that latex beads were inside MIO-M1 cells and not above or below the cells (Figure 17B). Therefore, for the subsequent experiments, MIO-M1 cells were incubated with 0.0025% fluorescent latex beads for 2h.

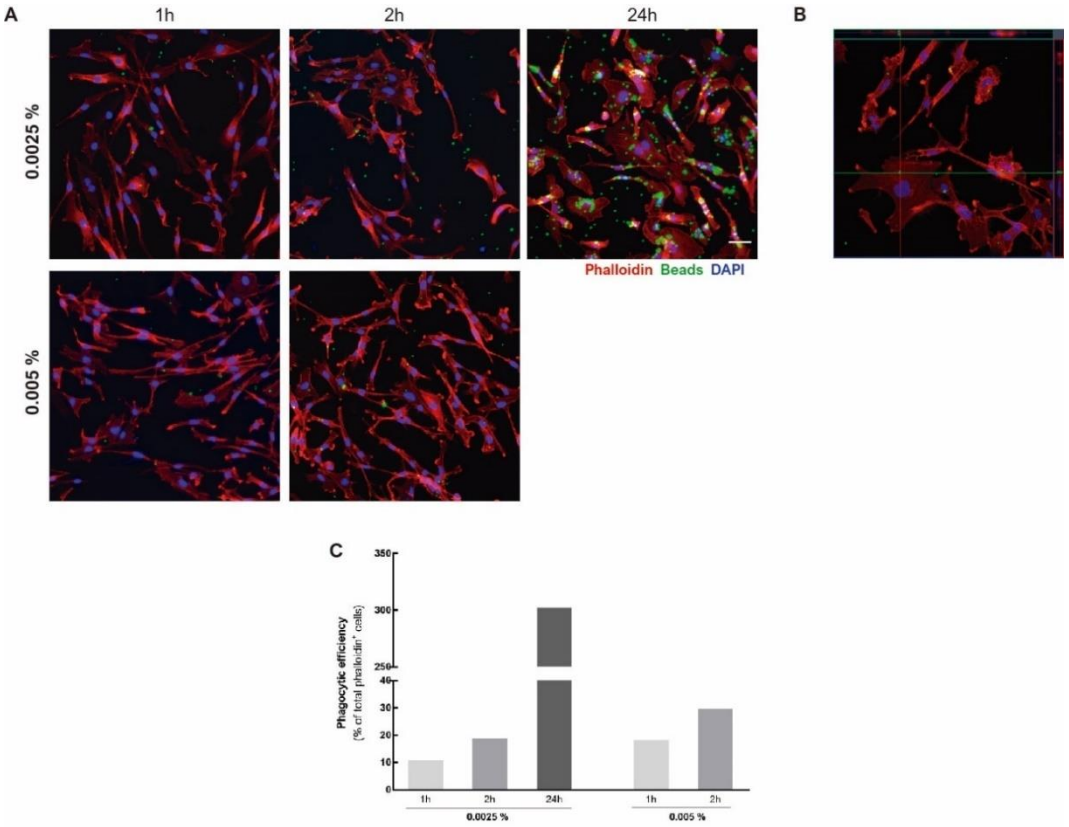

Figure 17 Phagocytosis of latex beads by MIO-M1 cells. MIO-M1 cultures were incubated with 0.0025% and 0.005% fluorescent latex beads (green) for 1h, 2h, and 24h **A**. Representative images of engulfed latex beads by MIO-M1 cells stained with phalloidin (red). Nuclei were counterstained with DAPI (blue). **B.** Orthogonal image demonstrating MIO-M1 engulfment of latex beads. **C.** Phagocytic efficiency of MIO-M1 cells obtained from 1 independent experiment. Scale bar: 50 μm.

Then, the effect of the incubation of BV-2 derived MVs in MIO-M1 cells that were exposed to EHP or atmospheric pressure in the phagocytic efficiency was assessed (Figure 18A). In control conditions, the phagocytic efficiency was 32.3±5.88% (n=3), and the presence of MV-CT or MV-EHP did not change the phagocytic efficiency of MIO-M1 cells (32.8±4.83% and 31.28±6.48%, respectively, n=3, Figure 18B). The phagocytic efficiency after MIO-M1 cells exposure to EHP for 24h was 43.0±6.22% (n=3, Figure 18B). Under EHP conditions, the exposure to MV-CT or MV-EHP did not significantly change the phagocytic efficiency (42.7±14.44 and 36.6±6.64%, respectively, n=3, Figure 18B).

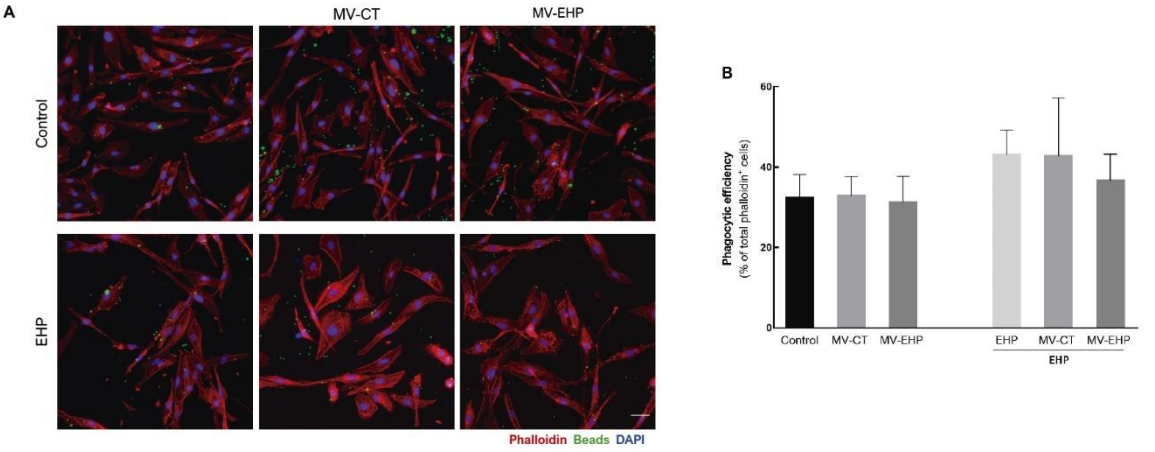

Figure 18 Effect of MVs derived from microglia under EHP and normal conditions in MIO-M1 cells phagocytic efficiency. MIO-M1 cells were incubated with MV-CT and MV-EHP and cultured in normal pressure or exposed to EHP for 24h. **A**. Phagocytosis was evaluated with fluorescent latex beads (green). MIO-M1 cells were stained with phalloidin (red). Nuclei were counterstained with DAPI (blue). **B.** Phagocytic efficiency was calculated from 3 independent experiments, performed in duplicate. Scale bar: 50 μm.

Then, the role of MVs in cell-to-cell communication within the retina was further investigated using an animal model.

3.10 BV-2 cells-derived microvesicles are internalized by retinal cells *in vivo*

MVs derived from BV-2 cells cultured in atmospheric pressure (MV-CT) or EHP (MV-EHP) were labelled with PHK67. Labelled MV-CT and MV-EHP were injected into the vitreous of C57Bl/6J mice. Retinal whole-mounts were prepared 24h post-injection, and DAPI staining allowed the observation of nuclei at the GCL. Green puncta, likely

corresponding to PKH67 labelled MVs, were observed in retinas injected with MV-CT and MV-EHP (n=3, Figure 19). No noticeable PKH67 staining was observed in the negative control performed (n=1, Figure 19 top row). Upon intravitreal injection, more labelled MV-EHP were observed in the retinas when compared with labelled MV-CT (Figure 19).

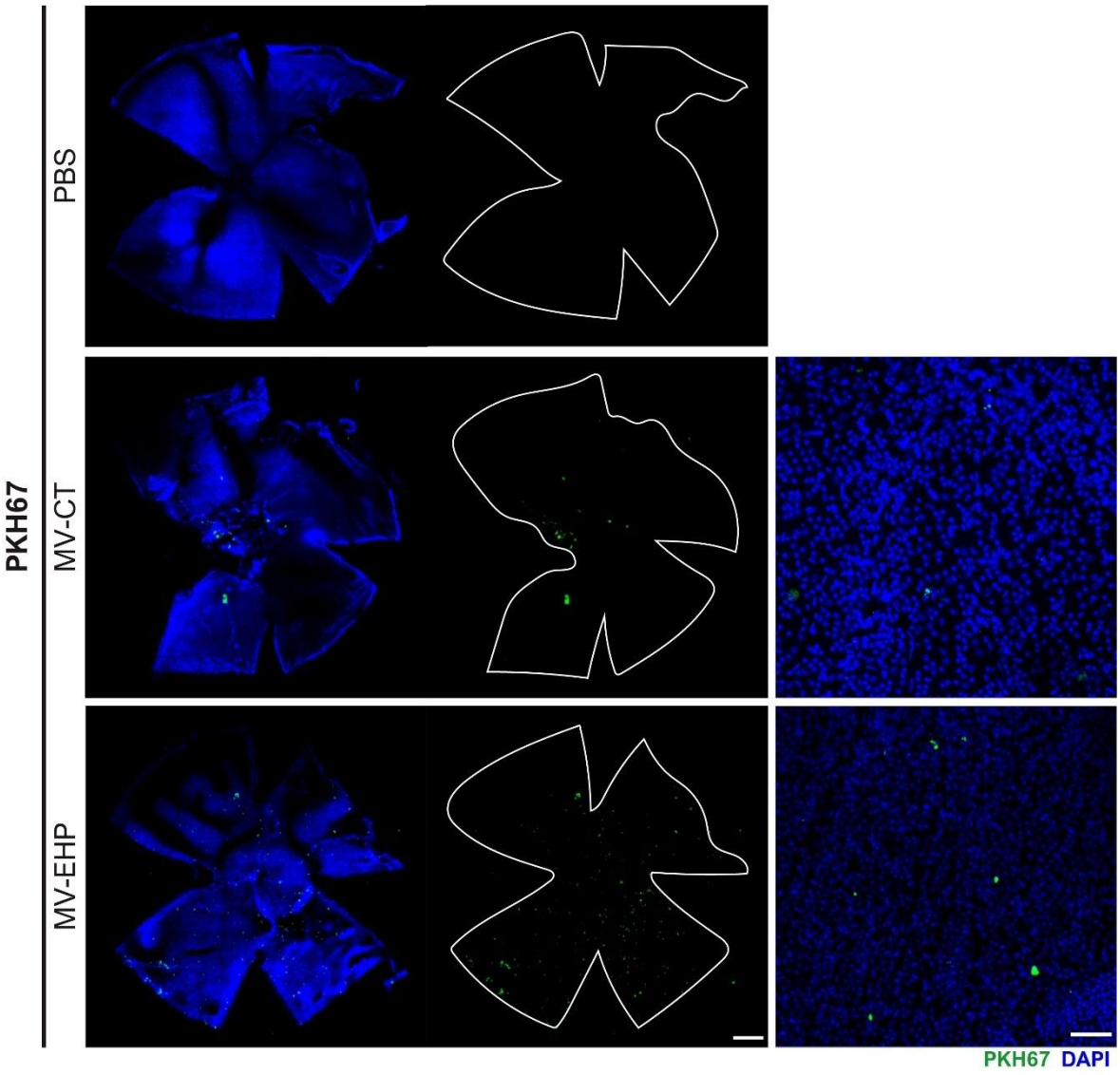

Figure 19 MVs derived from BV-2 cells interact with cells in the retina. MV-CT and MV-EHP were labelled with PKH67 and injected in the vitreous of C57BL/6J mice. Whole-mount preparations were acquired in a confocal microscope. MV-CT and MV-EHP labelled with PKH67 (green) were observed in the retinas. Nuclei were stained with DAPI (blue). Scale bar: 500 μm. The right panel shows a magnification of PKH67-labelled MVs acquired in confocal microscope. Scale bar: 50 μm.

3.11 Effect of BV-2-derived microvesicles injection in the integrity of the retina of C57BL/6J mice

Following intravitreal injection of MVs derived from BV-2 cells, OCT was performed to examine retinal structure and thickness at 24h and 7 days post-injection (Figure 20A).

The total retinal thickness, determined between the GCL and RPE, was assessed using the OCT images (Figure 20A). The retinal thickness of control retinas was 200.2±0.97 μm (n=5, Figure 20B), which is in accordance with previous results[284,285]. Analysis of the results showed no major differences in retinal structure or retinal thickness between conditions (Figure 20A). The intravitreal injection of MVs did not change total retinal thickness 24h and 7 days post-injection. Data showed very similar thickness after MV-CT and MV-EHP injection for 24h (200.4±1.42 μm and 200.3±1.60 μm, respectively for MV-CT and MV-EHP, n=14 and n=13) and 7 days post-injection (200.9±2.23 μm and 199.4±1.19 μm, respectively for MV-CT and MV-EHP, n=7), comparing to naïve retinas (Figure 20B).

During the OCT exam, distinctive puncta were detected in the vitreous cavity (Figure 20A). This finding was previously associated with the presence of vitreous immune cell infiltrates in several models of disease[7,286–288]. Cell infiltrates were detected in the vitreous of animals injected with MVs 24h after injection (Figure 20A). Densitometric analysis revealed that injection of MVs increased the presence of cell infiltrates in the vitreous, and MV-EHP appeared to cause a higher presence of infiltrates in the vitreous cavity compared to MV-CT at 24h (n=12, Figure 20C). Considerably fewer cells were observed 7 days after MVs injection, and a significant decrease was found for MV-EHP (n=6, Figure 20C) when compared with MV-CT ($p<0.05$). The presence of immune cells in the vitreous is associated with inflammation and BRB breakdown[7,289]. Therefore, fluorescein angiography was performed at 24h post-MVs injection to evaluate vascular leakage as a measurement of BRB integrity. No evident leakage of fluorescein was observed in untreated animals (Figure 20D). In animals injected with MV-CT and MV-EHP after 24h, the angiograms exhibited regions with a diffuse green cloud, showing extravascular fluorescein, indicating vascular leakage (Figure 20D), a sign of BRB impairment.

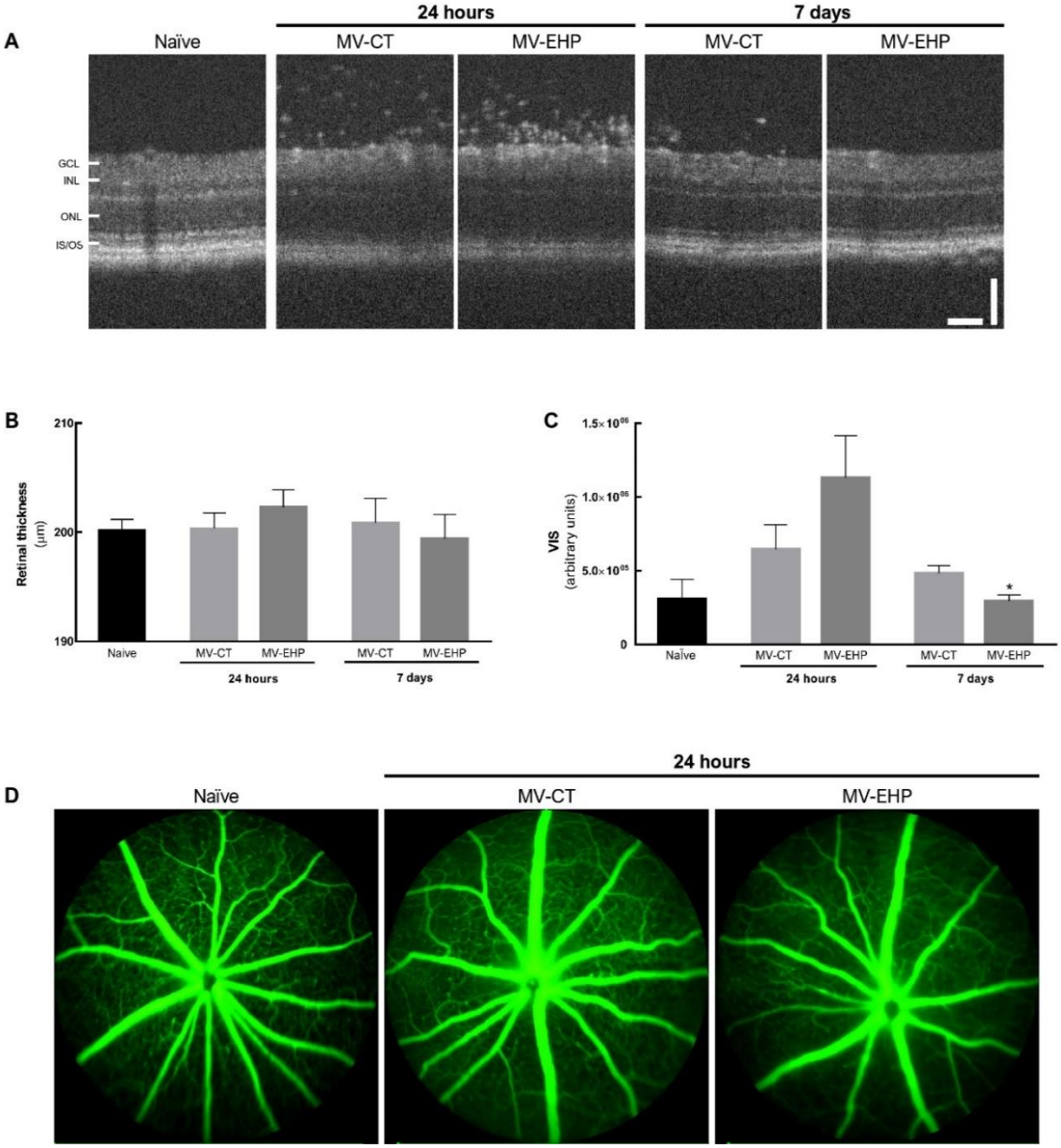

Figure 20 Effect of BV-2-derived microvesicles injection in the integrity of the retina of C57BL/6J mice evaluated by OCT and fluorescein angiography. A. Representative images of retinal tomographic scans, showing the presence of cells in the vitreous of animals injected with MV-CT and MV-EHP after 24h and 7 days. GCL - ganglion cell layer; INL - inner nuclear layer; ONL - outer nuclear layer; IS/OS- inner and outer segments of photoreceptors. Scale bar: 50 μm. **B.** Total retinal thickness was determined after segmentation of the GCL and the RPE and the results were obtained from 5 to 14 independent experiments. Scale bars: 50 μm. **C.** Assessment of the cell infiltrates present in the vitreous cavity following MVs injections by densitometric analysis. Results from 5 to 14 independent experiments. *$p<0.05$, different from MV-CT at 7 days, unpaired t test. **D.** Fluorescein angiography was performed after intraperitoneal injection of 5% fluorescein in naïve animals and in animals that were previously (24h) injected with MVs. The images represent the distribution of fluorescein across the retina.

3.12 BV-2 derived microvesicles modulate the protein levels of pro-inflammatory mediators 24h post-injection

The effect of MVs derived from BV-2 cells in the inflammatory response of the retina was determined by assessing the protein levels of 18 kDa translocator protein (TSPO, a biomarker of microglial reactivity), pro-IL-1β, and iNOS by WB (Figure 21). The intravitreal injection of MV-CT and MV-EHP increased the protein levels of TSPO 24h after injection (n=3, Figure 21A) as well as iNOS (n=3, Figure 21C). On the contrary, MVs decreased the protein levels of pro-IL-1β (n=3, Figure 21B) in retinal protein extracts, when compared with naïve animals. 7 days post-MVs injection TSPO protein levels were slightly increased compared with naïve retinas (n=3), however, TSPO appeared to decrease between 24h and 7 days after injection. Pro-IL-1β expression returned to levels similar to those of the naïve after 7 days (n=3). iNOS protein levels were undetected at 7 days post-MVs injection. Overall, the increase in TSPO and iNOS protein suggests that MVs from BV-2 cells cause retinal inflammation 24h post-injection. This situation seems transient since at 7 days post-injection of MVs, the protein levels of TSPO, pro-IL-1β (and likely iNOS) may be similar to naïve animals. Additionally, the release of pro-inflammatory cytokines, such as IL-1β is described during inflammation[290]. Therefore, the decrease in pro-IL-1β at 24h could indicate increased release of the cytokine after the MVs injection.

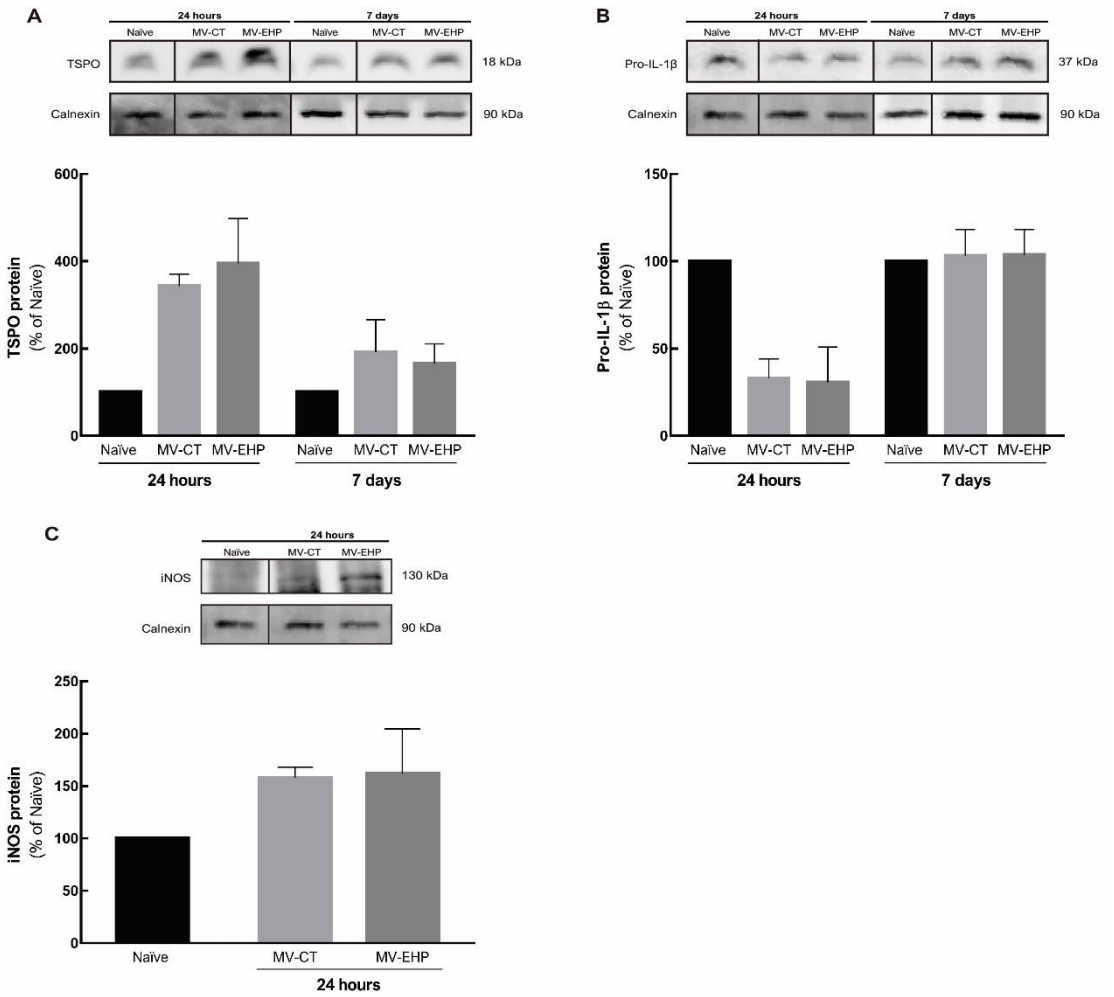

Figure 21 Effect of intravitreal injection of MVs from microglia under EHP and normal conditions in inflammation markers. Eyes were intravitreally injected with MV-CT and MV-EHP. TSPO (**A**), pro-IL-1β (**B**), and iNOS (**C**) protein levels were assessed by WB. Results were normalized to calnexin and expressed as percentage of control retinas (naïve animals). Data obtained from 3 independent experiments and one naïve sample.

3.13 Intravitreal injection of BV-2 derived microvesicles triggers Müller cell reactivity

The effect of MVs derived from microglia in Müller cells was assessed by WB to determine the protein levels of vimentin, GS, and GFAP. When comparing the two types of MVs within the same time point no statistically significant changes in the protein levels of vimentin, GS and GFAP were observed after MVs injection (Figure 22A-C). More than the effect of the type of MVs, it seems that the protein levels of vimentin and GS change with the time point. 24h after injection, MVs did not change the expression

levels of vimentin (n=3, Figure 22A). The protein levels of vimentin were 65.7±12.4 and 66.6±15.3% of naïve (n=3, Figure 22A). 7 days after injection, for MV-CT and MV-EHP, respectively. Additionally, 24h after MV-CT and MV-EHP injection the GS protein levels were, respectively, 85.4±5.7 and 86.5±10.5% of naïve (n=3), and 7 days post-injection protein levels were 125±16.5 and 127.7±21.1% of naïve, for MV-CT and MV-EHP, respectively (n=3, Figure 22B).

Alterations in GFAP expression levels were quantified by WB (Figure 22C). The results revealed that the injection of MVs shows a tendency to an increase in GFAP expression levels in the retina 24h (135±20.1 and 169.6±17.3% of naïve, for MV-CT and MV-EHP, respectively, n=3) and 7 days post-injection (191.6±17.3 and 222±67.2% of naïve, for MV-CT and MV-EHP, respectively, n=3) when compared to naïve animals (Figure 22C). GFAP is usually expressed in astrocytes, although Müller cells in detrimental conditions can also express this protein[65]. Therefore, by immunolabelling in vertical retinal sections for GFAP, it is possible to infer Müller cell reactivity (Figure 22D). GFAP immunoreactivity was observed in Müller cells in some conditions. The presence of GFAP in Müller cells was scored, as follows: as low levels if present only in the peripheral retina; high if immunolabelling was also detected in the central or other parts or throughout the whole retina; and none if no GFAP was observed in Müller cells. The analysis suggested that MVs injection promoted the expression of GFAP in Müller cells at 24h, MV-CT triggered a higher increase (n=9) while MV-EHP induced mild expression (n=8, Figure 22E). At 7 days, MV-EHP promoted an increase of GFAP in Müller cells, with more than 50% of animals with GFAP present in Müller cells (n=8, Figure 22E). However, the effect of MV-CT 7 days after injection was moderate, with most of the eyes analysed presenting low to none alterations in GFAP distribution in the retina (n=9, Figure 22E).

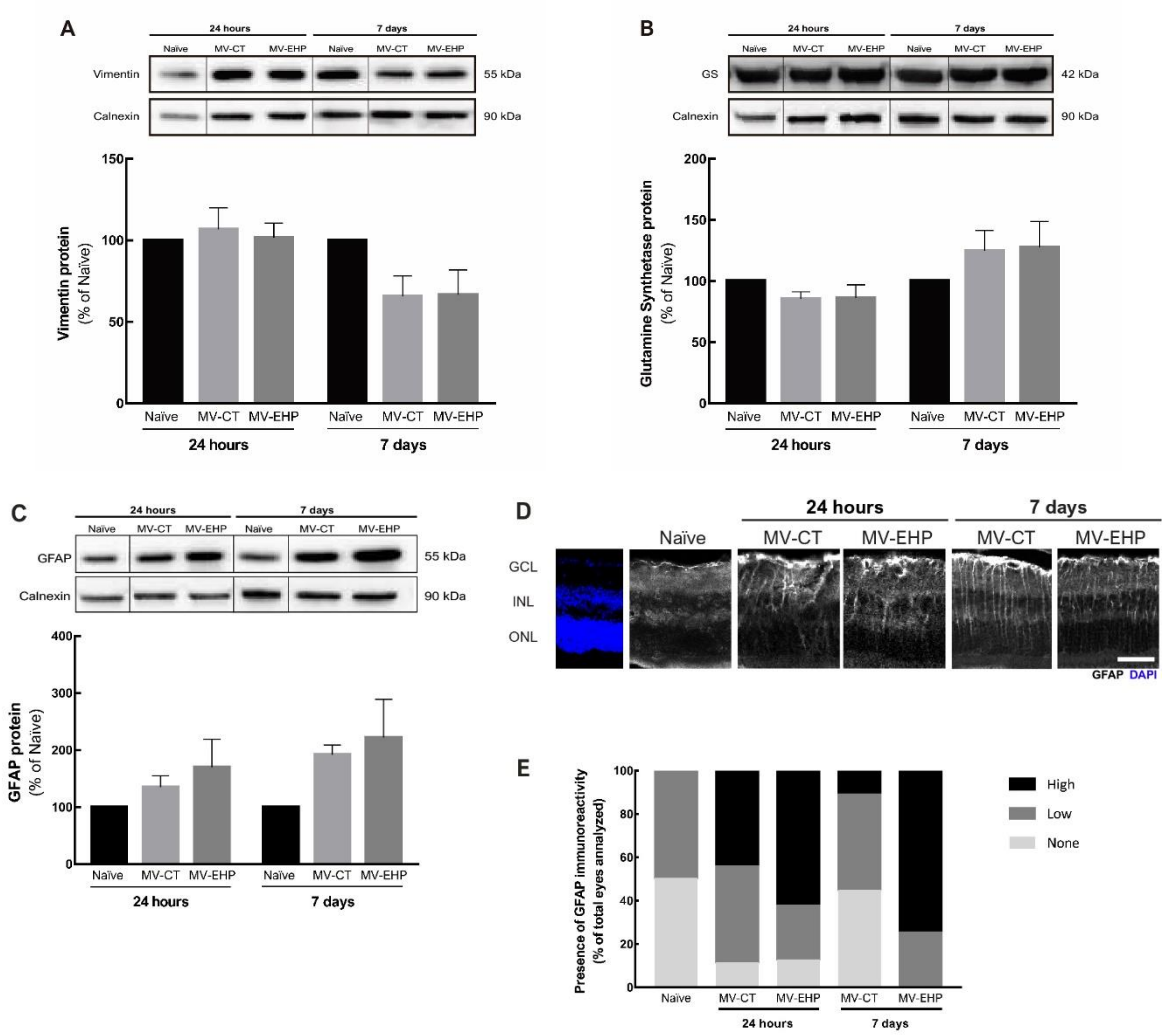

Figure 22 Effect of intravitreal injection of MVs from microglia under EHP and normal conditions in Müller cells protein markers of reactivity. Eyes were intravitreally injected with MV-CT and MV-EHP. Vimentin (**A**), GS (**B**), and GFAP (**C**) protein levels were assessed by WB. Results were normalized to calnexin and expressed as percentage of control retinas (naïve animals). Data obtained from 3 independent experiments and one naïve sample. **D.**24h and 7 days after MVs injection Müller cells reactivity was evaluated after immunolabeling for GFAP (white). Nuclei were stained with DAPI (blue). GCL - ganglion cell layer; INL - inner nuclear layer; ONL - outer nuclear layer. Scale bar: 50 μm. **E.** Qualitative assessment of GFAP presence in Müller cells. High – GFAP expression in peripheral retina and centre or expressed throughout the retina; Low – GFAP detected only in the peripheral retina; None – no GFAP labelling is detected. Results from 2 to 9 independent experiments.

3.14 Intravitreal injection of BV-2 derived microvesicles change the phenotype of retinal microglial cells

The number of microglial cells and microglia reactivity were evaluated 24h and 7 days post intravitreal injection of MV-CT and MV-EHP (Figure 23). The total number of microglia cells was assessed by immunolabelling with ionized calcium-binding adapter molecule 1 (Iba1, microglial marker, Figure 23B). The results between groups did not present significant alterations at 24h (9.0±1.59 and 6.5±0.54 $Iba1^+$ cells/mm, for MV-CT and MV-EHP, respectively, n=9 and n=8) and 7 days (7.8±0.92 and 7.0±0.47 $Iba1^+$ cells/mm, for MV-CT and MV-EHP, respectively, n=9 and n=8) compared with untreated naïve retinas (8.4±0.43 $Iba1^+$ cells/mm, n=2 Figure 23B). Reactive microglia were identified as $Iba1^+$ cells expressing MHC-II ($MHC\text{-}II^+$ $Iba1^+$ cells), as we reported previously[180,260]. A significant increase in the number of reactive microglia was observed 24h after MV-CT injection (15.6±3.41% of total microglia, n=9) when compared with naïve animals (1.2±0.28% of total microglia, n=2, Figure 23C), which indicates that MV-CT trigger retinal microglia activation. Additionally, the intravitreal injection of MV-EHP appeared to increase in the number of reactive microglia 24h post injection (9.1±2.85% of total microglia, n=8). Microglia reactivity was sustained at 7 days post MVs injection (12.7±2.29 and 10.6±2.71% of total microglia, for MV-CT and MV-EHP, respectively, n=9 and n=8, Figure 23C), and no significant alterations were found between MV-CT and MV-EHP at this time point.

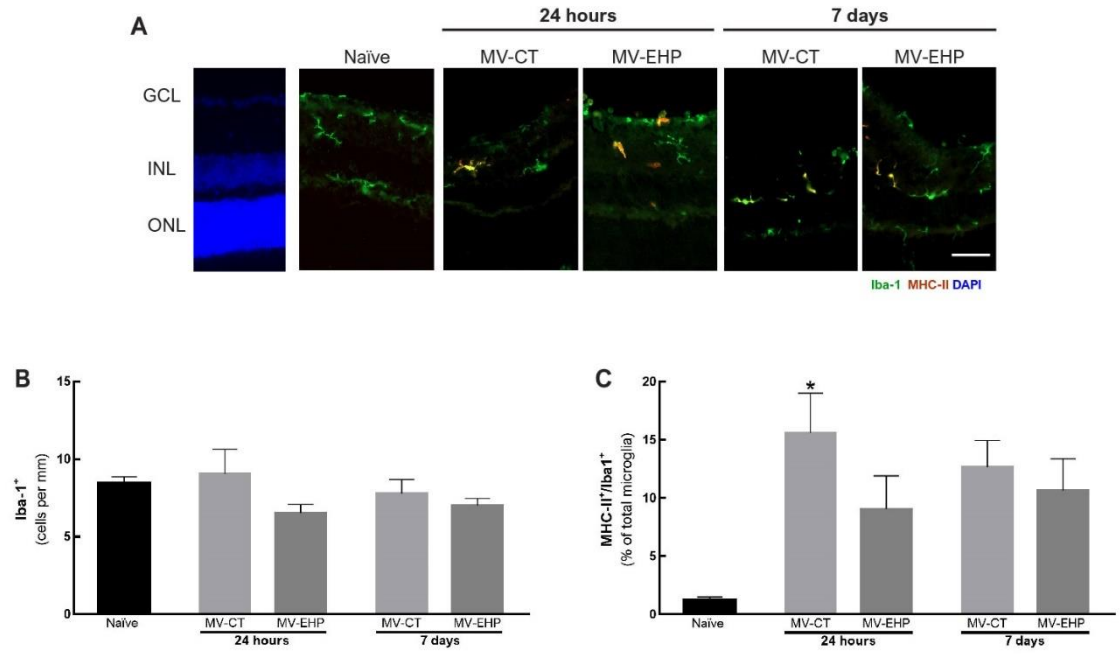

Figure 23 Intravitreal injection of MVs derived from BV-2 cells induced microglia activation in the retina. A. Isolated MVs from BV-2 cells exposed to EHP and normal conditions were injected in the vitreous. Microglial reactivity was assessed by immunolabelling for Iba1 (green) and MHC-II (red). Nuclei were stained with DAPI (blue). GCL - ganglion cell layer; INL - inner nuclear layer; ONL - outer nuclear layer. Scale bar: 50 μm. **B.** The number of microglial cells (Iba1$^+$ cells) per mm was counted in each condition, from 3 to 9 independent experiments. **C.** The number of reactive microglial cells (MHC-II$^+$ Iba1$^+$ cells) was determined, and results are presented as percentage of total microglia (Iba1$^+$ cells). Results from 2 to 9 independent experiments. *p<0.05, different from naïve, Kruskall-Wallis test, followed by Dunn's multiple comparison test.

3.15 MVs increased cell death at 24h and change the number of RGC 7 days post injection

The effect of MVs derived from BV-2 cells in retinal cell death and RGC number were assessed by TUNEL assay and immunolabelling for Brn3a, a marker of RGC, respectively (Figure 24A and Figure 25A). When injected with MV-CT there were 0.7±0.17 TUNEL$^+$ cells/mm and 0.1±0.02 TUNEL$^+$ cells/mm at 24h (n=9) and 7 days (n=7) after injection, when compared with naïve retinas (0.2±0.1 TUNEL$^+$ cells/mm, n=2, Figure 23B). While, when injected with MV-EHP there were 0.8±0.23 TUNEL$^+$ cells/mm and 0.2±0.07 TUNEL$^+$ cells/mm at 24h (n=7) and 7 days (n=8) after injection (Figure 24B). At 24h both MVs injected significantly decreased the number of Brn3a$^+$ cells (40.0±4.00 and 37.5±2.52 Brn3a$^+$ cells/mm, for MV-CT and MV-EHP,

respectively, n=9 and n=8) compared to naïve retinas (66.2±5.50 Brn3a$^+$ cells/mm, n=4, Figure 25B). In addition, 7 days after intravitreal injection, the number of Brn3a$^+$ cells was substantially decreased by MV-EHP (26.5±2.53 Brn3a$^+$ cells/mm, n=8, Figure 25C) when compared to naïve retinas and compared with MV-CT (43.32±6.70 Brn3a$^+$ cells per mm, n=8) at the same time point (Figure 25B). These results show that MVs derived from microglia induced retinal cell death and RGC loss *in vivo*.

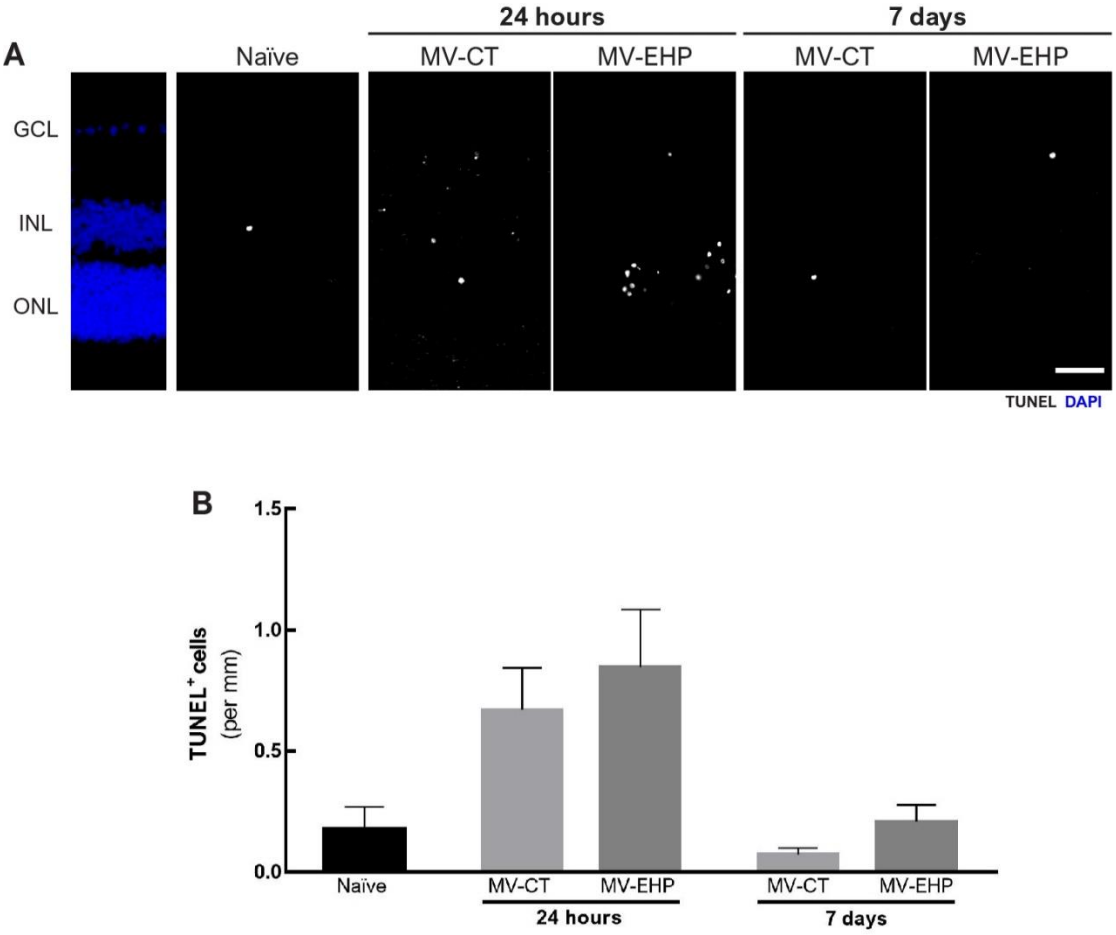

Figure 24 Intravitreal injection of MVs derived from BV-2 cells increased retinal cell death. A. Cell death was assessed by TUNEL assay (white) after intravitreal injection of MV-CT and MV-EHP. The nuclei were labelled with DAPI (blue). GCL - ganglion cell layer; INL - inner nuclear layer; ONL - outer nuclear layer. Scale bar: 50 μm. **B.** The number of TUNEL$^+$ cells was counted and expressed per mm of retina. Results were obtained from 2 to 9 independent experiments.

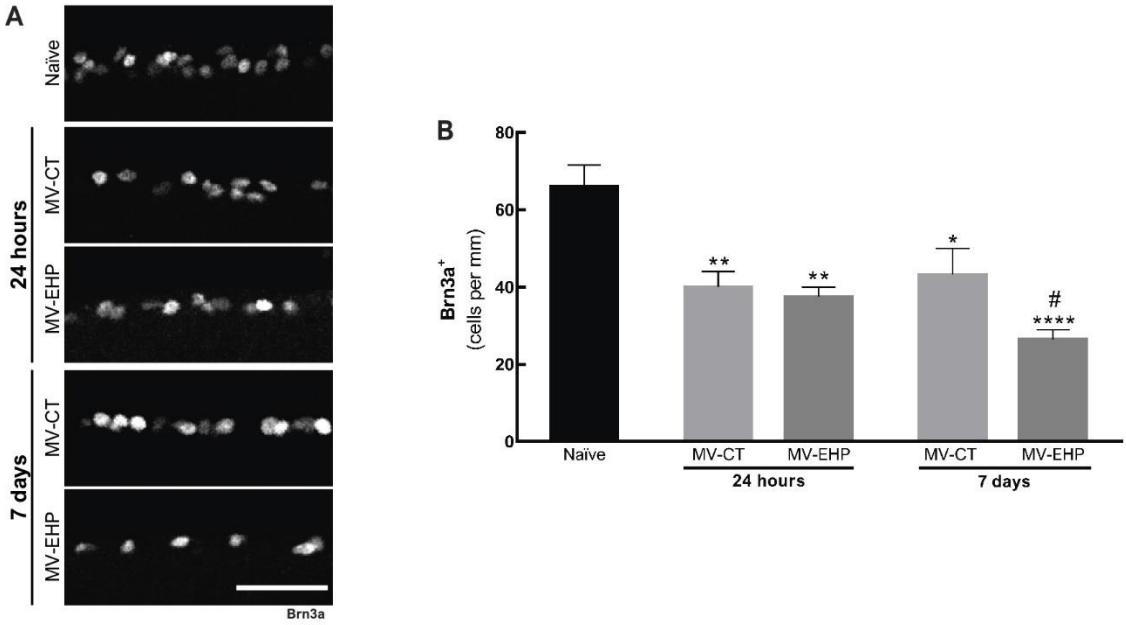

Figure 25 MVs isolated from BV-2 cells exposed to EHP and normal conditions induced loss of retinal ganglion cells. A. RGC were immunolabeled for Brn3a (white). Scale bar: 50 μm **B.** The number of Brn3a$^+$ cells was counted and expressed per mm of section. Results were obtained from 2 to 9 independent experiments. *p<0.05, **<0.005, ****<0.0001 different from naïve retinas, one-way ANOVA Multiple comparisons, followed by Dunnett's multiple comparisons test. #p<0.05, different from MV-CT at 7 days, unpaired t test.

Chapter 4

Discussion

4. Discussion

Glaucoma is the second leading cause of blindness worldwide and it is characterized by optic nerve atrophy and RGC death[84]. The main risk factor of glaucoma is elevated IOP and the treatments currently applied are focused on IOP control[87]. Evidence provided by human post-mortem samples from glaucoma subjects and experimental models strongly supports the contribution of neuroinflammation to RGC degeneration in glaucoma[38,93,180,291]. However, the mechanisms that drive retinal inflammation in glaucoma remain unclear. Therefore, it is of utmost importance to study the mechanisms that contribute to glaucomatous neurodegeneration since this might help in the development of novel therapeutic strategies.

Microglia and Müller cells play important roles in maintaining the homeostasis of the retinal tissue[21]. Microglia patrol the retinal tissue seeking alterations and sensing distressful signals[22]. Müller cells provide structural and functional support to the retina and protect the tissue from damage during noxious situations[35]. Glial activation is associated with neuroinflammation in glaucomatous conditions[292]. Microglia-mediated neuroinflammation contributes to retinal neurodegeneration, and following an injury, microglia cell reactivity precedes Müller cell gliosis[33,293]. MVs are EVs that are involved in cell-to-cell communication, as they carry a variety of molecules, including lipids, proteins, and genetic material[141,143]. Previous studies reported the release of MVs from a wide range of cells and their function in several disorders, such as cancer and neurodegenerative diseases[190]. The contribution of microglial MVs to retinal inflammation is unknown. Herein, we studied whether MVs derived from microglia can modulate Müller cells response.

Microglia affect cell function by releasing various mediators and EVs. Shedding of MVs from microglia, in their resting state or upon activation, is a known concept[222]. Moreover, MVs shed by microglia can spread the inflammatory signal, contributing to the progression of diseases[178,186,247]. In the present work, microglial cells (BV-2 cell line) were exposed to EHP to mimic elevated IOP. Previous studies reported the effects of EHP in BV-2 cells, showing that EHP impacts BV-2 response similar to what is described in

glaucomatous conditions[93,94]. Characterization of the isolated samples of EVs from BV-2 cells is a crucial step to properly analyse and categorise EVs. EVs samples isolated by ultracentrifugation may contain contaminants including small organelles, undesired fractions of EVs, and other cellular debris. However, ultracentrifugation is a frequently used method since no reagents that could potentially affect the EVs are used and allows isolation from large volumes of biological fluids at a relatively low cost[151]. The NTA results showed the size distribution was within the 100-800 nm range, which is consistent with the characteristics of MVs[143]. Additionally, TEM allowed to confirm that the isolated vesicles are MVs. Flotilin-1 and calnexin were detected in the MVs. Flotillin-1 is a protein typically expressed by EVs (exosomes and MVs), present in domains of the cell membrane which are involved in vesicle trafficking[144,201,294]. Previous studies showed that EHP modulates the purinergic system of BV-2 microglial cells, increasing the extracellular levels of ATP without causing cell death[95]. Therefore, apoptotic bodies are most likely absent from the vesicles isolated from BV-2 cells exposed to EHP. Calnexin was detected in EVs to a lower extend when comparing with total cell lysates, as reported by others[274], thus contamination of the preparation with other cell compartments or cell debris can not be excluded. Overall, the results indicated that the obtained samples of EVs from BV-2 cells were enriched with MVs. In the future, it would be interesting to explore specific MV markers along with the content within the MVs, to further characterize MVs released by microglial cells and to provide insight into the role of MVs in the inflammatory signal. For example, Slingshot 3 phosphatase and ATP-dependent RNA helicase DDX25 were enriched in MVs fractions derived from microglial cells and were only recently identified in EVs[246], suggesting that these two proteins may be used as selective markers of microglial MVs.

Müller cells are the main glial cell type of the retina and are known to promote RCG survival during pathological conditions, like glaucoma[65]. Müller cells release factors that support the function of retinal neurons, such as neurotrophic factors[37]. In response to retinal injuries, Müller cells become activated, changing their phenotype and these alterations can promote neuroprotection or contribute to neurodegeneration[39].

The response of microglial and Müller cells has been described in a wide range of retinal pathologies, and crosstalk between the glial cells appears to be required[74,75,77,78,80].

However, the mechanisms of how microglia and Müller cells coordinate their communication remain unclear. MIO-M1 cells, a human Müller cell line, were employed to investigate the role of MVs in the cellular communication between microglia and Müller cells. We started by analysing whether MVs derived from microglia could interact with MIO-M1 cells. The MVs were labelled with PKH67, a fluorescent lipid membrane (lipophilic) dye, allowing EVs visualization and tracking in recipient cells[295–297]. We observed that MIO-M1 cells were labelled with PKH67, indicating that MVs from microglial cells have the potential to interact with Müller cells. Nevertheless, the lipophilic dye labelling method has limitations[298,299], and the use of other techniques to label EVs must be considered.

MVs selectively transfer the content from their parent cells to recipient cells, likely altering cellular response, and ultimately, the fate of the recipient cells[221]. We studied the effects of MVs from microglia on the response of MIO-M1 cells, under EHP or atmospheric pressure. We demonstrated that microglial-derived MVs from control conditions (MV-CT) may protect MIO-M1 cells from apoptosis *in vitro*. The incubation of MIO-M1 cells with MV-CT appeared to protect them from cell death, under normal conditions and EHP, whereas MV-EHP did not cause major alterations. Meanwhile, the total cell count comparison between MVs and EHP treated cultures, and control cultures did not reveal significant differences in the overall number of cells. Taking the different outcomes when MIO-M1 cells are exposed to MV-CT or MV-EHP, one may suggest that microglial derived MVs from different conditions carry different contents, affecting receiving cells through different mechanisms. The content of microglial-derived MVs is hardly identified, although, there may be a resemblance in the effects of MVs and exosomes. Recent studies showed that microglial exosomes can play a beneficial role, protecting photoreceptors from hypoxia-induced apoptosis via miRNAs transfer[300]. Likewise, during retinal ischemia, human mesenchymal stem cell exosomes protect retinal cells from death[301,302].

Previous studies indicate that MVs shed by microglia can transfer pro-inflammatory factors, such as IL-1β, TNF, inflammasome complex components[230,233,235]. MVs are also able to carry miRNAs, such as miRNA-155, a well-characterized microglia pro-inflammatory miRNA[303], and miRNA-200c[240,241]. Remarkably, myeloid cell activation

highly increases the expression of pro-inflammatory mediators, allowing MVs to propagate inflammation[240,304,305]. Exosomes from microglia have been reported to have a neuroprotective role in retinopathy of prematurity, alleviating photoreceptors apoptosis on account of the high expression of miRNA-24-3p[300]. Similarly, miRNA-126 and miRNA-296 transferred by MVs derived from endothelial progenitor cells decrease renal cell apoptosis in a kidney injury model of ischemia-reperfusion injury[306]. Moreover, bioinformatic studies revealed that mesenchymal stem cells MVs cargo comprises miRNAs, such as miRNA-21 and miRNA-34a, that are involved in various cellular functions, participating in cell death, proliferation, and survival[307]. Little is known about the molecular composition of MVs produced by microglial cells in different environments. However, these miRNAs not yet describe in MVs from microglial cells may be transferred by these vehicles and contribute to the protective effects herein observed.

During noxious conditions, Müller cells became reactive and increase the expression of GFAP and vimentin[39,69]. Also, Müller cell gliosis is accompanied by the downregulation of GS expression[126]. In this work, MIO-M1 cells did not express substantial alterations in Müller cells gliotic markers, under EHP alone and when treated with microglial MVs under atmospheric pressure or EHP. There are two possible explanations. One is that the conditions used, such as the magnitude and the duration of pressure elevation and concentration of MVs, were not enough to cause alterations. For example, Holcombe et al described that the IOP threshold of~70 mmHg for the maintenance of retinal perfusion and IOPs elevated ≤70 mmHg was consistent with the maintenance of Müller cell function in rat glaucomatous model *in vivo*[45]. However, other reports demonstrate that 40 mmHg induces a significant change in Müller cells gliotic markers[98]. This suggests that other experimental pressure conditions should be tested. Another possibility is that MIO-M1 cells are secreting neurotrophins and other trophic factors that may be refraining the reactivity of the cells, in an autocrine manner. In fact, in this study, challenging MIO-M1 cells with EHP for 24h, demonstrated that elevated pressure induced an overall increase in the expression of chemokines, growth factors, and pro- and anti-inflammatory cytokines. A full characterization of the response of MIO-M1 cells to EHP, differing the magnitude and the time, including the analysis of the cell secretome may be helpful in the future. Previous works have shown how similar human MIO-M1 are to human Müller

cells96. However, others reported that primary mice Müller cells cultures are more alike to human Müller cells than the modified cell line MIO-M197. Therefore, it would be interesting to use the mouse primary Müller cell culture, developed during this work, to explore how much the results potentially diverge from the ones obtained using the MIO-M1 cell line.

Inflammation mediated by retinal glial cells contributes to RGC loss. Although inflammatory responses are usually considered to be mediated by microglia[24], Müller cells also detect detrimental stimuli and release inflammatory mediators[69] that might impact the survival of RGCs[41,43]. The production of NO in Müller cells is mainly caused by activation of iNOS[308], whose expression is increased in response to harmful stimuli[65]. Increased levels of NO have been reported to negatively impact the retinal cells in several diseases, including glaucoma[309,310]. However, NO is an essential mediator in several homeostatic processes in the retina, contributing to the regulation of blood flow and synaptic transmission, and the reduction of NO levels may also contribute to adverse effects[311,312]. Surprisingly, there was a trend to a decrease in the protein levels of iNOS in MIO-M1 cells exposed to EHP, an effect further accentuated in the presence of MV-CT. One possible explanation would be the feedback regulation of NO in which the NO levels increased in MIO-M1 cells in EHP inhibiting iNOS expression[313]. On the other hand, EHP exposure could trigger other mechanisms that modulate the intracellular assembly of iNOS in MIO-M1 cells. The iNOS protein is synthesized as a monomer, iNOS inactive subunits, and its dimerization assembles the dimeric active iNOS form, enabling the protein to catalyse NO[314]. Interferences with the dimeric assembly could prevent the dimerization of the enzyme and, consequently, decreasing the expression and NO levels. Interestingly, challenging microglial cells with EHP triggers oxidative and nitrosative stress, through the increase of NO and iNOS expression[93,315]. These findings indicate that the metabolic alterations triggered by elevated pressure are potentially conditioned by cell type. The content carried by these two populations of vesicles might be different that contribute to distinct MIO-M1 cells response.

The pro-inflammatory cytokine IL-1β is a potential mediator of retinal inflammation, that once released induces an immune response and tissue damage[316,317]. The evaluation of mRNA and protein levels of IL-1β in retinal organotypic cultures and

primary retinal neural cell cultures revealed that exposure to EHP increases IL-1β production[92,93], additionally, microglia cells were identified as the cells releasing this cytokine[3]. Exosomes derived from microglial cells exposed to EHP promoted microglia reactivity, increasing the levels of pro-inflammatory mediators, such as IL-1β[180]. Moreover, Müller cells respond to activated microglia upregulating IL-1β levels[77]. The incubation of MIO-M1 cells with MV-CT and MV-EHP, and exposure to atmospheric pressure or EHP did not induce major alterations in pro-IL-1β levels assessed by WB. However, the cytokine array analysis revealed a substantial decreased in IL-1β expression in MIO-M1 cells incubated with MV-CT and MV-EHP at atmospheric pressure. IL-1β, as well as other mediators produced by cells, present two forms, the pro, and the mature form, and assuming that the cytokine array detects only the matured form this could explain the discrepancy observed in the results. Therefore, we cannot rule out the hypothesis that MVs derived from microglial cells induced the release of IL-1β by MIO-M1 cells, without causing a major alteration in pro-IL-1β expression. The data obtained by cytokine array analysis provided more information regarding the expression of inflammatory factors in MIO-M1 cells. Interestingly, we observed an overall increase in inflammatory mediators, such as chemoattractant factors (I-309, MCP-1, RANTES, MCP-3, TARC, MDC, Eotaxin-2, GRO, ENA-78, NAP-2, MIG, and SDF-1) and pro-inflammatory cytokines (IL-1α, IL-15, SCF, and oncostatin), expressed by cells under EHP, whereas as MVs, in general, decreased it. Interestingly, the exposure of MIO-M1 cells to EHP increased the expression of RANTES and MCP-1, mediators of microglia activation signalling[27], which was not the case when cells were in the presence of MVs from microglia, suggesting that in the absence of microglia, Müller cells send stress signals to induce a microglial response. Moreover, under EHP MIO-M1 cells increased pro-angiogenic factor expression (ENA-78, SDF-1, MIG, NAP-2, VEGF, and angiogenin[279]), whereas with MVs most of these factors presented low expression levels. Additionally, TIMP-2, an anti-angiogenic factor[279], was only increased in MIO-M1 cells incubated with MVs. These results may indicate that Müller cells under EHP conditions shift towards a pro-inflammatory phenotype, showing their capacity to induce inflammation and recruit immune cells to the injury site, characteristics already described in retinal diseases[318–322]. Furthermore, these results also corroborate the existence of the crosstalk between microglia and Müller cells[79,80,323], since microglial-derived MVs modulated the production

of cytokines and chemokines in Müller cells. In addition, MV-CT and MV-EHP caused slightly different profiles of expression, indicating that MVs derived from microglia at distinct pressure conditions cause different responses in Müller cells. It is noteworthy that few mediators, such as GRO-α and FGF-4, when highly increased in MIO-M1 cells exposed to EHP were also increased in the presence of MV-EHP, while a decrease was identified in MV-CT incubation. This tendency concedes the possibility that MV-EHP may favour an analogous effect to EHP. Additionally, the increased synthesis of GRO-α and ENA-78 possibly indicates a stronger chemoattractant effect on neutrophils recruitment[324,325] in MIO-M1 cells incubated with MV-EHP. Neutrophilic inflammation has previously been identified in glaucoma animal models[326,327]. Moreover, not much is unknown about the FGF-4 role in the retina. Though, in the brain, this growth factor promotes neuronal proliferation and differentiation[328]. Likewise, the FGF was reported to be involved in lens regeneration in urodele amphibians eyes[329]. However, it does not play a role in RGC survival in an adult pig retina, being FGF-9 possibly responsible for that function[330]. EHP exposure increased the levels of other FGFs that may engage in neuroprotective mechanisms. For example, the release of FGFs by Müller cells can prevent the osmotic swelling of retinal cells[331], which can contribute to edema and neurodegeneration in retinal diseases[65,332].

Previous studies have documented the ability of Müller cells to provide neuroprotection to photoreceptors and RCG, releasing several neurotrophic factors (BDNF, LIF, CNTF, GDNF) essential to neuron survival[37,126]. Our results showed that MIO-M1 cells incubated with MV-CT and MV-EHP, and exposed to atmospheric pressure or EHP tended to decrease the expression of BDNF, whereas no substantial alterations were detected in LIF. Additionally, the cytokine array detected decreased levels of LIF in MIO-M1 cells exposed to EHP and incubated with MVs, whereas BDNF was only decreased in the presence of MVs. Contradictory to prior studies BDNF levels appeared to decrease, however, Müller cells can release pro-BDNF, indicating that under the experimental conditions MIO-M1 may induce neuroprotection. Therefore, the neuroprotective activity of MIO-M1 cells under EHP remains unclear. Moreover, exposure to EHP increased most of the neurotrophic factors production in MIO-M1 cells,

while MVs from microglial cells decreased it, showing that MVs may impact MIO-M1 cells function.

Nevertheless, Müller cells phagocyte cell debris, dead cells, and pathogens under normal and detrimental conditions[59–61]. Herein, we demonstrate that MIO-M1 cells are capable of phagocyte latex beads under normal and EHP conditions. Additionally, elevated pressure slightly increased the phagocytic capacity of MIO-M cells. Others reported that the same pressure conditions trigger an increase of the phagocytic function in microglia[93,95,315]. Activated microglial cells can decrease the phagocytic capacity of Müller cells[59,81], suggesting that microglia and Müller cells communicate with each other. MVs could be a possible mechanism of communication between these cells. However, in our conditions, no alterations were observed in the phagocytic capacity of MIO-M1 cells in the presence of MVs derived from microglia. Interestingly, exosomes isolated from EHP-activated microglial cells increase the phagocytic efficiency of BV-2 cells and retinal microglia[180].

To further investigate the role of microglia derived MVs in cell-to-cell communication, MVs were intravitreally injected into mice eyes. MVs administration triggered BRB breakdown, glial reactivity, retinal cell death, and, consequently, RGC loss.

In the literature, studies show an increase in total retinal thickness in glaucoma patients[285,333]. However, reports described no changes in total retinal thickness in animal glaucoma models[334,335]. In our results, no meaningful alterations were observed in animals intravitreally injected with MVs from microglial cells. Nevertheless, 24h and 7 days post-injection of MV-CT and MV-EHP, cell infiltrates were detected in the vitreous, accompanied by vascular leakage. These results indicate that microglia derived MVs induced BRB breakdown. Prior studies in animal glaucomatous models and glaucoma patients have shown that vascular leakage at the optic disc is related to higher IOP levels, showing BRB dysfunction of the optic disc[326,336–338]. In addition, changes in the vasculature permeability during glaucomatous insults allow bloodstream circulating cells to enter the retinal tissue[339]. Immune cell infiltration has previously been demonstrated in glaucoma injury in response to inflammatory signalling induced by the damaged local tissue[339–341]. Bamforth, Lightman, and Greenwood described similar effects after injection of IL-1β into the vitreous of rats[289]. MVs can transfer IL-1β[149], indicating pro-

inflammatory cytokines as a potential mediator carried by MV-CT and MV-EHP accountable in the induced retinal inflammation. We observed a distinction in the effects of MV-CT and MV-EHP within each time-point after MVs exposure, as well as a tendency for tissue recovery overtime since fewer infiltrates were detected after 7 days. This data shows that MVs from microglia may propagate inflammation, and contribute to the premise that vesicles from environmentally different cultured parent cells may trigger different mechanisms[143].

In this model, BRB breakdown was accompanied by increased expression of pro-inflammatory markers TSPO and iNOS in the retinas of mice 24h post MVs intravitreal injection. Additionally, at 7 days, the expression levels of the inflammatory markers TSPO and pro-IL-1β tended to normal values, suggesting a recovery of the tissue over time, consistent with the "retreat" of the vitreous immune infiltrates. Up-regulation of pro-inflammatory mediators is associated with inflammation in glaucomatous injury[312,342–345]. Interestingly, at 24h pro-IL-1β levels were decreased, which was not consistent with prior findings, that described increase production of IL-1β in glaucoma models and patients[346–350]. Nevertheless, this does not invalidate the possibility of inflammation, as mature IL-1β production and release may be increased, along with the expression on the corresponding post-transcriptional inflammation associated microRNA. More experiments are needed to assess the role of microglia MVs in inflammation and their effects on IL-1β metabolism within the retina.

Glial cell activation is a common response to retinal injuries[37,293]. The intravitreal administration of MVs derived from microglial cells induced Müller cells activation, exhibited by dysregulation of vimentin, GS, and GFAP levels. However, in this work, Müller cells did not express a typical phenotype associated with Müller cells reactivity. In response to glaucoma and glaucomatous like insults, Müller cells frequently increase GFAP and vimentin expression and decrease GS levels[65,351,352]. This observation suggests that, in the retina, Müller cells response to microglia-derived MVs may differ from typical gliotic changes induced by other retinal injuries. Nevertheless, retinal GFAP expression was up-regulated, suggesting astrocyte and Müller cells activation triggered by microglial-derived MVs[353]. Likewise, it was recently described an increase in $GFAP^+$ retinal glial cells after intravitreal delivery of exosomes derived from umbilical cord mesenchymal stem

cells[354]. Interestingly, MV-EHP induced a long-term and acute response of Müller cells. At 7 days, GFAP immunolabeling revealed a sustained upregulation of the intermediate filament by MV-EHP, while retinas injected with MV-CT showed mild GFAP staining over time, proving once again the different impacts of MV-CT and MV-EHP. Previous studies described the decrease in GS expression as a feature in the early stages of primary glaucoma[355]. However, extracellular glutamate could accumulate causing neuronal damage[65,356]. In some situations, Müller cells may try to regain glutamate function and upregulated GS expression[98,357,358]. Similarly, Müller cells may undergo an equivalent response after MVs exposure. The intermediate filament proteins, like GFAP and vimentin, are essential to maintain Müller cell integrity[359]. Under noxious conditions GFAP increase expression is accompanied by vimentin up-regulation, characterizing reactive Müller cells[65]. Contrary, in this work, we observed an increase in retinal GFAP levels associated with a decrease in vimentin expression 7 days post MVs injection, suggesting that GFAP tries to compensate for vimentin loss[359]. Furthermore, the intravitreal administration of MVs from microglial cells induced microglial reactivity. We observed an increased expression of TSPO and MHC-II$^+$/Iba1$^+$ cells, markers associated with microglia activation in the retina[343,345,360]. Moreover, MV-CT triggered to some extent a higher response in microglial cells, whereas MV-EHP promoted a higher expression of GFAP in Müller cells. For that reason, one may speculate that MV-CT and MV-EHP target different cells in the retina. Another possible explanation is that MVs from different microglial origins potentially prompt distinct mechanisms in the inner retina, even if targeting the same recipient cell. We could not determine if the induced glial reactivity results from direct interaction of microglia-derived MVs with Müller and microglial cells or a consequence of MVs communication with other retinal cells, which subsequently triggers glial cells activation. Overall, our results are in line with prior studies that demonstrate that MVs propagate inflammation *in vivo*[186,240].

In glaucoma, neuroinflammation due to glial cell activation has been described to contribute to RGC loss[38,65,93,293]. In these experiments, intravitreal injection of MVs from microglial cells tended to increase retinal cell death at 24h post-injection and decreased the number of RGC, indicating that MVs from control microglia and reactive microglia affect retinal homeostasis and impact RGC survival. Moreover, MV-EHP induced a

substantial decrease in RCG number, showing that during glaucoma, elevated IOP might promote the release of MVs by activated microglia, which over time may contribute to the dissemination of the inflammatory signal and RGC death. However, similar results were observed in retinas administered with MVs isolated from microglial cells at atmospheric pressure, suggesting that microglial MVs may not play a role in inflammation propagation during retinal neuroinflammation. Therefore, the role of microglial-derived MVs in neuroinflammation is still uncertain and more studies are needed to further understand the importance of these vesicles in glaucoma disease.

Remarkably, in the retina the impact of both populations of MVs from microglia, MV-CT, and MV-EHP, was comparable, the sustained overall inflammatory profile that ultimately prompts RGC loss overtime. These results indicate that microglial MVs may spread the neuroinflammatory signal, in the inner retina, regardless of content carried by these vehicles. Additionally, the impact of microglial-derived exosomes in neuroinflammation is more pronounced than the effects of MVs. Exosomes from microglia were recently identified as important players in the propagation of neuroinflammation in the diseased retina, demonstrating that exosomes derived from reactive microglial cells can mediate retinal inflammation[180]. Indeed, exosomes from non-reactive microglia did not cause inflammation, however, we found that MVs from microglia cultured in control pressure spread the inflammatory stimuli. Therefore, while microglial exosomes contribute to retinal degeneration, modulating the inflammatory signal, one may speculate that MVs do not play a crucial role in glaucomatous degeneration since both MVs populations trigger a similar response in the retina.

Chapter 5

Concluding remarks and future perspectives

5. Concluding remarks and future perspectives

The results presented in this thesis show that EHP potentially induces alterations in the secretion of neurotrophins and other trophic factors by MIO-M1 cells. Likewise, the MVs derived from microglia altered the MIO-M1 cells mediators production, in addition, induced retinal inflammation and retinal cell death.

Our results demonstrate that:

- The exposure of MIO-M1 cells to EHP for 24h did not cause Müller cell reactivity, suggesting that these cells may be resistant to the conditions tested.
- The exposure of MIO-M1 cells to EHP changed the levels of several chemokines, growth factors, and pro and anti-inflammatory factors. Additionally, MIO-M1 cells seem to decrease the expression of the pro-inflammatory marker iNOS.

- Microglial cells released MVs, both when cultured in control pressure and when challenged with EHP. These MVs are able to interact with Müller cells and retinal cells.

- The exposure of MIO-M1 cells to MVs derived from microglia showed that:
  - MV-CT appear to protect MIO-M1 cells from apoptotic cell death.
  - MIO-M1 cells altered the expression of pro-inflammatory cytokines, chemokines, and trophic factors upon incubation with MVs.

- The intravitreal injection of MV in the vitreous of C57BL/6J mice allowed us to conclude:
  - Microglial-derived MVs interacted with cells in the retina.
  - MVs derived from microglia caused vascular leakage and the presence of cells in the vitreous.
  - Microglia-derived MVs increased the expression of inflammatory markers.
  - Microglia-derived MVs promoted neuroinflammation and Müller cells and microglia reactivity.
  - Microglia-derived MVs triggered cell death.

- Both, MV-CT and MV-EHP, impacted RGC survival.

Overall, MVs induce glial reactivity; MV-CT trigger a significant effect in microglial activation, whereas MV-EHP induce higher levels of Müller cells reactivity. Furthermore, both MVs prompted RGC loss, however, MV-EHP caused more damage when compared with MV-CT.

Further experiments must be performed to uncover the role played by MVs derived from microglia in Müller cells. Lipophilic dyes are not the most reliable labelling procedure, they often cause false-positive signals, due to non-specific labelling of EVs and other cellular components, except when one holds a pure sample of EVs entirely devoid of other cellular contaminants[298]. Additionally, in cellular EVs uptake assays, PKH dyes can produce background signals, due to staining of cells caused by unbound dyes retained by recipient cells[299]. Therefore, it would be interesting to apply another method to label EVs. One suggestion is the transfection of cells with reporter [361,362] Still, this procedure also presents limitations, since EVs can express heterogeneity in similar or different cell types, restringing to a subpopulation of EVs. Moreover, the clarification of the effects of EHP in these cells, specifically the evaluation of glutamine and NO production, would be important to elucidate the role of the crosstalk of microglia and Müller cells in a context with elevated pressure. In addition, it would be fascinating to further explore the inflammatory mediators released after the intravitreal injection of MVs, considering that MV-EHP caused a higher increase in Müller cell reactivity and RCG loss compared with MV-CT. Nevertheless, taking into consideration the effects caused by MV-CT, it would be interesting to analyse the content of these two populations of vesicles, which might explain the different effects. The analysis of the individual layers of the retina as well as the identification of the immune cells present in the vitreous may provide additional indications of the effects caused by MVs in the retina of mice. Furthermore, some experiments need to be repeated in order to increase the number of independent experiments.

Chapter 6

References

6. References

1. Augustine, G. J. *et al. Neuroscience*. (Sinauer Associates, Inc., 2004).
2. Lammert, E., Zeeb, M. & Physiology, O. Metabolism of Human Diseases. in *Metabolism of Human Diseases* 59–65 (2014). doi:10.1007/978-3-7091-0715-7.
3. Sunderland, D. K. & Sapra, A. Physiology, Aqueous Humor Circulation. in *StatPearls* (2020).
4. Remington, L. A. Retina. in *Clinical Anatomy and Physiology of the Visual System* 61–92 (2012).
5. Klaassen, I., Van Noorden, C. J. F. & Schlingemann, R. O. Molecular basis of the inner blood-retinal barrier and its breakdown in diabetic macular edema and other pathological conditions. *Prog. Retin. Eye Res.* **34**, 19–48 (2013).
6. Cunha-Vaz, J., Bernardes, R. & Lobo, C. Blood-retinal barrier. *Eur. J. Ophthalmol.* **21**, 3–9 (2011).
7. Chu, C. J. *et al.* Multimodal analysis of ocular inflammation using the endotoxin-induced uveitis mouse model. *DMM Dis. Model. Mech.* **9**, 473–481 (2016).
8. Urbančič, M., Kloboves Prevodnik, V., Petrovič, D. & Globočnik Petrovič, M. A flow cytometric analysis of vitreous inflammatory cells in patients with proliferative diabetic retinopathy. *Biomed Res. Int.* **2013**, 1–8 (2013).
9. Nair, A. P., Sahu, G. R., Tejwani, S. & Ghosh, Arkasubhra Sethu, S. Increased infiltration of immune cell subsets and altered soluble factor profile in aqueous humor of glaucoma patients correlates with disease severity. *ARVO Annu. Meet. Abstr.* **60**, 674 (2019).
10. Crane, I. J. & Liversidge, J. Mechanisms of leukocyte migration across the blood-retina barrier. *Semin. Immunopathol.* **30**, 165–177 (2008).
11. Kolb, H. How the Retina Works. *Am. Sci.* **91**, 28 (2003).
12. Joselevitch, C. Human retinal circuitry and physiology. *Psychol. Neurosci.* **1**, 141–165 (2008).
13. Molday, R. S. & Moritz, O. L. Photoreceptors at a glance. *J. Cell Sci.* **128**, 4039–4045 (2015).
14. Perry, V. H. & Walker, M. Amacrine cells, displaced amacrine cells and interplexiform cells in the retina of the rat. *Proc. R. Soc. Lond. B. Biol. Sci.* **208**, 415–431 (1980).
15. Ball, A. K. & Dickson, D. H. Displaced amacrine and ganglion cells in the newt retina. *Exp. Eye Res.* 199–213 (1983).
16. Keyser, K. T. *et al.* Amacrine, ganglion, and displaced amacrine cells in the rabbit retina express nicotinic acetylcholine receptors. *Vis. Neurosci.* **17**, 743–752 (2000).
17. Wassle, H. & Boycott, B. B. Functional architecture of the mammalian retina. *Physiol. Rev.* **71**, 447–480 (1991).
18. Sanes, J. R. & Masland, R. H. The Types of Retinal Ganglion Cells: Current Status and Implications for Neuronal Classification. *Annu. Rev. Neurosci.* **38**, 221–246 (2015).
19. Boia, R. *et al.* Neuroprotective strategies for retinal ganglion cell degeneration: Current status and challenges ahead. *Int. J. Mol. Sci.* **21**, 1–39 (2020).
20. Kolb, H. Glial Cells of the Retina. *The Organization of the Retina and Visual System [Internet]* 1–9 (2001).

21. Vecino, E., Rodriguez, F. D., Ruzafa, N., Pereiro, X. & Sharma, S. C. Glia-neuron interactions in the mammalian retina. *Prog. Retin. Eye Res.* **51**, 1–40 (2016).
22. Debasis Nayak, Theodore L. Roth, and D. B. M. Microglia Development and function. *Annu. Rev.* **32**, 367–402 (2014).
23. Helmut, K., Hanisch, U. K., Noda, M. & Verkhratsky, A. Physiology of microglia. *Physiol. Rev.* **91**, 461–553 (2011).
24. Silverman, S. M. & Wong, W. T. Microglia in the retina: Roles in development, maturity, and disease. *Annu. Rev. Vis. Sci.* **4**, 45–77 (2018).
25. Schafer, D. P. *et al.* Microglia Sculpt Postnatal Neural Circuits in an Activity and Complement-Dependent Manner. *Neuron* **74**, 691–705 (2012).
26. Guttenplan, K., Blum, J. & Bennett, M. A role for microglia in retinal development. *J. Neurosci.* **38**, 9126–9128 (2018).
27. Langmann, T. Microglia activation in retinal degeneration. *J. Leukoc. Biol.* **81**, 1345–1351 (2007).
28. Anderson, S. R. *et al.* Complement targets newborn retinal ganglion cells for phagocytic elimination by microglia. *J. Neurosci.* **39**, 2025–2040 (2019).
29. Jonas, R. A. *et al.* The spider effect: Morphological and orienting classification of microglia in response to stimuli in vivo. *PLoS One* **7**, 1–12 (2012).
30. Todd, L. *et al.* Reactive microglia and IL1β/IL-1R1-signaling mediate neuroprotection in excitotoxin-damaged mouse retina. *J. Neuroinflammation* **16**, 1–19 (2019).
31. Madeira, M. H., Boia, R., Santos, P. F., Ambrósio, A. F. & Santiago, A. R. Contribution of microglia-mediated neuroinflammation to retinal degenerative diseases. *Mediators Inflamm.* **2015**, 15 (2015).
32. Karlstetter, M., Ebert, S. & Langmann, T. Microglia in the healthy and degenerating retina: Insights from novel mouse models. *Immunobiology* **215**, 685–691 (2010).
33. Bosco, A., Steele, M. R. & Vetter, M. L. Early microglia activation in a mouse model of chronic glaucoma. *J. Comp. Neurol.* **519**, 599–620 (2011).
34. Almasieh, M., Wilson, A. M., Morquette, B., Cueva Vargas, J. L. & Di Polo, A. The molecular basis of retinal ganglion cell death in glaucoma. *Prog. Retin. Eye Res.* **31**, 152–181 (2012).
35. Newman, E. & Reichenbach, A. The Muller cell: A functional element of the retina. *Trends Neurosci.* **19**, 307–312 (1996).
36. Liu, B., Hunter, D. J., Smith, A. A., Chen, S. & Helms, J. A. The capacity of neural crest-derived stem cells for ocular repair. *Birth Defects Res. Part C - Embryo Today Rev.* **102**, 299–308 (2014).
37. Vecino, E., Rodriguez, F. D., Ruzafa, N., Pereiro, X. & Sharma, S. C. Glia-neuron interactions in the mammalian retina. *Prog. Retin. Eye Res.* **51**, 1–40 (2016).
38. Reichenbach, A. & Bringmann, A. Glia of the human retina. *Glia* **68**, 768–796 (2020).
39. Reichenbach, A. & Bringmann, A. New functions of Müller cells. *Glia* **61**, 651–678 (2013).
40. Rhee, K. Do *et al.* CNTF-mediated protection of photoreceptors requires initial activation of the cytokine receptor gp130 in Müller glial cells. *Proc. Natl. Acad. Sci. U. S. A.* **110**, E4520–E4529 (2013).
41. Pereiro, X., Miltner, A. M., La Torre, A. & Vecino, E. Effects of Adult Müller Cells

and Their Conditioned Media on the Survival of Stem Cell-Derived Retinal Ganglion Cells. *Cells* **9**, 1–17 (2020).
42. Zhou, W. ting *et al.* Electrical stimulation ameliorates light-induced photoreceptor degeneration in vitro via suppressing the proinflammatory effect of microglia and enhancing the neurotrophic potential of Müller cells. *Exp. Neurol.* **238**, 192–208 (2012).
43. Ruzafa, N. & Vecino, E. Effect of Müller cells on the survival and neuritogenesis in retinal ganglion cells. *Arch. Soc. Esp. Oftalmol.* **90**, 522–526 (2015).
44. Derouiche, A. & Rauen, T. Coincidence of L-glutamate/L-aspartate transporter (GLAST) and glutamine synthetase (GS) immunoreactions in retinal glia: Evidence for coupling of GLAST and GS in transmitter clearance. *J. Neurosci. Res.* **42**, 131–143 (1995).
45. Holcombe, D. J., Lengefeld, N., Gole, G. A. & Barnett, N. L. The effects of acute intraocular pressure elevation on rat retinal glutamate transport. *Acta Ophthalmol.* **86**, 408–414 (2008).
46. Bringmann, A., Grosche, A., Pannicke, T. & Reichenbach, A. GABA and glutamate uptake and metabolism in retinal glial (Müller) cells. *Front. Endocrinol. (Lausanne).* **4**, 1–14 (2013).
47. Skytt, D. M. *et al.* Glia-Neuron Interactions in the Retina Can Be Studied in Cocultures of Müller Cells and Retinal Ganglion Cells. *Biomed Res. Int.* **2016**, (2016).
48. Bringmann, A. *et al.* Role of retinal glial cells in neurotransmitter uptake and metabolism. *Neurochem. Int.* **54**, 143–160 (2009).
49. Schütte, M. & Werner, P. Redistribution of glutathione in the ischemic rat retina. *Neurosci. Lett.* **246**, 53–56 (1998).
50. Ahuja, P., Caffé, A. R., Ahuja, S., Ekström, P. & Van Veen, T. Decreased glutathione transferase levels in rd1/rd1 mouse retina: Replenishment protects photoreceptors in retinal explants. *Neuroscience* **131**, 935–943 (2005).
51. Martin, K. R. G. *et al.* Gene therapy with brain-derived neurotrophic factor as a protection: Retinal ganglion cells in a rat glaucoma model. *Investig. Ophthalmol. Vis. Sci.* **44**, 4357–4365 (2003).
52. Cao, K. *et al.* Protection of the retinal ganglion cells: Intravitreal injection of resveratrol in mouse model of ocular hypertension. *Investig. Ophthalmol. Vis. Sci.* **61**, 1–12 (2020).
53. Telegina, D. V., Kolosova, N. G. & Kozhevnikova, O. S. Immunohistochemical localization of NGF, BDNF, and their receptors in a normal and AMD-like rat retina. *BMC Med. Genomics* **12**, (2019).
54. Harada, C. *et al.* Potential role of glial cell line-derived neurotrophic factor receptors in Müller glial cells during light-induced retinal degeneration. *Neuroscience* **122**, 229–235 (2003).
55. Van Adel, B. A., Arnold, J. M., Phipps, J., Doering, L. C. & Ball, A. K. Ciliary neurotrophic factor protects retinal ganglion cells from axotomy-induced apoptosis via modulation of retinal glia in vivo. *J. Neurobiol.* **63**, 215–234 (2005).
56. Pfeiffer, B., Grosche, J., Reichenbach, A. & Hamprecht, B. Immunocytochemical demonstration of glycogen phosphorylase in Müller (glial) cells of the mammalian retina. *Glia* **12**, 62–67 (1994).
57. Pfeiffer-Guglielmi, B. *et al.* Glycogen phosphorylase isozyme pattern in mammalian

retinal Müller (glial) cells and in astrocytes of retina and optic nerve. *Glia* **49**, 84–95 (2005).
58. Barry S. Winkler, Arnold, M. J., Brassell, M. A. & Puro, D. G. Energy Metabolism in Human Retinal Müller Cells Barry. **44**, 735–745 (2000).
59. Mart, G., Bejarano-escobar, R., Hortensia, S. & Francisco-morcillo, J. Müller glia and phagocytosis of cell debris in retinal tissue. *J. Anat.* 471–483 (2017).
60. Morris, A. C., Schroeter, E. H., Bilotta, J., Wong, R. O. L. & Fadool, J. M. Cone Survival Despite Rod Degeneration in XOPS-mCFP Transgenic Zebrafish. *Invest Ophthalmol Vis Sci.* **46**, 4762–4771 (2005).
61. Rosenthal, A. R. & Appleton, B. Histochemical localization of intraocular copper foreign bodies. *Am. J. Ophthalmol.* **79**, 613–625 (1975).
62. Nishizono, H., Muratat, Y., Tanakat, M., Soji, T. & Herberts, D. C. Evidence that Müller cells can phagocytize egg-lecithin-coated silicone particles. *Tissue Cell* **25**, 305–310 (1993).
63. Tout, S., Chan-Ling, T., Holländer, H. & Stone, J. The role of Müller cells in the formation of the blood-retinal barrier. *Neuroscience* **55**, 291–301 (1993).
64. Eichler, W., Yafai, Y., Wiedemann, P. & Reichenbach, A. Angiogenesis-related factors derived from retinal glial (Müller) cells in hypoxia. *Neuroreport* **15**, 1633–1637 (2004).
65. Bringmann, A. *et al.* Müller cells in the healthy and diseased retina. *Prog. Retin. Eye Res.* **25**, 397–424 (2006).
66. Kofuji, P. *et al.* Genetic inactivation of an inwardly rectifying potassium channel (kir4.1 Subunit) in mice: Phenotypic impact in retina. *J. Neurosci.* **20**, 5733–5740 (2000).
67. Agte, S. *et al.* Müller glial cell-provided cellular light guidance through the vital guinea-pig retina. *Biophys. J.* **101**, 2611–2619 (2011).
68. Franze, K. *et al.* Müller cells are living optical fibers in the vertebrate retina. *Proc. Natl. Acad. Sci. U. S. A.* **104**, 8287–8292 (2007).
69. T. Michael, N., Mona W., G., Gholam A., P. & Mark O. M., T. Massive Retinal Gliosis. A Reactive Proliferation of Müller Cells. *Arch Ophthalmol* **104**, 1383–1389 (1986).
70. Enayati, S. *et al.* Electrical Stimulation Induces Retinal Müller Cell Proliferation and Their Progenitor Cell Potential. *Cells* **9**, 781 (2020).
71. Ramachandran R., Fausett B.V., G. D. Ascl1A regulates Müller glia dedifferentiation and retina regeneration via a Lin-28 dependent, let7 miRNA signaling pathway. *Nat. Cell Biol.* **7**, 1959–1967 (2010).
72. Roesch, K. *et al.* The transcriptome of retinal Müller glial cells. *J. Comp. Neurol.* **509**, 225–238 (2008).
73. Fischer, A. J. & Reh, T. A. Potential of Müller glia to become neurogenic retinal progenitor cells. *Glia* **43**, 70–76 (2003).
74. Seitz, R., Ohlmann, A. & Tamm, E. R. The role of Müller glia and microglia in glaucoma. *Cell Tissue Res.* **353**, 339–345 (2013).
75. Bosco, A. *et al.* Neurodegeneration severity can be predicted from early microglia alterations monitored in vivo in a mouse model of chronic glaucoma. *DMM Dis. Model. Mech.* **8**, 443–455 (2015).
76. Xu, H., Chen, M. & Forrester, J. V. Para-inflammation in the aging retina. *Prog. Retin. Eye Res.* **28**, 348–368 (2009).

77. Wang, M., Ma, W., Zhao, L., Fariss, R. N. & Wong, W. T. Adaptive Müller cell responses to microglial activation mediate neuroprotection and coordinate inflammation in the retina. *J. Neuroinflammation* **8**, 173 (2011).
78. Conedera, F. M., Pousa, A. M. Q., Mercader, N., Tschopp, M. & Enzmann, V. Retinal microglia signaling affects Müller cell behavior in the zebrafish following laser injury induction. *Glia* **67**, 1150–1166 (2019).
79. Wang, M. *et al.* Macroglia-microglia interactions via TSPO signaling regulates microglial activation in the mouse retina. *J. Neurosci.* **34**, 3793–3806 (2014).
80. Harada, T. *et al.* Microglia-Müller glia cell interactions control neurotrophic factor production during light-induced retinal degeneration. *J. Neurosci.* **22**, 9228–9236 (2002).
81. Bejarano-escobar, R., Blasco, M., Martín-partido, G. & Francisco-morcillo, J. Light-induced degeneration and microglial response in the retina of an epibenthonic pigmented teleost : age-dependent photoreceptor susceptibility to cell death. *J. Exp. Biol.* **215**, 3799–3812 (2012).
82. Weinreb, R. N., Aung, T. & Medeiros, F. A. The pathophysiology and treatment of glaucoma: A review. *JAMA - J. Am. Med. Assoc.* **311**, 1901–1911 (2014).
83. Tham, Y. C. *et al.* Global prevalence of glaucoma and projections of glaucoma burden through 2040: A systematic review and meta-analysis. *Ophthalmology* **121**, 2081–2090 (2014).
84. Jonas, J. B. *et al.* Glaucoma. *Lancet* **390**, 2183–2193 (2017).
85. Drance S, Anderson DR, S. M. Collaborative Normal- Tension Glaucoma Study Group. Risk factors for progression of visual field abnormalities in normal-tension glaucoma. *Am J Ophthalmol* **131**, 699–708 (2001).
86. Walland, M. J. *et al.* Failure of medical therapy despite normal intraocular pressure. *Clin. Exp. Ophthalmol.* **34**, 827–836 (2006).
87. Cohen, L. P. & Pasquale, L. R. Clinical characteristics and current treatment of glaucoma. *Cold Spring Harb. Perspect. Med.* **4**, 1–16 (2014).
88. Johnson, T. V. & Tomarev, S. I. Rodent models of glaucoma. *Brain Res. Bull.* **81**, 349–358 (2010).
89. Pang, I. H. & Clark, A. F. Inducible rodent models of glaucoma. *Prog. Retin. Eye Res.* **75**, 100799 (2020).
90. Aires, I. D., Ambrósio, A. F. & Santiago, A. R. Modeling Human Glaucoma: Lessons from the in vitro Models. *Ophthalmic Res.* **57**, 77–86 (2017).
91. Liu, Q. *et al.* Oxidative stress is an early event in hydrostatic pressure-induced retinal ganglion cell damage. *Investig. Ophthalmol. Vis. Sci.* **48**, 4580–4589 (2007).
92. Madeira, M. H. *et al.* Adenosine A2AR blockade prevents neuroinflammation-induced death of retinal ganglion cells caused by elevated pressure. *J. Neuroinflammation* **12**, 1–13 (2015).
93. Aires, I. D. *et al.* Blockade of microglial adenosine A2A receptor suppresses elevated pressure-induced inflammation, oxidative stress, and cell death in retinal cells. *Glia* **67**, 896–914 (2019).
94. Madeira, M. H. *et al.* Selective A2A receptor antagonist prevents microglia-mediated neuroinflammation and protects retinal ganglion cells from high intraocular pressure-induced transient ischemic injury. *Transl. Res.* **169**, 112–128 (2015).
95. Rodrigues-neves, A. C., Aires, I. D., Vindeirinho, J. & Boia, R. Elevated Pressure

Changes the Purinergic System of Microglial Cells. **9**, 1–12 (2018).
96. Sappington, R. M. & Calkins, D. J. Pressure-Induced Regulation of IL-6 in Retinal Glial Cells : Involvement of the Ubiquitin / Proteasome Pathway and NF B. *Invest. Ophthalmol. Vis. Sci.* **47**, 3860–3869 (2006).
97. Xue, W. *et al.* Gene Expression Changes in Retinal Müller (Glial) Cells Exposed to Elevated Pressure. *Curr. Eye Res.* **36**, 754–767 (2011).
98. Yu, J. U. N. *et al.* In vitro effect of adenosine A2A receptor antagonist SCH 442416 on the expression of glutamine synthetase and glutamate aspartate transporter in rat retinal Müller cells at elevated hydrostatic pressure. *Oncol. Rep.* **27**, 748–752 (2012).
99. Yu, J. U. N. *et al.* In vitro effect of adenosine on the mRNA expression of Kir 2 . 1 and Kir 4 . 1 channels in rat retinal Müller cells at elevated hydrostatic pressure. 617–620 (2012) doi:10.3892/etm.2012.457.
100. Lee, S. J. *et al.* Pressure-Induced Alterations in PEDF and PEDF-R Expression : Implications for Neuroprotective Signaling in Glaucoma. *J. Clin. Exp. Ophthalmol.* **6**, 491 (2015).
101. Reardon, M. J. Neuroinflammation: The devil is in the details. *J. Thorac. Cardiovasc. Surg.* **156**, 598–599 (2018).
102. Tong, Y. *et al.* Analyzing cytokines as biomarkers to evaluate severity of glaucoma. *Int. J. Ophthalmol.* **10**, 925–930 (2017).
103. Chua, J. *et al.* Expression profile of inflammatory cytokines in aqueous from glaucomatous eyes. *Mol. Vis.* **18**, 431–438 (2012).
104. Tsai, D. C. *et al.* Significant variation of the elevated nitric oxide levels in aqueous humor from patients with different types of glaucoma. *Ophthalmologica* **216**, 346–350 (2002).
105. Goyal, A., Srivastava, A., Sihota, R. & Kaur, J. Evaluation of oxidative stress markers in aqueous humor of primary open angle glaucoma and primary angle closure glaucoma patients. *Curr. Eye Res.* **39**, 823–829 (2014).
106. Rokicki, W., Zalejska-Fiolka, J., Pojda-Wilczek, D., Kabiesz, A. & Majewski, W. Oxidative stress in the red blood cells of patients with primary open-angle glaucoma. *Clin. Hemorheol. Microcirc.* **62**, 369–378 (2016).
107. Luo, C. *et al.* Glaucomatous tissue stress and the regulation of immune response through glial toll-like receptor signaling. *Investig. Ophthalmol. Vis. Sci.* **51**, 5697–5707 (2010).
108. Tezel, G. Immune regulation toward immunomodulation for neuroprotection in glaucoma. *Curr. Opin. Pharmacol.* **13**, 23–31 (2013).
109. Russo, R. *et al.* Retinal ganglion cell death in glaucoma: Exploring the role of neuroinflammation. *Eur. J. Pharmacol.* **787**, 134–142 (2016).
110. Wilson, G. N., Inman, D. M., Dengler-Crish, C. M., Smith, M. A. & Crish, S. D. Early pro-inflammatory cytokine elevations in the DBA/2J mouse model of glaucoma. *J. Neuroinflammation* **12**, 1–13 (2015).
111. Bosco, A. *et al.* Reduced retina microglial activation and improved optic nerve integrity with minocycline treatment in the DBA/2J mouse model of glaucoma. *Investig. Ophthalmol. Vis. Sci.* **49**, 1437–1446 (2008).
112. Bosco, A. *et al.* Early Reduction of Microglia Activation by Irradiation in a Model of Chronic Glaucoma. *PLoS One* **7**, e43602–e43602 (2012).
113. Breen, K. T. *et al.* Loss of fractalkine signaling exacerbates axon transport

dysfunction in a chronic model of glaucoma. *Front. Neurosci.* **10**, 1–15 (2016).
114. Sappington, R. M. & Calkins, D. J. Contribution of TRPV1 to microglia-derived IL-6 and NFκB translocation with elevated hydrostatic pressure. *Investig. Ophthalmol. Vis. Sci.* **49**, 3004–3017 (2008).
115. Sappington, R. M., Chan, M. & Calkins, D. J. Interleukin-6 protects retinal ganglion cells from pressure-induced death. *Investig. Ophthalmol. Vis. Sci.* **47**, 2932–2942 (2006).
116. Echevarria, F. D., Formichella, C. R. & Sappington, R. M. Interleukin-6 deficiency attenuates retinal ganglion cell axonopathy and glaucoma-related vision loss. *Front. Neurosci.* **11**, 1–14 (2017).
117. Nakazawa, T. *et al.* Tumor necrosis factor-α mediates oligodendrocyte death and delayed retinal ganglion cell loss in a mouse model of glaucoma. *J. Neurosci.* **26**, 12633–12641 (2006).
118. Tezel, G., Li, L. Y., Patil, R. V. & Wax, M. B. TNF-α and TNF-α receptor-1 in the retina of normal and glaucomatous eyes. *Investig. Ophthalmol. Vis. Sci.* **42**, 1787–1794 (2001).
119. Balaiya, S., Edwards, J., Tillis, T., Khetpal, V. & Chalam, K. V. Tumor necrosis factor-alpha (TNF-α) levels in aqueous humor of primary open angle glaucoma. *Clin. Ophthalmol.* **5**, 553–556 (2011).
120. Roh, M. *et al.* Etanercept, a widely used inhibitor of tumor necrosis factor-α (TNF-α), prevents retinal ganglion cell loss in a rat model of glaucoma. *PLoS One* **7**, 1–13 (2012).
121. Chidlow, G., Ebneter, A., Wood, J. P. M. & Casson, R. J. Evidence supporting an association between expression of major histocompatibility complex II by microglia and optic nerve degeneration during experimental glaucoma. *J. Glaucoma* **25**, 681–691 (2016).
122. Liu, S. *et al.* Tracking retinal microgliosis in models of retinal ganglion cell damage. *Investig. Ophthalmol. Vis. Sci.* **53**, 6254–6262 (2012).
123. Bordone, M. P. *et al.* Involvemente of microglia in early axoglial alteration of the optic nerve induced by experimental Glaucoma. *J Neurochem* **142**, 323–337 (2017).
124. Takeda, A. *et al.* Microglia mediate non-cell-autonomous cell death of retinal ganglion cells. *Glia* **66**, 2366–2384 (2018).
125. Boia, R. *et al.* Treatment with A 2A receptor antagonist KW6002 and caffeine intake regulate microglia reactivity and protect retina against transient ischemic damage. *Nat. Publ. Gr.* 1–12 (2017) doi:10.1038/cddis.2017.451.
126. Bringmann, A. *et al.* Cellular signaling and factors involved in Müller cell gliosis: Neuroprotective and detrimental effects. *Prog. Retin. Eye Res.* **28**, 423–451 (2009).
127. Hirrlinger, P. G., Ulbricht, E., Iandiev, I., Reichenbach, A. & Pannicke, T. Alterations in protein expression and membrane properties during Müller cell gliosis in a murine model of transient retinal ischemia. *Neurosci. Lett.* **472**, 73–78 (2010).
128. Bolz, S. *et al.* K+ currents fail to change in reactive retinal glial cells in a mouse model of glaucoma. *Graefe's Arch. Clin. Exp. Ophthalmol.* **246**, 1249–1254 (2008).
129. Inman, D. M. & Horner, P. J. Reactive Nonproliferative Gliosis Predominates in a Chronic Mouse Model of Glaucoma. *Glia* **55**, 942–953 (2007).
130. Tezel, G., Chauhan, B. C., LeBlanc, R. P. & Wax, M. B. Immunohistochemical assessment of the glial mitogen-activated protein kinase activation in glaucoma.

Investig. Ophthalmol. Vis. Sci. **44**, 3025–3033 (2003).
131. Russo, R. *et al.* Impairment of Neuronal Glutamate Uptake and Modulation of the Glutamate Transporter GLT-1 Induced by Retinal Ischemia. *PLoS One* **8**, 1–10 (2013).
132. Taylor, S., Srinivasan, B., Wordinger, R. J. & Roque, R. S. Glutamate stimulates neurotrophin expression in cultured Müller cells. *Mol. Brain Res.* **111**, 189–197 (2003).
133. Tezel, G. & Wax, M. B. Hypoxia-inducible factor 1α in the glaucomatous retina and optic nerve head. *Arch. Ophthalmol.* **122**, 1348–1356 (2004).
134. Ergorul, C. *et al.* Hypoxia inducible factor-1α (HIF-1α) and some HIF-1 target genes are elevated in experimental glaucoma. *J. Mol. Neurosci.* **42**, 183–191 (2010).
135. Tezel, G. & Wax, M. B. The mechanisms of hsp27 antibody-mediated apoptosis in retinal neuronal cells. *J. Neurosci.* **20**, 3552–3562 (2000).
136. Chang, Z. Y., Yeh, M. K., Chiang, C. H., Chen, Y. H. & Lu, D. W. Erythropoietin Protects Adult Retinal Ganglion Cells against NMDA-, Trophic Factor Withdrawal-, and TNF-α-Induced Damage. *PLoS One* **8**, 1–14 (2013).
137. King, C. E. *et al.* Erythropoietin is both neuroprotective and neuroregenerative following optic nerve transection. *Exp. Neurol.* **205**, 48–55 (2007).
138. O'Reilly, A. M., Currie, R. W. & Clarke, D. B. HspB1 (Hsp 27) expression and neuroprotection in the retina. *Mol. Neurobiol.* **42**, 124–132 (2010).
139. Foxton, R. H. *et al.* VEGF-A is necessary and sufficient for retinal neuroprotection in models of experimental glaucoma. *Am. J. Pathol.* **182**, 1379–1390 (2013).
140. Barnett, N. L., Pow, D. V. & Bull, N. D. Differential perturbation of neuronal and glial glutamate transport systems in retinal ischaemia. *Neurochem. Int.* **39**, 291–299 (2001).
141. Raposo, G. & Stoorvogel, W. Extracellular vesicles: Exosomes, microvesicles, and friends. *J. Cell Biol.* **200**, 373–383 (2013).
142. Rufino-Ramos, D. *et al.* Extracellular vesicles: Novel promising delivery systems for therapy of brain diseases. *J. Control. Release* **262**, 247–258 (2017).
143. Van Niel, G., D'Angelo, G. & Raposo, G. Shedding light on the cell biology of extracellular vesicles. *Nat. Rev. Mol. Cell Biol.* **19**, 213–228 (2018).
144. Kowal, J. *et al.* Proteomic comparison defines novel markers to characterize heterogeneous populations of extracellular vesicle subtypes. *Proc. Natl. Acad. Sci. U. S. A.* **113**, E968–E977 (2016).
145. Yuana, Y. *et al.* Handling and storage of human body fluids for analysis of extracellular vesicles. *J. Extracell. Vesicles* **4**, 1–12 (2015).
146. Masyuk, A. I. *et al.* Biliary exosomes influence cholangiocyte regulatory mechanisms and proliferation through interaction with primary cilia. *Am. J. Physiol. - Gastrointest. Liver Physiol.* **299**, 990–999 (2010).
147. Aalberts, M. *et al.* Identification of distinct populations of prostasomes that differentially express prostate stem cell antigen, annexin A1, and GLIPR2 in humans. *Biol. Reprod.* **86**, 1–8 (2012).
148. Cocucci, E., Racchetti, G. & Meldolesi, J. Shedding microvesicles: artefacts no more. *Trends Cell Biol.* **19**, 43–51 (2009).
149. Turola, E., Furlan, R., Bianco, F., Matteoli, M. & Verderio, C. Microglial microvesicle secretion and intercellular signaling. *Front. Physiol.* **3**, 1–11 (2012).
150. Abels, E. R. & Breakefield, X. O. Introduction to Extracellular Vesicles: Biogenesis,

RNA Cargo Selection, Content, Release, and Uptake. *Physiol. Behav.* **36**, 301–312 (2016).
151. Konoshenko, M. Y., Lekchnov, E. A., Vlassov, A. V & Laktionov, P. P. Isolation of Extracellular Vesicles : General Methodologies and Latest Trends. *Biomed Res. Int.* **2018**, 8545347 (2018).
152. Taylor, D. D. & Shah, S. Methods of isolating extracellular vesicles impact down-stream analyses of their cargoes. *Methods* **87**, 3–10 (2015).
153. Théry, C. *et al.* Minimal information for studies of extracellular vesicles 2018 (MISEV2018): a position statement of the International Society for Extracellular Vesicles and update of the MISEV2014 guidelines. **3078**, (2018).
154. Wang, W., Luo, J. & Wang, S. Recent Progress in Isolation and Detection of Extracellular Vesicles for Cancer Diagnostics. *Adv. Healthc. Mater.* **7**, 1–27 (2018).
155. Mincheva-Nilsson, L., Baranov, V., Nagaeva, O. & Dehlin, E. Isolation and characterization of exosomes from cultures of tissue explants and cell lines. *Curr. Protoc. Immunol.* **2016**, 14.42.1-14.42.21 (2016).
156. Ramirez, M. I. *et al.* Technical challenges of working with extracellular vesicles. *Nanoscale* **10**, 881–906 (2018).
157. Boulanger, C. *et al.* Methodological Guidelines to Study Extracellular Vesicles. *Circ. Res.* **120**, 1632–1648 (2017).
158. Vestad, B. *et al.* Size and concentration analyses of extracellular vesicles by nanoparticle tracking analysis: a variation study. *J. Extracell. Vesicles* **6**, 1–12 (2017).
159. Szatanek, R. *et al.* The Methods of Choice for Extracellular Vesicles (EVs) Characterization. *Int. J. Mol. Sci.* **18**, 1153 (2017).
160. Cizmar, P. & Yuana, Y. Detection and Characterization of Extracellular Vesicles by Transmission and Cryo-Transmission Electron Microscopy. in *Extracellular Vesicles: Methods and Protocols, Methods in Molecular Biology* vol. 1660 221–232 (2017).
161. Bastos-Amador, P. *et al.* Proteomic analysis of microvesicles from plasma of healthy donors reveals high individual variability. *J. Proteomics* **75**, 3574–3584 (2012).
162. Kalra, H. *et al.* Comparative proteomics evaluation of plasma exosome isolation techniques and assessment of the stability of exosomes in normal human blood plasma. *Proteomics* **13**, 3354–3364 (2013).
163. Haraszti, R. A. *et al.* High-resolution proteomic and lipidomic analysis of exosomes and microvesicles from different cell sources. *J. Extracell. Vesicles* **5**, 1–14 (2016).
164. Altadill, T. *et al.* Enabling metabolomics based biomarker discovery studies using molecular phenotyping of exosome-like vesicles. *PLoS One* **11**, 1–17 (2016).
165. Sokolova, V. *et al.* Characterisation of exosomes derived from human cells by nanoparticle tracking analysis and scanning electron microscopy. *Colloids Surfaces B Biointerfaces* **87**, 146–150 (2011).
166. Colombo, M., Raposo, G. & Théry, C. Biogenesis, secretion, and intercellular interactions of exosomes and other extracellular vesicles. *Annu. Rev. Cell Dev. Biol.* **30**, 255–289 (2014).
167. Hessvik, N. P. & Llorente, A. Current knowledge on exosome biogenesis and release. *Cell. Mol. Life Sci.* **75**, 193–208 (2018).
168. Stuffers, S., Sem Wegner, C., Stenmark, H. & Brech, A. Multivesicular endosome biogenesis in the absence of ESCRTs. *Traffic* **10**, 925–937 (2009).
169. Subra, C., Laulagnier, K., Perret, B. & Record, M. Exosome lipidomics unravels

lipid sorting at the level of multivesicular bodies. *Biochimie* **89**, 205–212 (2007).
170. Hemler, M. E. Tetraspanin Proteins Mediate Cellular Penetration, Invasion, and Fusion Events and Define a Novel Type of Membrane Microdomain. *Annu. Rev. Cell Dev. Biol.* **19**, 397–422 (2003).
171. Wubbolts, R. *et al.* Proteomic and biochemical analyses of human B cell-derived exosomes: Potential implications for their function and multivesicular body formation. *J. Biol. Chem.* **278**, 10963–10972 (2003).
172. Van Niel, G., Porto-Carreiro, I., Simoes, S. & Raposo, G. Exosomes: A common pathway for a specialized function. *J. Biochem.* **140**, 13–21 (2006).
173. Mathieu, M., Martin-Jaular, L., Lavieu, G. & Théry, C. Specificities of secretion and uptake of exosomes and other extracellular vesicles for cell-to-cell communication. *Nat. Cell Biol.* **21**, 9–17 (2019).
174. Valadi, H. *et al.* Exosome-mediated transfer of mRNAs and microRNAs is a novel mechanism of genetic exchange between cells. *Nat. Cell Biol.* **9**, 654–659 (2007).
175. Nolte'T Hoen, E. N. M. *et al.* Deep sequencing of RNA from immune cell-derived vesicles uncovers the selective incorporation of small non-coding RNA biotypes with potential regulatory functions. *Nucleic Acids Res.* **40**, 9272–9285 (2012).
176. Pegtel, D. M. & Gould, S. J. Exosomes. *Annu. Rev. Biochem.* **88**, 487–514 (2019).
177. Asai, H. *et al.* Depletion of microglia and inhibition of exosome synthe. *Nat. Neurosci.* **18**, 1584–1593 (2015).
178. Porro, C., Panaro, M. A., Lofrumento, D. D., Hasalla, E. & Trotta, T. The multiple roles of exosomes in Parkinson's disease: an overview. *Immunopharmacol. Immunotoxicol.* **41**, 469–476 (2019).
179. Marie, G. *et al.* Acceleration of α-synuclein aggregation by exosomes. *J. Biol. Chem.* **290**, 2969–2982 (2015).
180. Aires, I. D. *et al.* Exosomes derived from microglia exposed to elevated pressure amplify the neuroinflammatory response in retinal cells. *Glia1. Aires, I. D. al. Exosomes Deriv. from microglia Expo. to Elev. Press. amplify neuroinflammatory response Retin. cells. Glia 1–20 (2020).* 1–20 (2020).
181. Wolf, P. The Nature and Significance of Platelet Products in Human Plasma PETER. *Connect. Tissue Res.* **13**, 269–288 (1967).
182. Stein, J. M. & Luzio, J. P. Ectocytosis caused by sublytic autologous complement attack on human neutrophils. The sorting of endogenous plasma-membrane proteins and lipids into shed vesicles. *Biochem. J.* **274**, 381–386 (1991).
183. Kolotuev, I., Apaydin, A. & Labouesse, M. Secretion of hedgehog-related peptides and WNT during Caenorhabditis elegans development. *Traffic* **10**, 803–810 (2009).
184. Théry, C., Ostrowski, M. & Segura, E. Membrane vesicles as conveyors of immune responses. *Nat. Rev. Immunol.* **9**, 581–593 (2009).
185. Lacroix, R. *et al.* Microvesicles and Cancer Associated Thrombosis. *Semin. Thromb. Hemost.* **45**, 593–603 (2019).
186. Verderio, C. *et al.* Myeloid microvesicles are a marker and therapeutic target for neuroinflammation. *Ann. Neurol.* **72**, 610–624 (2012).
187. Minciacchi, V. R., Freeman, M. R. & Di Vizio, D. Extracellular Vesicles in Cancer: Exosomes, Microvesicles and the Emerging Role of Large Oncosomes. *Semin. Cell Dev. Biol.* **40**, 41–51 (2015).
188. Meckes, D. G. & Raab-Traub, N. Microvesicles and Viral Infection. *J. Virol.* **85**,

12844–12854 (2011).
189. Carandini, T. *et al.* Microvesicles: What is the role in multiple sclerosis? *Front. Neurol.* **6**, 1–7 (2015).
190. Piccin, A., Murphy, W. G. & Smith, O. P. Circulating microparticles: pathophysiology and clinical implications. *Blood Rev.* **21**, 157–171 (2007).
191. John McCullough, Leremy A. Colf, and W. I. S. Membrane Fission Reactions of the Mammalian ESCRT Pathway. *Annu Rev Biochem* **23**, 1–7 (2013).
192. Leventis, P. A. & Grinstein, S. The distribution and function of phosphatidylserine in cellular membranes. *Annu. Rev. Biophys.* **39**, 407–427 (2010).
193. Slotte, J. P., Hedström, G., Rannström, S. & Ekman, S. Effects of sphingomyelin degradation on cell cholesterol oxidizability and steady-state distribution between the cell surface and the cell interior. *BBA - Biomembr.* **985**, 90–96 (1989).
194. Neufeld, E. B. *et al.* Intracellular trafficking of cholesterol monitored with a cyclodextrin. *J. Biol. Chem.* **271**, 21604–21613 (1996).
195. Tepper, A. D. *et al.* Sphingomyelin hydrolysis to ceramide during the execution phase of apoptosis results from phospholipid scrambling and alters cell-surface morphology. *J. Cell Biol.* **150**, 155–164 (2000).
196. Muralidharan-Chari, V. *et al.* ARF6-Regulated Shedding of Tumor Cell-Derived Plasma Membrane Microvesicles. *Curr. Biol.* **19**, 1875–1885 (2009).
197. Wehman, A. M., Poggioli, C., Schweinsberg, P., Grant, B. D. & Nance, J. The P4-ATPase TAT-5 inhibits the budding of extracellular vesicles in C. elegans embryos. *Curr. Biol.* **21**, 1951–1959 (2011).
198. Bianco, F. *et al.* Acid sphingomyelinase activity triggers microparticle release from glial cells. *EMBO J.* **28**, 1043–1054 (2009).
199. Gasser, O. & Schifferli, J. A. Activated polymorphonuclear neutrophils disseminate anti-inflammatory microparticles by ectocytosis. *Blood* **104**, 2543–2548 (2004).
200. Muralidharan-Chari, V., Clancy, J. W., Sedgwick, A. & D'Souza-Schorey, C. Microvesicles: Mediators of extracellular communication during cancer progression. *J. Cell Sci.* **123**, 1603–1611 (2010).
201. Beneventano, M. *et al.* Shedding of microvesicles from microglia contributes to the effects induced by metabotropic glutamate receptor 5 activation on neuronal death. *Front. Pharmacol.* **8**, 1–10 (2017).
202. Clancy, J. W., Zhang, Y., Sheehan, C. & D'Souza-Schorey, C. An ARF6-Exportin-5 Axis Delivers pre-miRNA Cargo to Tumor Microvesicles. *Nat Cell Biol.* **21**, 856–866 (2019).
203. Afroze, S. H., Uddin, M. N., Cao, X., Asea, A. & Gizachew, D. Internalization of exogenous ADP-ribosylation factor 6 (Arf6) proteins into cells. *Mol. Cell. Biochem.* **354**, 291–299 (2011).
204. Zhang, L. *et al.* Microvesicles Derived from Human Embryonic Neural Stem Cells Inhibit the Apoptosis of HL-1 Cardiomyocytes by Promoting Autophagy and Regulating AKT and mTOR via Transporting HSP-70. *Stem Cells Int.* **2019**, 15 (2019).
205. Belov, L. *et al.* Extensive surface protein profiles of extracellular vesicles from cancer cells may provide diagnostic signatures from blood samples. *J. Extracell. Vesicles* **5**, 1–12 (2016).
206. Ramachandra, L. *et al.* Mycobacterium tuberculosis synergizes with ATP to induce release of microvesicles and exosomes containing major histocompatibility complex

class II molecules capable of antigen presentation. *Infect. Immun.* **78**, 5116–5125 (2010).
207. Chiva-Blanch, G. *et al.* Monocyte-derived circulating microparticles (CD14+, CD14+/CD11b+ and CD14+/CD142+) are related to long-term prognosis for cardiovascular mortality in STEMI patients. *Int. J. Cardiol.* **227**, 876–881 (2017).
208. Andrews, A. M., Lutton, E. M., Merkel, S. F. & Razmpour, R. Mechanical Injury Induces Brain Endothelial-Derived Microvesicle Release : Implications for Cerebral Vascular Injury during Traumatic Brain Injury. *Front. Cell. Neurosci.* **10**, 1–13 (2016).
209. Unterberg, A. W., Stover, J., Kress, B. & Kiening, K. L. Edema and brain trauma. *Neuroscience* **129**, 1021–1029 (2004).
210. Elmore, S. Apoptosis: A Review of Programmed Cell Death. *Toxicol. Pathol.* **35**, 495–516 (2007).
211. Poon, I. K. H., Lucas, C. D., Rossi, A. G. & Ravichandran, K. S. Apoptotic cell clearance: Basic biology and therapeutic potential. *Nat. Rev. Immunol.* **14**, 166–180 (2014).
212. Hristov, M., Erl, W., Linder, S. & Weber, P. C. Apoptotic bodies from endothelial cells enhance the number and initiate the differentiation of human endothelial progenitor cells in vitro. *Blood* **104**, 2761–2766 (2004).
213. Coleman, M. L. *et al.* Membrane blebbing during apoptosis results from caspase-mediated activation of ROCK I. **3**, 339–346 (2001).
214. Demchenko, A. P. Beyond annexin V: Fluorescence response of cellular membranes to apoptosis. *Cytotechnology* **65**, 157–172 (2013).
215. Friedl, P., Vischer, P. & Freyberg, M. A. The role of thrombospondin-1 in apoptosis. *Cell. Mol. Life Sci.* **59**, 1347–1357 (2002).
216. Takizawa, F., Tsujial, S. & Nagasawa, S. Enhancement of macrophage phagocytosis upon iC3b deposition on apoptotic cells. *FEBS Lett* **397**, 269–272 (1996).
217. Erwig, L. P. & Henson, P. M. Clearance of apoptotic cells by phagocytes. *Cell Death Differ.* **15**, 243–250 (2008).
218. Van Engeland, M., Nieland, L. J. W., Ramaekers, F. C. S., Schutte, B. & Reutelingsperger, C. P. M. Annexin V-affinity assay: A review on an apoptosis detection system based on phosphatidylserine exposure. *Cytometry* **31**, 1–9 (1998).
219. Johnny C. Akers, David Gonda, Ryan Kim, B.S., Bob S. Carter, C. C. C. Biogenesis of extracellular vesicles (EV): exosomes, microvesicles, retrovirus-like vesicles, and apoptotic bodies Johnny. *J Neurooncol* 1–11 (2013).
220. Bergsmedh, A. *et al.* Horizontal transfer of oncogenes by uptake of apoptotic bodies. *Proc. Natl. Acad. Sci. U. S. A.* **98**, 6407–6411 (2001).
221. Paolicelli, R. C., Bergamini, G. & Rajendran, L. Cell-to-cell Communication by Extracellular Vesicles: Focus on Microglia. *Neuroscience* **405**, 148–157 (2019).
222. Prada, I., Furlan, R., Matteoli, M. & Verderio, C. Classical and unconventional pathways of vesicular release in microglia. *Glia* **61**, 1003–1017 (2013).
223. Visentin, S. & Levi, G. Protein kinase C involvement in the resting and interferon-γ-induced K+ channel profile of microglial cells. *J. Neurosci. Res.* **47**, 233–241 (1997).
224. Ferrari, D. *et al.* The P2X 7 Receptor: A Key Player in IL-1 Processing and Release . *J. Immunol.* **176**, 3877–3883 (2006).

225. Verhoef, P. A., Estacion, M., Schilling, W. & Dubyak, G. R. P2X7 Receptor-Dependent Blebbing and the Activation of Rho-Effector Kinases, Caspases, and IL-1β Release. *J. Immunol.* **170**, 5728–5738 (2003).
226. Morelli, A. *et al.* Extracellular ATP Causes ROCK I-dependent Bleb Formation in P2X7-transfected HEK293 Cells. *Mol. Biol. Cell* **14**, 2655–2664 (2003).
227. Duan, S. & Neary, J. T. P2X7 Receptors: Properties and Relevance to CNS Function. *Glia* **54**, 738–746 (2006).
228. MacKenzie, A. *et al.* Rapid secretion of interleukin-1β by microvesicle shedding. *Immunity* **15**, 825–835 (2001).
229. Qu, Y., Franchi, L., Nunez, G. & Dubyak, G. R. Nonclassical IL-1β Secretion Stimulated by P2X7 Receptors Is Dependent on Inflammasome Activation and Correlated with Exosome Release in Murine Macrophages. *J. Immunol.* **179**, 1913–1925 (2007).
230. Bianco, F. *et al.* Astrocyte-Derived ATP Induces Vesicle Shedding and IL-1β Release from Microglia. *J. Immunol.* **174**, 7268–7277 (2005).
231. Pizzirani, C. *et al.* Stimulation of P2 receptors causes release of IL-1B – loaded microvesicles from human dendritic cells. *Immunobiology* **109**, 3856–3864 (2007).
232. Qu, Y. *et al.* P2X7 receptor-stimulated secretion of MHC-II-containing exosomes requires the ASC/NLRP3 inflammasome but is independent of caspase-1. *J Immunol* **182**, 5052–5062 (2009).
233. Sarkar, A., Mitra, S., Mehta, S., Raices, R. & Wewers, M. D. Monocyte derived microvesicles deliver a cell death message via encapsulated caspase-1. *PLoS One* **4**, (2009).
234. Dubyak, G. R. P2X7 receptor regulation of non-classical secretion from immune effector cells. *Cell. Microbiol.* **14**, 1697–1706 (2012).
235. Hide, I. *et al.* Extracellular ATP triggers tumor necrosis factor-α release from rat microglia. *J. Neurochem.* **75**, 965–972 (2000).
236. Illes, P. P2X7 Receptors Amplify CNS Damage in Neurodegenerative Diseases. *Int. J. Mol. Sci.* **21**, 5996 (2020).
237. Furlan, R. Cytokines Stimulate the Release of Microvesicles from Myeloid Cells Independently from the P2X7 Receptor/Acid Sphingomyelinase Pathway. *Front. Immunol.* **9**, 1–15 (2018).
238. Fiebich, B. L., Akter, S. & Akundi, R. S. The two-hit hypothesis for neuroinflammation : role of exogenous ATP in modulating inflammation in the brain. *Front. Cell. Neurosci.* **8**, 1–11 (2014).
239. Nair, C. E. Mac, Schlamp, C. L., Montgomery, A. D., Shestopalov, V. I. & Nickells, R. W. Retinal glial responses to optic nerve crush are attenuated in Bax -deficient mice and modulated by purinergic signaling pathways. *J. Neuroinflammation* **13**, 93 (2016).
240. Kumar, A. *et al.* Microglial-derived microparticles mediate neuroinflammation after traumatic brain injury. *J. Neuroinflammation* **14**, 1–17 (2017).
241. Wu, B. *et al.* Glutaminase-containing microvesicles from HIV-1-infected macrophages and immune-activated microglia induce neurotoxicity. *Mol. Neurodegener.* **10**, 1–11 (2015).
242. Stary, C. M. *et al.* miR-200c Contributes to Injury From Transient Focal Cerebral Ischemia by Targeting Reelin. *Stroke* **46**, 551–556 (2015).
243. Tang, M. *et al.* Protective action of B1R antagonist against cerebral ischemia-

reperfusion injury through suppressing miR-200c expression of Microglia-derived microvesicles. *Neurol. Res.* **39**, 612–620 (2017).
244. Antonucci, F. *et al.* Microvesicles released from microglia stimulate synaptic activity via enhanced sphingolipid metabolism. *EMBO J.* **31**, 1231–1240 (2012).
245. Thomas, L. M. & Salter, R. D. Activation of macrophages by P2X7-induced microvesicles from myeloid cells is mediated by phospholipids and is partially dependent on TLR4. *J Immunol.* **185**, 3740–3749 (2010).
246. Drago, F. *et al.* ATP modifies the proteome of extracellular vesicles released by microglia and influences their action on astrocytes. *Front. Pharmacol.* **8**, 1–14 (2017).
247. Joshi, P. *et al.* Microglia convert aggregated amyloid-β into neurotoxic forms through the shedding of microvesicles. *Cell Death Differ.* **21**, 582–593 (2014).
248. Lehmann-horn, K. *et al.* Myeloid microvesicles in cerebrospinal fluid are associated with myelin damage and neuronal loss in mild cognitive impairment and Alzheimer disease. *Ann. Neurol.* **76**, 813–825 (2014).
249. Joshi, P. *et al.* Microglia convert aggregated amyloid-β into neurotoxic forms through the shedding of microvesicles. *Cell Death Differ.* **21**, 582–593 (2014).
250. Vargas, D. L., Nascimbene, C., Krishnan, C., Zimmerman, A. W. & Pardo, C. A. Neuroglial activation and neuroinflammation in the brain of patients with autism. *Ann. Neurol.* **57**, 67–81 (2005).
251. Suzuki, K. *et al.* Microglial activation in young adults with autism spectrum disorder. *Arch. Gen. Psychiatry* **70**, 49–58 (2013).
252. Prada, I. *et al.* Glia-to-neuron transfer of miRNAs via extracellular vesicles: a new mechanism underlying inflammation-induced synaptic alterations. *Acta Neuropathol.* **135**, 529–550 (2018).
253. Umapathy, N. S., Li, W., Mysona, B. A., Smith, S. B. & Ganapathy, V. Expression and function of glutamine transporters SN1 (SNAT3) and SN2 (SNAT5) in retinal Müller cells. *Investig. Ophthalmol. Vis. Sci.* **46**, 3980–3987 (2005).
254. Hicks, D. & Courtois, Y. The growth and behaviour of rat retinal Müller cells in vitro 1. An improved method for isolation and culture. *Exp. Eye Res.* **51**, 119–129 (1990).
255. Navneet, S. *et al.* Hyperhomocysteinemia-induced death of retinal ganglion cells: The role of Müller glial cells and NRF2. *Redox Biol.* **24**, 101199 (2019).
256. Chu, V. *et al.* In Vitro Characterization of a Spontaneously Immortalized Human MÜller Cell Line (MIO-M1). *Invest. Ophthalmol. Vis. Sci.* **43**, 864–869 (2002).
257. Aires, I. D. *et al.* Blockade of microglial adenosine A 2A receptor suppresses elevated pressure-induced inflammation, oxidative stress, and cell death in retinal cells. *Glia* **67**, 896–914 (2019).
258. Soares, A. R. *et al.* Gap junctional protein Cx43 is involved in the communication between extracellular vesicles and mammalian cells. *Sci. Rep.* **5**, 1–14 (2015).
259. Pan, X. D. *et al.* Microglial phagocytosis induced by fibrillar β-amyloid is attenuated by oligomeric β-amyloid: Implications for Alzheimer's disease. *Mol. Neurodegener.* **6**, 45 (2011).
260. Aires, I. D. *et al.* Intravitreal injection of adenosine A2A receptor antagonist reduces neuroinflammation, vascular leakage and cell death in the retina of diabetic mice. *Sci. Rep.* **9**, 1–14 (2019).
261. Stifter, J. *et al.* Neuroprotection and neuroregeneration of retinal ganglion cells

after intravitreal carbon monoxide release. *PLoS One* **12**, 1–24 (2017).
262. Dabin, I. & Barnstable, C. J. Rat retinal müller cells express Thy-1 following neuronal cell death. *Glia* **14**, 23–32 (1995).
263. Fischer, A. J. & Reh, T. A. Exogenous growth factors stimulate the regeneration of ganglion cells in the chicken retina. *Dev. Biol.* **251**, 367–379 (2002).
264. Kubrusly, R. C. C. *et al.* Expression of functional dopaminergic phenotype in purified cultured Müller cells from vertebrate retina. *Neurochem. Int.* **53**, 63–70 (2008).
265. Kubrusly, R. C. C. *et al.* Expression of functional receptors and transmitter enzymes in cultured Muller cells. *Brain Res.* **1038**, 141–149 (2005).
266. Dráberová, E. *et al.* Class III β-tubulin is constitutively coexpressed with glial fibrillary acidic protein and nestin in midgestational human fetal astrocytes: Implications for phenotypic identity. *J. Neuropathol. Exp. Neurol.* **67**, 341–354 (2008).
267. Lawrence, J. M. *et al.* MIO-M1 Cells and Similar Müller Glial Cell Lines Derived from Adult Human Retina Exhibit Neural Stem Cell Characteristics. *Stem Cells* **25**, 2033–2043 (2007).
268. Kaur, G. & Dufour, J. M. Cell lines: Valuable tools or useless artifacts. *Spermatogenesis* **2**, 1–5 (2012).
269. Vohra, R. *et al.* Disturbed mitochondrial function restricts glutamate uptake in the human Müller glia cell line, MIO-M1. *Mitochondrion* **36**, 52–59 (2017).
270. Mohammad, G. *et al.* Rho-associated protein kinase-1 mediates the regulation of inflammatory markers in diabetic retina and in retinal Müller cells. *Ann. Clin. Lab. Sci.* **48**, 137–145 (2018).
271. Chu-Tan, J. A. *et al.* MicroRNA-124 dysregulation is associated with retinal inflammation and photoreceptor death in the degenerating retina. *Investig. Ophthalmol. Vis. Sci.* **59**, 4094–4105 (2018).
272. Bull, N. D., Limb, G. A. & Martin, K. R. Human Müller stem cell (MIO-M1) transplantation in a rat model of glaucoma: Survival, differentiation, and integration. *Investig. Ophthalmol. Vis. Sci.* **49**, 3449–3456 (2008).
273. Matsuda, M. *et al.* Cellular stress response in human Müller cells (MIO-M1) after bevacizumab treatment. *Exp. Eye Res.* **160**, 1–10 (2017).
274. Tucher, C. *et al.* Extracellular vesicle subtypes released from activated or apoptotic T-lymphocytes carry a specific and stimulus-dependent protein cargo. *Front. Immunol.* **9**, 1–13 (2018).
275. Willms, E. *et al.* Cells release subpopulations of exosomes with distinct molecular and biological properties. *Sci. Rep.* **6**, 1–12 (2016).
276. Juel, H. B., Faber, C., Udsen, M. S., Folkersen, L. & Nissen, M. H. Chemokine expression in retinal pigment epithelial ARPE-19 cells in response to coculture with activated T cells. *Investig. Ophthalmol. Vis. Sci.* **53**, 8472–8480 (2012).
277. Lucin, K. M. & Wyss-Coray, T. Immune Activation in Brain Aging and Neurodegeneration: Too Much or Too Little? *Neuron* **64**, 110–122 (2009).
278. Taub, D. D. Chemokine-leukocyte interactions: The voodoo that they do so well. *Cytokine Growth Factor Rev.* **7**, 355–376 (1996).
279. Costa, C., Incio, J. & Soares, R. Angiogenesis and chronic inflammation: Cause or consequence? *Angiogenesis* **10**, 149–166 (2007).
280. Li, X., Liu, J., Hoh, J. & Liu, J. *Müller cells in pathological retinal angiogenesis*.

Translational Research vol. 207 (Elsevier Inc., 2019).
281. Xia, X. *et al.* Oncostatin M protects rod and cone photoreceptors and promotes regeneration of cone outer segment in a rat model of retinal degeneration. *PLoS One* **6**, 1–6 (2011).
282. Xia, X. *et al.* Protection of pattern electroretinogram and retinal ganglion cells by oncostatin M after optic nerve injury. *PLoS One* **9**, 1–7 (2014).
283. Wahl, V. *et al.* Osteopontin inhibits osmotic swelling of retinal glial (Müller) cells by inducing release of VEGF. *Neuroscience* **246**, 59–72 (2013).
284. Kutsyr, O. *et al.* Gradual Increase in Environmental Light Intensity Induces Oxidative Stress and Inflammation and Accelerates Retinal Neurodegeneration. *Retin. Cell Biol.* **61**, 1–19 (2020).
285. Sennlaub, F., Raoul, W., Paques, M. & Bemelmans, A. Spectral-Domain Optical Coherence Tomography of the Rodent Eye : Highlighting Layers of the Outer Retina Using Signal Averaging and Comparison with Histology. *PLoS One* **9**, 1–9 (2014).
286. Rezzola, S. *et al.* Inflammation and N-formyl peptide receptors mediate the angiogenic activity of human vitreous humour in proliferative diabetic retinopathy. *Diabetologia* **60**, 719–728 (2017).
287. Sharma, R. K. *et al.* Immune Profiling of T Cells Infiltrating Vitreous Humor in Tubercular Uveitis. *Immunol. Invest.* **47**, 615–631 (2018).
288. Yuan, Z. *et al.* The anti-inflammatory effect of minocycline on endotoxin-induced uveitis and retinal inflammation in rats. *Mol. Vis.* **25**, 359–372 (2019).
289. Bamforth, S. D., Lightman, S. L. & Greenwood, J. Ultrastructural analysis of interleukin-1β-induced leukocyte recruitment to the rat retina. *Investig. Ophthalmol. Vis. Sci.* **38**, 25–35 (1997).
290. Ke Rena, R. T. Role of interleukin-1β during pain and inflammation Ke. *Bone* **23**, 1–7 (2011).
291. Vohra, R., Tsai, J. C. & Kolko, M. The Role of Inflammation in the Pathogenesis of Glaucoma. *Surv. Ophthalmol.* **58**, 311–320 (2013).
292. Sciences, V. & Madison, W. *Neuroinflammation in Glaucoma and Optic Nerve Damage*. *Molecular Biology of Eye Disease* (Elsevier Inc., 2015).
293. Chong, R. S. & Martin, K. R. Glial cell interactions and glaucoma. *Curr. Opin. Ophthalmol.* **26**, 73–77 (2015).
294. De Gassart, A., Géminard, C., Février, B., Raposo, G. & Vidal, M. Lipid raft-associated protein sorting in exosomes. *Blood* **102**, 4336–4344 (2003).
295. Morales-Kastresana, A. *et al.* Labeling extracellular vesicles for nanoscale flow cytometry. *Sci. Rep.* **7**, 1–10 (2017).
296. Mondal, A., Ashiq, K. A., Phulpagar, P., Singh, D. K. & Shiras, A. Effective Visualization and Easy Tracking of Extracellular Vesicles in Glioma Cells. *Biol. Proced. Online* **21**, 1–12 (2019).
297. Grange, C. *et al.* Microvesicles released from human renal cancer stem cells stimulate angiogenesis and formation of lung premetastatic niche. *Cancer Res.* **71**, 5346–5356 (2011).
298. Pužar Dominkuš, P. *et al.* PKH26 labeling of extracellular vesicles: Characterization and cellular internalization of contaminating PKH26 nanoparticles. *Biochim. Biophys. Acta - Biomembr.* **1860**, 1350–1361 (2018).
299. Takov, K., Yellon, D. M. & Davidson, S. M. Confounding factors in vesicle uptake

studies using fluorescent lipophilic membrane dyes. *J. Extracell. Vesicles* **6**, 1–15 (2017).
300. Xu, W. *et al.* Exosomes from Microglia Attenuate Photoreceptor Injury and Neovascularization in an Animal Model of Retinopathy of Prematurity. *Mol. Ther. Nucleic Acid* **16**, 778–790 (2019).
301. Moisseiev, E. *et al.* Protective Effect of Intravitreal Administration of Exosomes Derived from Mesenchymal Stem Cells on Retinal Ischemia. *Curr. Eye Res.* **42**, 1358–1367 (2017).
302. Mathew, B. *et al.* Mesenchymal stem cell-derived extracellular vesicles and retinal ischemia-reperfusion. *Biomaterials* **197**, 146–160 (2019).
303. Su, W. S., Aloi, M. S. & Garden, G. A. G. MicroRNAs mediating CNS inflammation: Small regulators with powerful potential. *Brain Behav Immun.* 1–8 (2016).
304. Yang, Y. *et al.* Inflammation leads to distinct populations of extracellular vesicles from microglia. *J. Neuroinflammation* **15**, 1–19 (2018).
305. Garzetti, L. *et al.* Activated macrophages release microvesicles containing polarized M1 or M2 mRNAs. *J. Leukoc. Biol.* **95**, 817–825 (2014).
306. Cantaluppi, V. *et al.* Microvesicles derived from endothelial progenitor cells protect the kidney from ischemia – reperfusion injury by microRNA-dependent reprogramming of resident renal cells. *Kidney Int.* **82**, 412–427 (2012).
307. Vallabhaneni, K. C. *et al.* Extracellular vesicles from bone marrow mesenchymal stem / stromal cells transport tumor regulatory microRNA , proteins , and metabolites. *Oncotarget* **6**, 4953–4967 (2014).
308. Du, Y., Sarthy, V. P. & Kern, T. S. Interaction between NO and COX pathways in retinal cells exposed to elevated glucose and retina of diabetic rats. *Am. J. Physiol. - Regul. Integr. Comp. Physiol.* **287**, 735–741 (2004).
309. Siu, A. W. *et al.* Total Retinal Nitric Oxide Production is Increased in Intraocular Pressure-elevated Rats. *Exp. Eye Res.* **75**, 401–406 (2002).
310. Park, S. H., Kim, J. H., Kim, Y. H. & Park, C. K. Expression of neuronal nitric oxide synthase in the retina of a rat model of chronic glaucoma. *Vision Res.* **47**, 2732–2740 (2007).
311. Goldstein, I. M., Ostwald, P. & Roth, S. Nitric oxide: A review of its role in retinal function and disease. *Vision Res.* **36**, 2979–2994 (1996).
312. Toda, N. & Nakanishi-Toda, M. Nitric oxide: Ocular blood flow, glaucoma, and diabetic retinopathy. *Prog. Retin. Eye Res.* **26**, 205–238 (2007).
313. Chang, K. *et al.* Nitric oxide supresses inducible nitric oxide synthase expression by inhibiting post-translational modification of IκB. *Exp. Mol. Med.* **36**, 311–324 (2004).
314. Albakri, Q. A. & Stuehr, D. J. Intracellular assembly of inducible NO synthase is limited by nitric oxide-mediated changes in heme insertion and availability. *J. Biol. Chem.* **271**, 5414–5421 (1996).
315. Ferreira-silva, J., Aires, I. D., Boia, R. & Ambrósio, A. F. Activation of Adenosine A 3 Receptor Inhibits Microglia Reactivity Elicited by Elevated Pressure. *Int. J. Mol. Sci.* **21**, 7218 (2020).
316. Rothwell, N. J. & Luheshi, G. N. Interleukin 1 in the brain: Biology, pathology and therapeutic target. *Trends Neurosci.* **23**, 618–625 (2000).
317. Wooff, Y., Man, S. M., Aggio-Bruce, R., Natoli, R. & Fernando, N. IL-1 family

members mediate cell death, inflammation and angiogenesis in retinal degenerative diseases. *Front. Immunol.* **10**, 1–21 (2019).
318. Garweg, J. G., Zandi, S., Pfister, I. B., Skowronska, M. & Gerhardt, C. Comparison of cytokine profiles in the aqueous humor of eyes with pseudoexfoliation syndrome and glaucoma. *PLoS One* **12**, 1–13 (2017).
319. Gao, X. *et al.* Chemokine (C-C motif) ligand 2 and chemokine (C-C motif) ligand 7 in angle-closure glaucoma. *Acta Ophthalmol.* **94**, e220–e224 (2016).
320. Ohira, S., Inoue, T., Iwao, K., Takahashi, E. & Tanihara, H. Factors influencing aqueous proinflammatory cytokines and growth factors in uveitic glaucoma. *PLoS One* **11**, 1–13 (2016).
321. Wang, Y. *et al.* Inflammatory cytokine profiles in eyes with primary angle-closure glaucoma. *Biosci. Rep.* **38**, 1–9 (2018).
322. Gajda-Derylo, B. *et al.* Comparison of cytokine/chemokine levels in aqueous humor of primary open-angle glaucoma patients with positive or negative outcome following trabeculectomy. *Biosci. Rep.* **39**, 1–11 (2019).
323. Abcouwer, S. F. Müller cell-microglia cross talk drives neuroinflammation in diabetic retinopathy. *Diabetes* **66**, 261–263 (2017).
324. Rutar, M., Natoli, R., Chia, R. X., Valter, K. & Provis, J. M. Chemokine-mediated inflammation in the degenerating retina is coordinated by Müller cells, activated microglia, and retinal pigment epithelium. *J. Neuroinflammation* **12**, 1–15 (2015).
325. Crane, I. J., Wallace, C. A., Mckillop-Smith, S. & Forrester, J. V. Control of chemokine production at the blood-retina barrier. *Immunology* **101**, 426–433 (2000).
326. Mangan, B. G. *et al.* Retinal pigment epithelial damage, breakdown of the blood-retinal barrier, and retinal inflammation in dogs with primary glaucoma. *Vet. Ophthalmol.* **10**, 117–124 (2007).
327. Scott, E. M., Boursiquot, N., Beltran, W. A. & Dubielzig, R. R. Early histopathologic changes in the retina and optic nerve in canine primary angle-closure glaucoma. *Vet. Ophthalmol.* **16**, 79–86 (2013).
328. Kosaka, N. *et al.* FGF-4 regulates neural progenitor cell proliferation and neuronal differentiation. *FASEB J.* **20**, 1484–1485 (2006).
329. Del Rio-Tsonis, K., Jung, J. C., Chiu, I. M. & Tsonis, P. A. Conservation of fibroblast growth factor function in lens regeneration. *Proc. Natl. Acad. Sci. U. S. A.* **94**, 13701–13706 (1997).
330. Kinkl, N. *et al.* Possible involvement of a fibroblast growth factor 9 (FGF9)-FGF receptor-3-mediated pathway in adult pig retinal ganglion cell survival in vitro. *Mol. Cell. Neurosci.* **23**, 39–53 (2003).
331. Vogler, S. *et al.* Endothelins Inhibit Osmotic Swelling of Rat Retinal Glial and Bipolar Cells by Activation of Growth Factor Signaling. *Neurochem. Res.* **41**, 2598–2606 (2016).
332. Pinar-Sueiro, S., Urcola, H., Agurtzane Rivas, M. & Vecino, E. Prevention of retinal ganglion cell swelling by systemic brimonidine in a rat experimental glaucoma model. *Clin. Exp. Ophthalmol.* **39**, 799–807 (2011).
333. Sezenöz, A. S. *et al.* The diagnostic ability of ganglion cell complex thickness-to-total retinal thickness ratio in glaucoma in a Caucasian population. *Turkish J. Ophthalmol.* **50**, 26–30 (2020).
334. Chan, K. C., Fu, Q. L., So, K. F. & Wu, E. X. Evaluation of the visual system in a

rat model of chronic glaucoma using manganese-enhanced magnetic resonance imaging. in *Annual International Conference of the IEEE Engineering in Medicine and Biology - Proceedings* 67–70 (2007).
335. Zhao, D. *et al.* Characterization of the circumlimbal suture model of chronic IOP elevation in mice and assessment of changes in gene expression of stretch sensitive channels. *Front. Neurosci.* **11**, 1–15 (2017).
336. Radius, R. L. & Anderson, D. R. Breakdown of the normal optic nerve head blood-brain barrier following acute elevation of intraocular pressure in experimental animals. *Investig. Ophthalmol. Vis. Sci.* **19**, 244–255 (1980).
337. Plange, N., Bienert, M., Remky, A. & Arend, K. O. Optic disc fluorescein leakage and intraocular pressure in primary open-angle glaucoma. *Curr. Eye Res.* **37**, 508–512 (2012).
338. Arend, O., Plange, N., Sponsel, W. E. & Remky, A. Pathogenetic aspects of the glaucomatous optic neuropathy: Fluorescein angiographic findings in patients with primary open angle glaucoma. *Brain Res. Bull.* **62**, 517–524 (2004).
339. Margeta, M. A. *et al.* CD163+ macrophages infiltrate axon bundles of postmortem optic nerves with glaucoma. *Graefes Arch Clin Exp Ophthalmol.* **256**, 2449–2456 (2018).
340. Howell, G. R. *et al.* Radiation treatment inhibits monocyte entry into the optic nerve head and prevents neuronal damage in a mouse model of glaucoma. *J. Clin. Invest.* **122**, 1246–1261 (2012).
341. Lad, E. M., Cousins, S. W., Arnam, J. S. Van & Proia, A. D. Abundance of infiltrating CD163+ cells in the retina of postmortem eyes with dry and neovascular age-related macular degeneration. *Graefes Arch Clin Exp Ophthalmol.* **253**, 1941–1945 (2015).
342. Ramirez, A. I. *et al.* The role of microglia in retinal neurodegeneration: Alzheimer's disease, Parkinson, and glaucoma. *Front. Aging Neurosci.* **9**, 1–21 (2017).
343. Wolf, S. A., Boddeke, H. W. G. M. & Kettenmann, H. Microglia in Physiology and Disease. *Annu. Rev. Physiol.* **79**, 619–643 (2017).
344. Gui, D. M., Yang, Y., Li, X. & Gao, D. W. Effect of erythropoietin on the expression of HIF-1 and iNOS in retina in chronic ocular hypertension rats. *Int. J. Ophthalmol.* **4**, 40–43 (2011).
345. Karlstetter, M., Nothdurfter, C., Aslanidis, A., Moeller, K. & Horn, F. Translocator protein (18 kDa) (TSPO) is expressed in reactive retinal microglia and modulates microglial inflammation and phagocytosis. *J. Neuroinflammation* **11**, 2–12 (2014).
346. Liu, X. *et al.* The effect of A2A receptor antagonist on microglial activation in experimental glaucoma. *Investig. Ophthalmol. Vis. Sci.* **57**, 776–786 (2016).
347. Li, L., Qin, J., Fu, T. & Shen, J. Fisetin rescues retinal functions by suppressing inflammatory response in a DBA/2J mouse model of glaucoma. *Doc. Ophthalmol.* **138**, 125–135 (2019).
348. Markiewicz, L. *et al.* Altered expression levels of MMP1, MMP9, MMP12, TIMP1, and IL-1 β as a risk factor for the elevated IOP and optic nerve head damage in the primary open-angle glaucoma patients. *Biomed Res. Int.* **2015**, 1–8 (2015).
349. ten Berge, J. C. *et al.* Intraocular cytokine profile and autoimmune reactions in retinitis pigmentosa, age-related macular degeneration, glaucoma and cataract. *Acta Ophthalmol.* **97**, 185–192 (2019).
350. Cho, K. J., Kim, J. H., Park, H. Y. L. & Park, C. K. Glial cell response and iNOS

expression in the optic nerve head and retina of the rat following acute high IOP ischemia-reperfusion. *Brain Res.* **1403**, 67–77 (2011).
351. Woldemussie, E., Wijono, M. & Ruiz, G. Müller cell response to laser-induced increase in intraocular pressure in rats. *Glia* **47**, 109–119 (2004).
352. Wurm, A. *et al.* Effects of Ischemia – Reperfusion on Physiological Properties of Müller Glial Cells in the Porcine Retina. *Retin. Cell Biol.* **52**, 3360–3367 (2011).
353. Hidenobu, T. *et al.* Up-regulation of glial fibrillary acidic protein in the retina of primate eyes with experimental glaucoma. *Arch Ophthalmol.* **115**, 752–756 (1997).
354. Pan, D., Chang, X., Xu, M., Zhang, M. & Zhang, S. UMSC-derived exosomes promote retinal ganglion cells survival in a rat model of optic nerve crush. *J. Chem. Neuroanat.* **96**, 134–139 (2019).
355. Chen, C. Te, Alyahya, K., Gionfriddo, J. R., Dubielzig, R. R. & Madl, J. E. Loss of glutamine synthetase immunoreactivity from the retina in canine primary glaucoma. *Vet. Ophthalmol.* **11**, 150–157 (2008).
356. Moreno, M. C. *et al.* Effect of glaucoma on the retinal glutamate/glutamine cycle activity. *FASEB J.* **19**, 1161–1162 (2005).
357. Yu, J. *et al.* Effect of high hydrostatic pressure on the expression of glutamine synthetase in rat retinal Müller cells cultured in vitro. *Exp. Ther. Med.* **2**, 513–516 (2011).
358. Zhang, S. D. *et al.* Detection of early neuron degeneration and accompanying glial responses in the visual pathway in a rat model of acute intraocular hypertension. *Brain Res.* **1303**, 131–143 (2009).
359. Lundkvist, A. *et al.* Under stress , the absence of intermediate filaments from Müller cells in the retina has structural and functional consequences. *J. Cell Sci.* **117**, 3481–3488 (2004).
360. Wang, K., Peng, B. & Lin, B. Fractalkine receptor regulates microglial neurotoxicity in an experimental mouse glaucoma model. *Glia* **62**, 1943–1954 (2014).
361. Chuo, S. T. Y., Chien, J. C. Y. & Lai, C. P. K. Imaging extracellular vesicles: Current and emerging methods. *J. Biomed. Sci.* **25**, 1–10 (2018).
362. Lai, C. P. *et al.* Visualization and tracking of tumour extracellular vesicle delivery and RNA translation using multiplexed reporters. *Nat. Commun.* **6**, (2015).